Nt

NASA Contractor Report 165163

(NASA-CR-165163) A MULTI-PURPOSE METHOD FOR ANALYSIS OF SPUR GEAR TOOTH LOADING Final Report (Cleveland State Univ.) 106 p HC A06/MF A01 CSCL 13I N82-10401 Unclas G3/37 27763

A MULTI-PURPOSE METHOD FOR ANALYSIS OF SPUR GEAR TOOTH LOADING

R. Kasuba, J. W. Evans, R. August, and J. L. Frater

Cleveland State University
Cleveland, Ohio 44115

October 1981

Prepared for

NATIONAL AERONAUTICS AND SPACE ADMINISTRATION
Lewis Research Center
Under Contract NAS3-18547

TABLE OF CONTENTS

NOMENCLATURE

C - Center distance

C_B - bearing damping

C_S - shaft damping

CP - circular pitch

CR - loading contact ratio

CR_T - theoretical contact ratio

DDELT - backlash

DF - dynamic load factor

E - Young's modulus

F - gear face width

FH - hub face width

FW - geat web thickness

G - torsional modulus

GP - gear tooth pair

HSF - hub torsional stiffness factor

J - mass moment of interia

JG - $1/2\ M_G(RBC)^2$

K - shaft stiffness

KG - gear mesh stiffness, N/m

KP - gear pair stiffness, N/m

M - mass

P - total mesh static load, normal

P_H - Hertz stress

PE - profile error

PM - profile modification

PSITP - static angular position

Q - static GP load, normal

QD - dynamic GP load, normal

QDT - total mesh dynamic load, normal

RA - roll angle

RATIP - RA at tip of involute

RAPP - RA at pitch point

RABOT - RA at bottom of involute

RBC - radius of base circle

RCP - radius to contacting point

RCCP - radius of curvature

RH - hub fixity radius

RRC - radius of root circle

SV - sliding velocity

TR - transmission ratio

δ - deflection

μ - Poisson's ratio

ξ - critical damping ratio, gear mesh

ξ_s - critical damping ratio, shafts

Ψ - dynamic displacement, rad

$\dot{\Psi}$ - dynamic velocity

$\ddot{\psi}$ - dynamic acceleration, rad/sec^2

Superscript:

' - instantaneous

Subscripts :

D - driving element

G - gear

HCR - high contact ratio gearing

i - mesh arc position

L - load element

NCR - normal contact ratio gearing

S - shafting

1 - Gear 1

2 - Gear 2

INTRODUCTION

Many advanced technology applications have a general requirement that the power to transmission weight ratio be increased. Engineers, as a result of these requirements, design gear systems to maximum load capacity. However, accurate determination of gear tooth loads and stresses under dynamic conditions is not currently possible. As a result, experience or engineering institution becomes the controlling factors in transmission design. The ability to accurately calculate the dynamic loads in geared systems becomes essential for advanced transmission design.

The concern with dynamic loads acting on gear teeth goes back at least to the eighteenth century. A first concentrated effort in defining dynamic loads was conducted by the ASME Research Committee on Dynamic Loads on Gear Teeth in the late 1920's and early 1930's. These studies presented a dynamic load equation more popularly known as Buckingham's Equations [1]*.

Between 1940 and mid 1950's another era in analyzing the dynamic loads in gear teeth developed. The studies conducted during this period utilized more detailed information on gear teeth deflection, and in addition, mass-equivalent spring models with wedge, cam, or sinusoidal type excitations were introduced [4, 6, 7, 9]. In general, this group of analyses could be considered as using an equivalent constant mesh stiffness model.

---

* Numbers in brackets designate references at the end of the paper.

Starting with the late 1950's, a variable gear mesh stiffness model was considered by a number of investigators [8, 10-12, 14-16, 18-21]. In these analyses, the gear mesh stiffness was assumed or calculated to be of periodic rectangular (or nearly rectangular) form, in other cases it was assumed that the stiffness could be of sinusoidal or trapezoidal forms. The main simplifications used either singly or in same combinations in these models can be generalized as follows:

a. Gear tooth errors have negligible effect or no effect on mesh stiffness. This implies that for a given load a gear with errors will have equal mesh stiffness as the same gear without errors.

b. Contact assumed to occur only on the line of action.

c. Analysis limited to contact ratios below 2.0.

d. The contact ratio and/or mesh stiffness is not affected by transmitted load, premature or delayed engagement.

e. Dynamic simulations based on uninterrupted periodic stiffness functions and error displacement strips.

In view of these limitations, the above gear mesh stiffness model can be defined as a fixed-variable gear mesh stiffness model (FVMS).

The gear mesh stiffness in engagement is probably the key element in the analysis of gear train dynamics. The gear mesh stiffness and the contact ratio are affected by many factors such as the transmitted loads, load sharing, gear tooth errors, profile modifications, gear tooth deflections, and position of contacting points.

By introducing these aspects, the calculated gear mesh stiffness can be defined as being a variable-variable mesh stiffness (VVMS) as opposed to the FVMS modeling. The need for an improved modeling or variable-variable gear mesh stiffness modeling has been recognized or initiated to some degree [11, 15, 16, 22-25, 27, 29, 33, 34].

In this study a large scale digitized approach (computer block diagram in Figure 1) was used for eliminating the previously indicated serious shortcomings of the FVMS modeling. The concept of the VVMS was expanded by introducing an iterative procedure to calculate the VVMS by solving the statically indeterminate problem of multi-pair contacts, changes in contact ratio, and mesh deflections. In both the static and dynamic portions of the analysis, the gear train was modeled as a rotating system rather than an equivalent mass-spring system excited by the error displacement strips or wedges.

The primary purpose of this study was to develop an uninterrupted static and dynamic analysis of a spur gear train. In both the static and dynamic portions, the gear train was modeled as a rotating system rather than an equivalent mass-spring system excited by the error displacement strips or wedges. At this time the modeling is limited to the condition that for a given gear all teeth have identical spacing and profiles (with or without surface imperfections). The surface imperfections-faults were simulated by introducing various sinusoidal profile errors and surface pitting. The extended modeling is illustrated by a few selected situations in the high contact ratio ($CR \geq 2$) and normal contact ratio ($CR < 2$) operating regimes.

OVERALL COMPUTER PROGRAM FLOW DIAGRAM

The developed digitized analytical method was programmed in FORTRAN IV. Functionally, the computer program is divided into the following three parts:

1. A set of subroutines to perform the static analysis. This set of subroutines can operate as a stand-alone unit. However, this set is needed to operate Sets 2 and 3.
2. A set of subroutines to perform the dynamic analysis.
3. A set of subroutines to perform the finite element analysis of gear tooth stresses. (Currently not an integral part of the entire system program package).

Figure 1 depicts in general terms the block diagram for the computer program. The main calling program reads in and prints the input information defining the gears. It then passes control first to the static analysis section and then sequentially to the dynamic analysis section and to the finite element section.

The MAIN1 routine performs the bookkeeping for the static analysis portion of the program. This routine calls the necessary subroutines to perform all the calculations required for the static analysis and the writing out of the results in the form of tables or X-Y plots.

The static analysis is accomplished primarily by means of three subroutines: MOD, SLOWM and DEFL.

The purposes of the MOD subroutine is to generate the XY coordinate system and digitize the gear tooth profiles from the addendum circle to the root circle for each gear. The MOD subroutine permits to build up a non-standard tooth form, or to introduce profile modifications, profile errors, and surface pits.

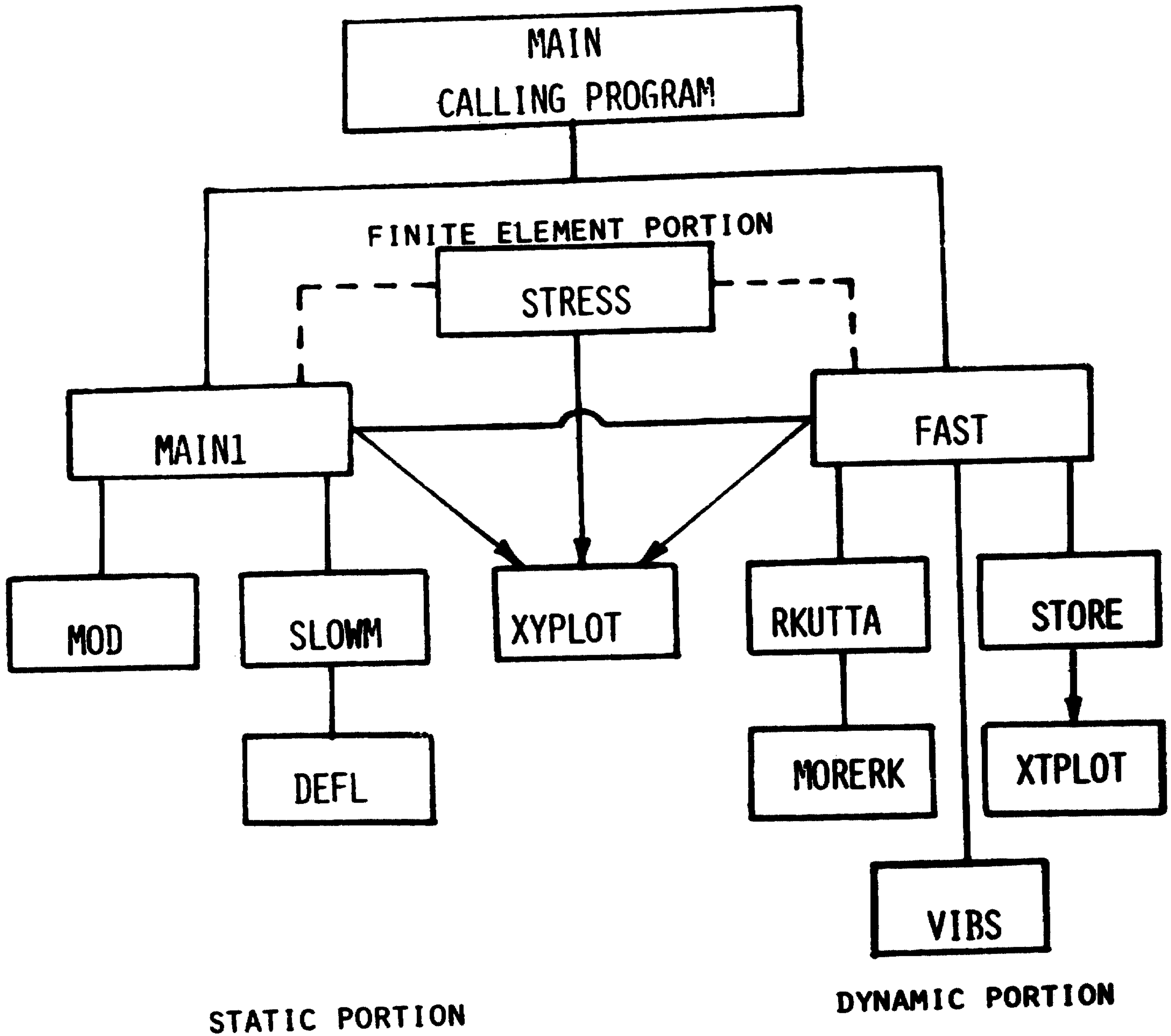

FIGURE 1 - COMPUTER PROGRAM BLOCK DIAGRAM

The SLOWM routine determines the contact points and the number of contacting gear tooth pairs, load sharing, stiffness functions, various positional vectors, sliding velocity vectors, transmission ratios, etc. as the gear tooth pairs move through the mesh arc. In the SLOWM routine all inertia forces and torques were taken to be negligible.

The DEFL subroutine is used in conjunction with the SLOWM routine to determine the individual gear tooth deflections.

The XYPLOT routine is used to cross plot as many as four dependent variables against a single independent variable.

The FAST routine is the main routine for the dynamic analysis. The routine consists of a number of subroutines listed below:

The VIBS subroutine is used to determine the eigenvalues and eigenvectors of the gear train and to set the length of the numerical integration run as well as the integration time steps.

The RKUTTA and the MORERK subroutines are used to numerically integrate the system of differential equations of motion. These routines utilize a fourth order Runge-Kutta integration scheme.

The STORE subroutine is used in conjunction with the XTPLOT routine to generate plots of the mesh stiffness function and the dynamic force variation versus time. The STORE subroutine features a recirculating memory provision and is used as a buffer between the integration routines and the XTPLOT routine.

The STRESS routine contains the finite element and grid generating subroutines to perform stress analysis of a gear tooth subjected to dynamic loads. At this time the STRESS routine is not an integral part of the entire program. Also see P. 74.

The principal executing subroutines are described in a greater detail in subsequent sections and Appendix.

STATIC MODEL - DETERMINATION OF GEAR TOOTH STIFFNESS AND LOAD SHARING

Before the variable-variable mesh stiffness (VVMS) can be determined, the actual contacting profiles must be developed. In this process, the profile modifications and errors must be considered.

It is customary to define the profile modifications and errors by means of a profile chart. In terms of an involute chart, the profile modifications (PM) and errors (PE) can be expressed as

$$M = PV(RA) \tag{1}$$

where

M = deviation from the line of action

RA = roll angle limited to active profile

PV = profile variation (error or amount of modification) as a function of RA

A true involute profile is defined by

$$M = PV(RA) = 0$$

The previously discussed MOD subroutine simulates an involute chart-gear tooth profi relationship shown in Figures 2 and 3. The simulated profile chart can accommodate the parabolic and straight line modifications of the tip and root zones, Figure 2a. The profile errors were approximated by sinusoidal representation. By varying the number of cycles and phase angle sinusoidal profile errors (Figures 2b, 2c) could describe a large number of practical the theoretical cases. A simulated surface pitting damage is shown in Figure 2e. The defined surface faults and their respective involute charts are then numerically transferred to the previously digitized true involute

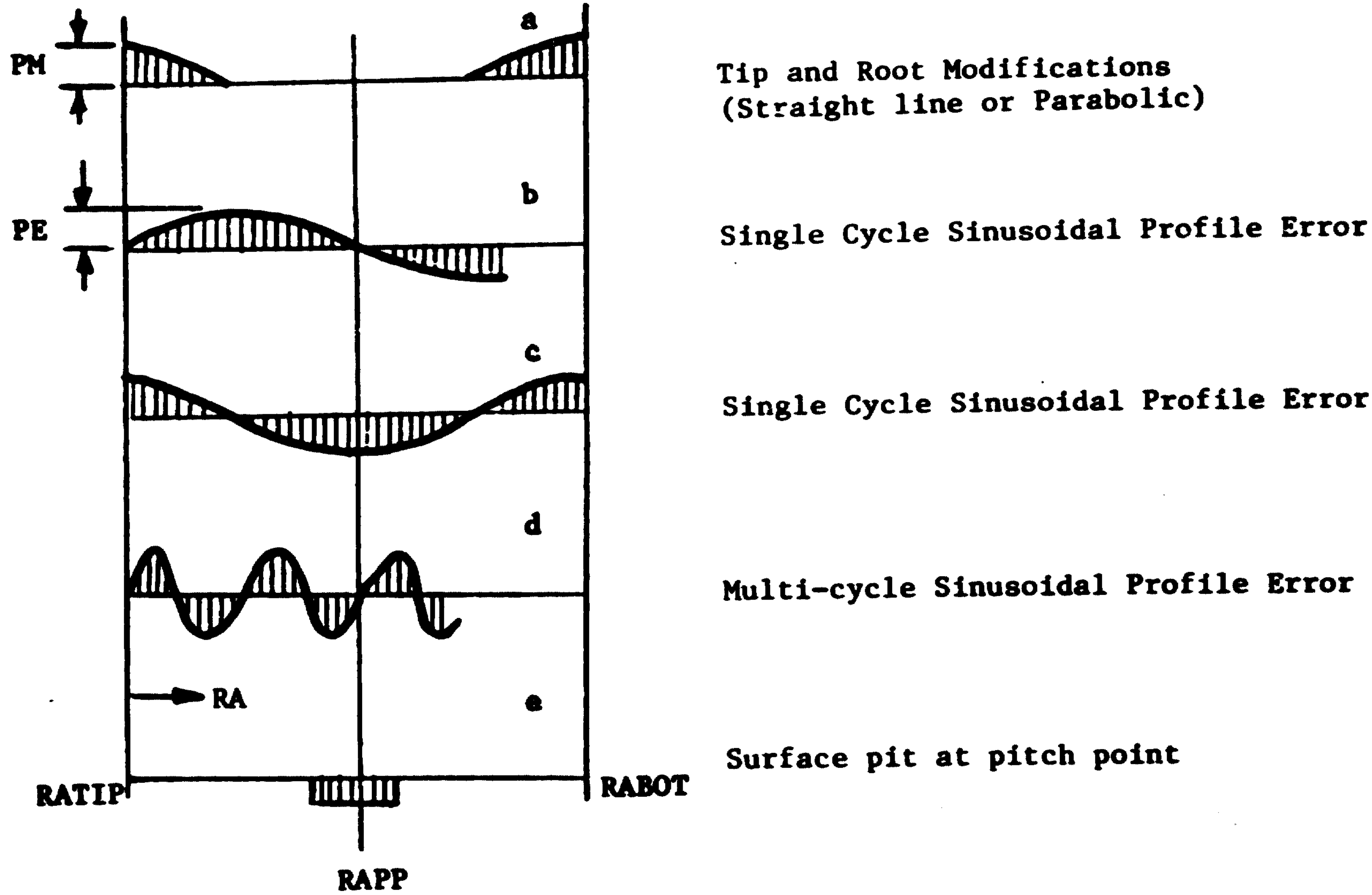

FIGURE 2 - SAMPLE SINULATED GEAR TOOTH PROFILE CHARTS

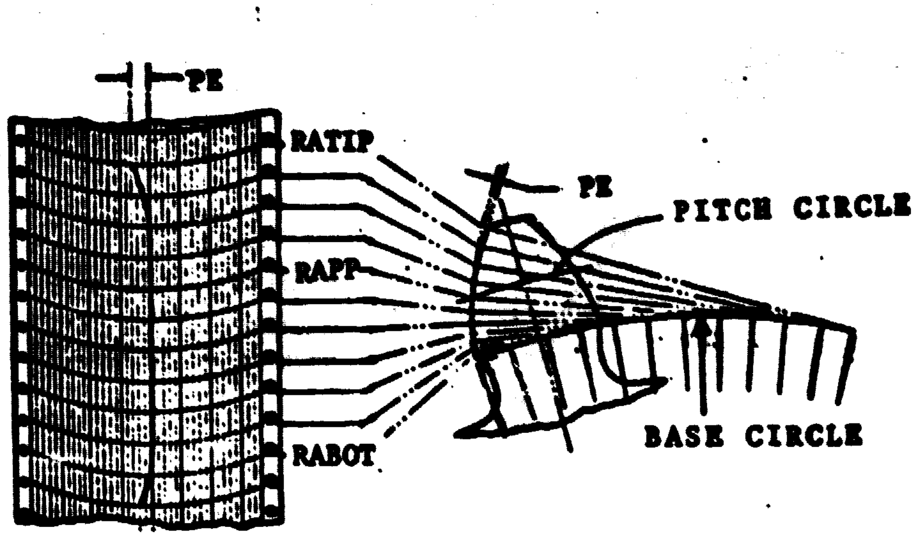

FIGURE 3 INVOLUTE CHART - PROFILE RELATIONSHIP

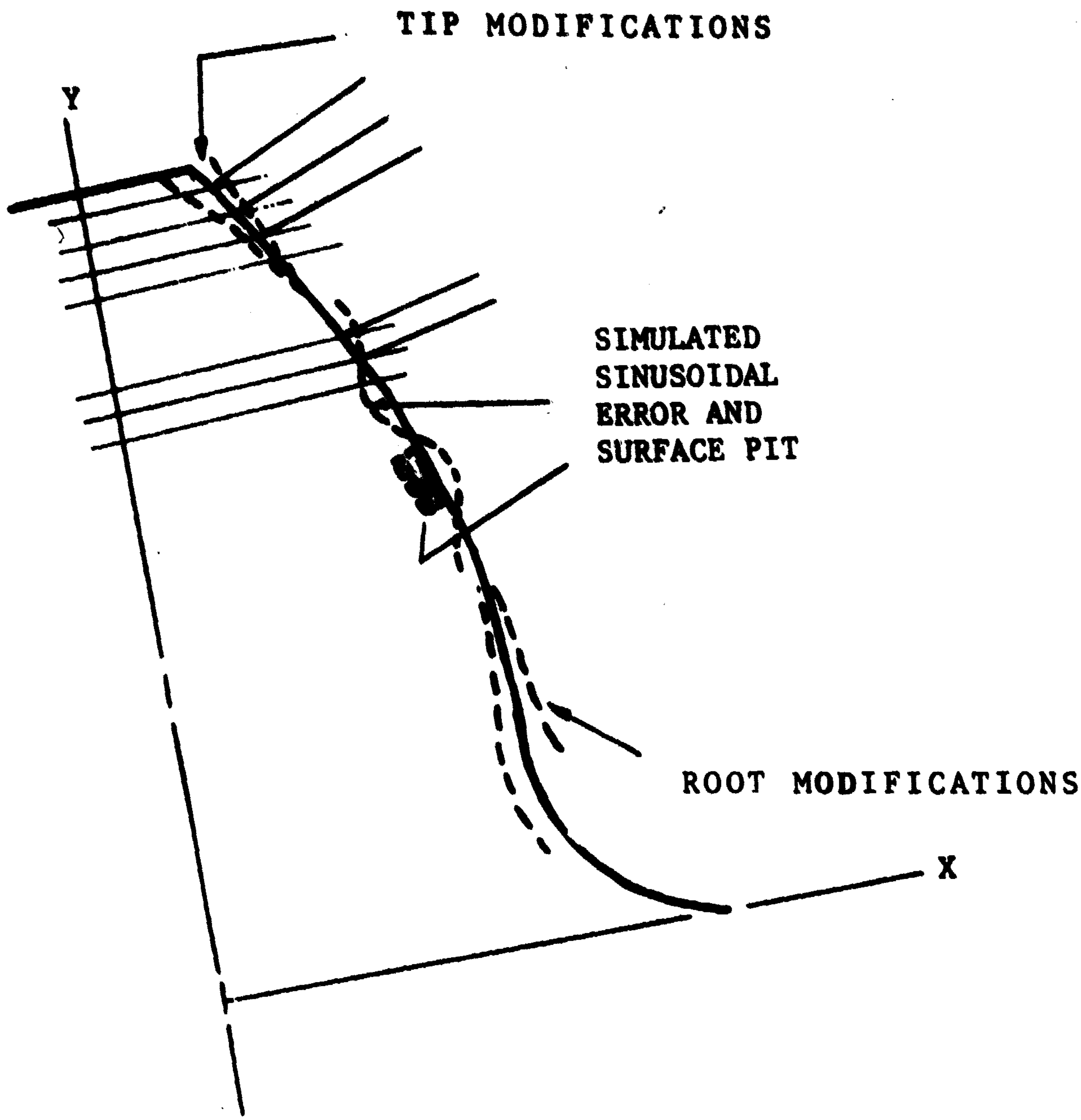

FIGURE 4 - GEAR TOOTH PROFILE MODEL

profile. This is accomplished by subtracting or adding the specified amounts of material perpendicularly to the true involute profile as shown in Figures 3 and 4.

After considering several types of "curved" segments and resulting numerical difficulties, straight line segments were chosen to connect the densely digitized points involving the "modified" gear teeth. Each gear tooth profile was defined by one to two hundred digitized points, depending on tooth size. One hundred points were used to define the gear tooth heights up to 25 mm (1 in.). Two hundred points were used to digitize the gear tooth profiles above 50 mm. (2 in.) in height. The intermediate tooth heights are proportionally digitized between one and two hundred points.

The digitized profile points incorporating the specified profile modifications and errors then are transferred to the SLOWM subroutine for establishing the points of contact, number of contacting gear tooth pairs, sliding velocity vectors, and the stiffness of the individual pairs as well as the variable-variable mesh stiffness.

Figures 4 and 5 will be used to illustrate the computerized method for determining the VVMS and other parameters. For this purpose three coordinate systems are used. Following Figure 5.

U, V - Fixed global coordinate system for the pinion and gear tooth profiles, gear 1 and gear 2, respectively.
The global system, (U, V), has its origin at the pinion center and its V-axis corresponds to the gear centerline.

X, Y - Local coordinate system fixed at the root of individual teeth for the pinion and gear, respectively. The origin O (X,Y) is located at the intersection of the centerline of the tooth and the line tangent to the root circle of the teeth. The Y-axes coincide with the tooth centerlines. The X, Y coordinate system is used in digitizing the profiles and for determining the appropriate deflections of the teeth.

W, Z - Intermediate coordinate system rotating with the pinion and gear respectively. The origins of the W, Z coordinate systems for each gear are at the respective gear centers. The Z-axes coincide with the tooth centerlines.

The transformations between the coordinate systems for each considered gear pair (k=1, n) are:

$$
\begin{aligned}
&W1 = X1;\ W2 = X2 \\
&Z1 = Y1 + RRO1;\ Z2 = Y2 + RRO2 \\
&U1 = W1 \sin PSI1TP(k) + Z1 \cos PSI1TP(k) \\
&V1 = -W1 \cos PSI1TP(k) + Z1 \sin PSI1TP(k) \\
&U2 = -W2 \cos (PSI2TP(k) - 1.5\pi) + Z2 \sin (PSI2TP(k) - 1.5\pi) \\
&V2 = C - [W2 \sin (PSI2TP(k) - 1.5\pi) + Z2 \cos (PSI2TP(k) - 1.5\pi)]
\end{aligned}
\qquad (2)
$$

For each angular position defined by PSI1TP (k) and PSI2TP(k) the profile coordinates (X,Y) are first transformed into an intermediate coordinate system, (W,Z), and then into a global coordinate system, (U, V).

In each transformation step, the first profile point (point 1) is located at the addendum circle, and the final point is located at the root. Each tooth is defined by the same number of digitized points.

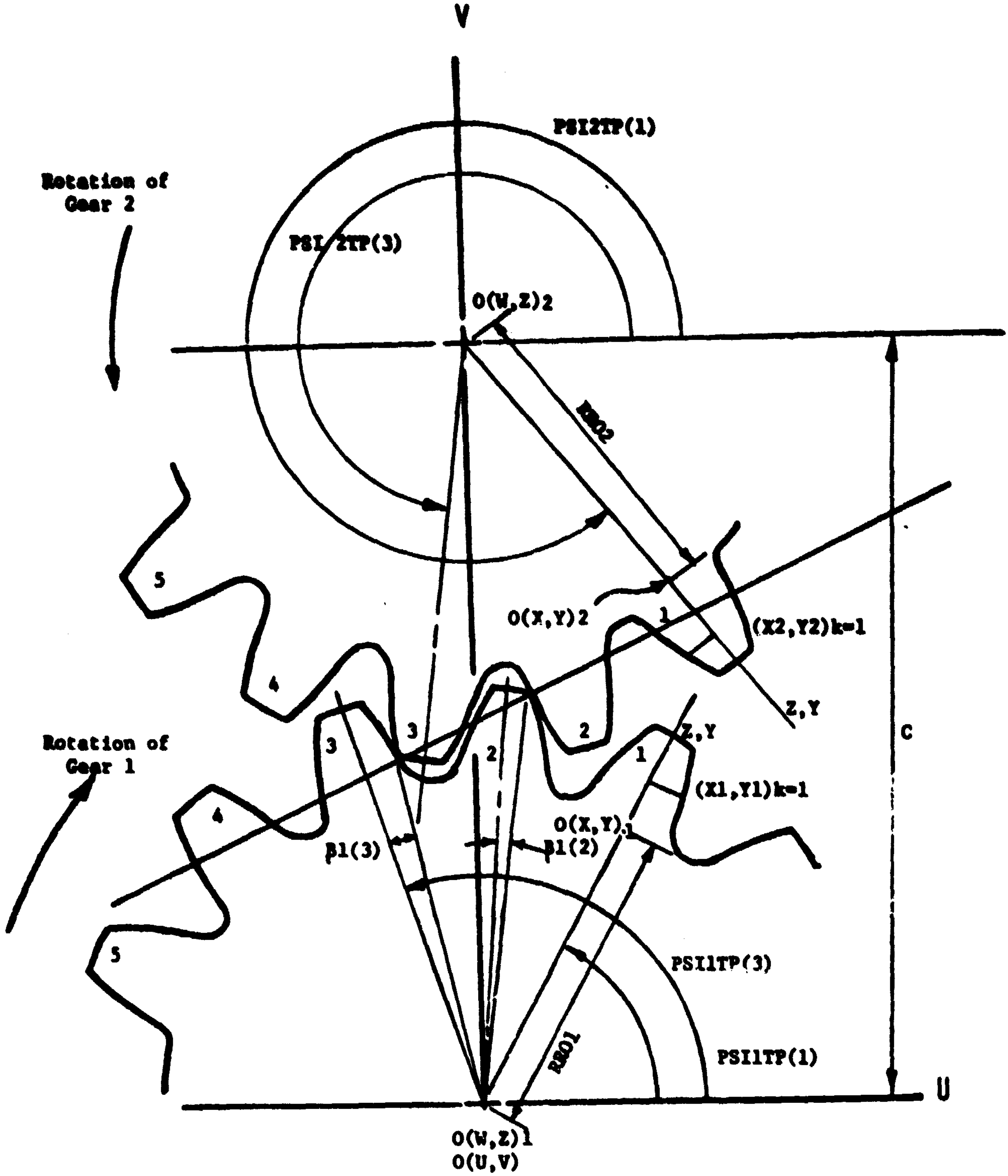

FIGURE 5 - GEAR TOOTH COORDINATE SYSTEM

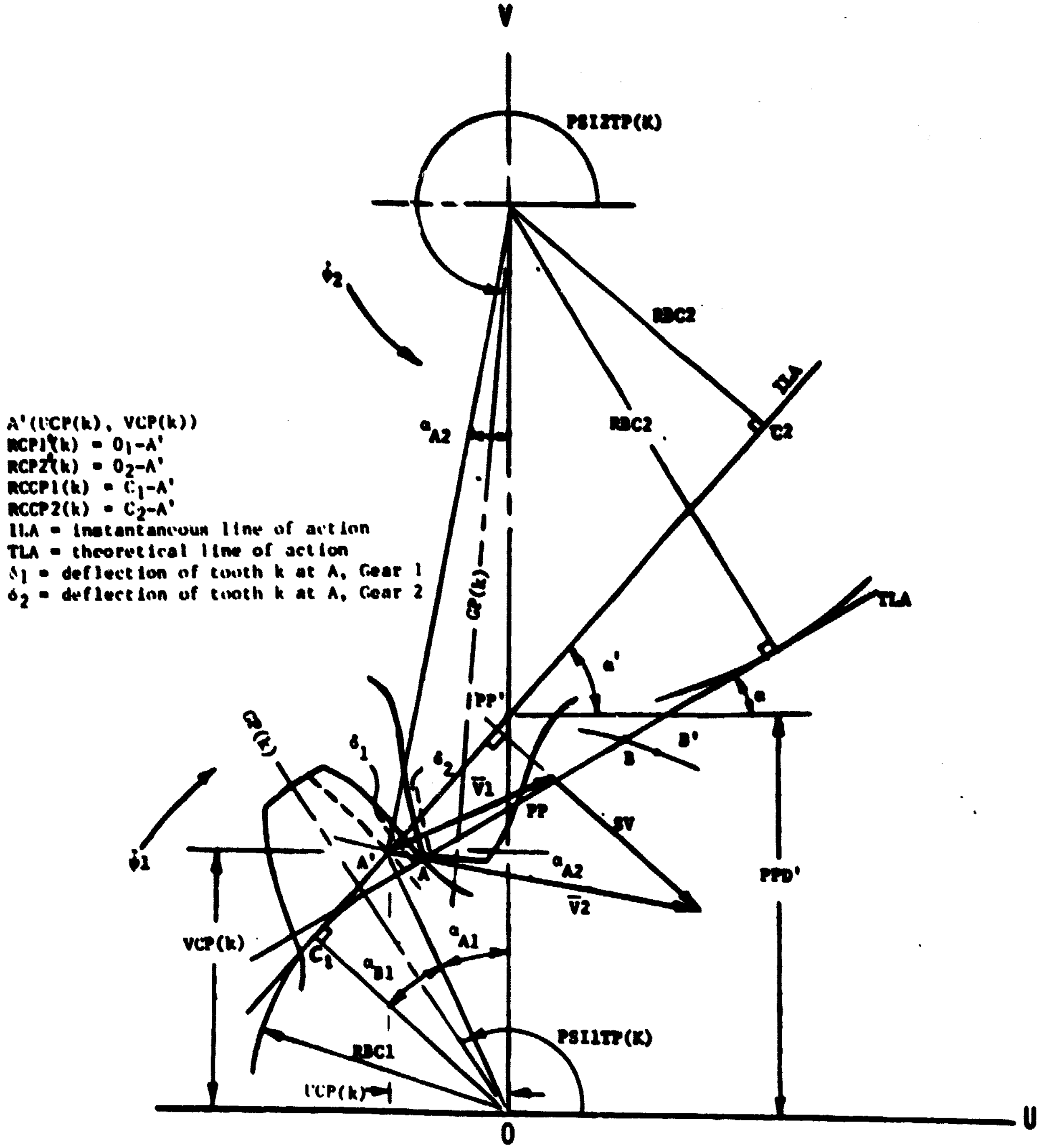

FIGURE 6 - INSTANTANEOUS CONTACT POINT FOR INCOMING TOOTH PAIR

For example, using 100 digitized profile points there are:

X1 (100), Y1 (100)		X2 (100), Y2 (100)	
W1 (100), Z1 (100)		W2 (100), Z2 (100)	
U1 (100), V1 (100)	Gear 1 k = 1, n	U2 (100), V2 (100)	Gear 2 k = 1, n

The locations of the contacting gear teeth and the number of contacting gear tooth pairs are determined by using a three step process. First, the gears are preloaded by a unit load and rotated by incrementing the PSI1TP (k) and PSI2TP (k) angles and examining the potential contact between the calculated (U1, V1) and U2, V2) profile points for several gear tooth pairs. The search technique is described in Appendix 1. The beginning and the end of the meshing arc are established by tracking the gear pair 3, (GP3) through its complete meshing arc. After the limiting points of mesh arc are determined the mesh arc is divided into fifty positions. Next, the gears are fully loaded for further analysis. The actual load sharing and deflections are calculated for fifty arc positions by tracking the movement of fully loaded gears through the established mesh arc.

By tracking five tooth pairs simultaneously, it is possible to analyze the mesh behavior for the contact ratios up to 3.0. Tracking seven tooth pairs instead of five expands the capacity of the program to analyze gear systems with contact ratios between 3.0 and 4.0, etc.

The gear tooth pair deflection $\delta(k)_i$ can be expressed in the following form:

$$\delta(k)_i = \delta_1(k)_i + \delta_2(k)_i + \delta_H(k)_i \tag{3}$$

$\delta_1(k)_i$ = deflection of the k^{th} tooth of gear 1 at mesh arc position i

$\delta_2(k)_i$ = deflection of the k^{th} tooth of gear 2 at mesh arc position i

$\delta_H(k)_i$ = localized Hertz deformation at the point of contact

For the contacting pairs, the gear tooth deflections $\delta_1(k)_i$ and $\delta_2(k)_i$ incorporate a number of constituent deflections; See [17] and Appendix 2,

$$\delta_1(k)_i = \delta_{M1}(k)_i + \delta_{N1}(k)_i + \delta_{S1}(k)_i + \delta_{B1}(k)_i + \delta_{R1}(k)_i \qquad (4)$$

and similarly for Gear 2. In equation (4),

δ_M = gear tooth deflection due to bending

δ_N = gear tooth deflection due to normal force

δ_S = gear tooth deflection due to shear force

δ_B = gear tooth deflection due to deformation of surrounding hub area (rocking action)

δ_R = gear tooth deflection due to gross torsion of the rim or hub (Appendix 2)

The gear tooth deflections can be considered as equivalent positive profile errors for the pinion and gears causing premature engagement and delayed disengagement [24, 29]. The presence of positive manufactured profile errors (material addition) will increase the total equivalent positive error at the point of contact thus moving it farther away from the theoretical line of contact and causing an earlier engagement. The negative profile errors or material removal at the tips will reduce the equivalent positive errors.

In the third step, the $\delta_1(k)_i$ and $\delta_2(k)_i$ and approportioned $\delta_H(k)_i$ deflections were returned to equations 2 and added perpendicularly to the respective digitized profiles in order to simulate the above gear behavior. Now, the iterative search and calculate process is repeated under the "loaded and deflected" conditions. In this step the contacting points and the mesh are determined under full load. These events are illustrated in Figure 5, where the limiting points of meshing arc occur at points A' and B' as compared to the theoretical true involute mesh arc A-B under no load. As a result, the contact arc, and therefore the contact ratio of the gears is increased. In the same procedural step, the final number of pairs in contact, locations of contacting points, gear tooth deflections, load sharing, stiffnesses, etc., are computed as the load gear tooth pairs move through the mesh arc (A'-B').

If the geometrical variations in surfaces do not permit contact in Steps 1 and 2, then the non-contacting gear teeth are still subjected to δ_R deflections. For example, if GP1 and GP3 are in contact, then for GP2

$$\delta_1(2)_i = \delta_{R1}(2)_i \text{ and } \delta_2(2)_i = \delta_{R2}(2)_i \tag{5}$$

These deflections are due to torque transmission at GP1 and GP3 and the resulting circumferential hub deformation at GP2. If the $\delta_{R1}(2)_i$ and $\delta_{R2}(2)_i$ deflections are sufficiently large to overcome the geometrical gap (errors) between the approaching teeth profiles of gears 1 and 2 at the angular position i, then the contact will be established for GP2. In this case the final load sharing and deflections will be recalculated on the basis of three contacting pairs (Step 3). These calculation methods can handle both the involute and non-involute gear actions, high contact ratio gearing, etc.

For any mesh arc position i, the calculated k^{th} gear tooth pair stiffness $KP(k)_i$, mesh stiffness KG_i, and load sharing incorporate the effects due to manufactured profile errors, profile modifications, and deflections by means of the iterated numerical solutions of equations 3 through 8.

The individual gear tooth pair stiffness can be expressed as

$$KP(k)_i = Q(k)_i / \delta(k)_i \tag{6}$$

If the effective errors prevent contact, $KP(k)_i = 0$.

The sum of gear tooth pair stiffnesses for all pairs in contact at position i represents the variable-variable mesh stiffness KGP

$$KGP_i = \sum_1^K KP(k)_i \tag{7}$$

The load carried by each of the pairs moving through the mesh arc in the static mode can be determined as

$$Q(k)_i = \frac{KP(k)_i}{KGP_i} (P) \tag{8}$$

where P is the total normal static load carried by the gears at any mesh position i in the static mode

$$P = \sum_1^K Q(k)_i \tag{9}$$

The contact ratio under non-conjugate action can be more properly defined as the ratio of the traversed arcs. For example, referring to Figures 5 and 6, the loaded contact ratios for an errorless gear pair can be approximated as

$$CR = \frac{A' - B'}{CP} \tag{10}$$

where

$$(A' - B') = [PSITP1\ (3)\ _{A'} - \beta1(3)] - [PSITP1(3) - \beta2(3)]\ _{B'} \tag{11}$$

$(A' - B')$ is the loaded arc length from GP3 first engagement to GP3 disengagement with $\beta1$ being the variable angle between the tooth centerline and the contacting point. In this modeling GP2, GP3 and GP4 participate in the mesh arc for $1<CR<2$; GP1, GP2, GP3, GP4, and GP5 participate in the mesh arc for $2<CR<3$, etc.

For the instances when the contact points are not on the theoretical lines of action (non-conjugate action) we must refer to instantaneous pressure angles, instantaneous lines of action and transmission ratios. The need for instantaneous lines of action were indicated in [15] and [23]. Utilizing Figure 6, the instantaneous parameters* for the contact point A' (defined by RCP1 and RCP2, or UCP(k) and VCP(k) in the U, V coordinate system) are:

PPD'	=	$RBC1/\cos(\alpha_{A1} + \alpha_{B1})$	Distance to instantaneous pitch point	(12)
α_{A1}	=	arcsin (UCP(k)/RCP1)		
α_{A2}	=	arcsin (UCP(k)/RCP2)		
α_{B1}	=	arctan (RCCP1/RBC1)		
α'	=	$\alpha_{A1} + \alpha_{B1}$	Instantaneous pressure angle	(13)
TR'	=	(C-PPD')/PPD'	Instantaneous transmission ratio	(14)
TR	=	RPC2/RPC1	Involute (theoretical) transmission ratio	(15)
RBC2'	=	RBC1xTR'	Instantaneous base circle, gear 2	(16)

---

* Designated by superscript '

$$RCCP1' = \sqrt{(RCP1)^2 - (RBC1)^2}$$ Equivalent instantaneous radius of curvature, gear 1 (17)

$$RCCP2' = \sqrt{(RCP2)^2 - (RBC2')^2}$$ Equivalent instantaneous radius of curvature, gear 2 (18)

The same procedure is used for determining the instantaneous parameters as the above gear pair k traverses the mesh arc and, similarly, for other gear pairs. The instantaneous transmission ratio TR' is influenced by the deformations in the contact zone and tooth profile errors. It is important to note that for no-load and no surface fault conditions TR' = TR, and similar analogy exists for other parameters.

If the actual loaded contact occurs above the theoretical line of action, the effective base circle radius of the driven gear will be decreased. Consequently, the instantaneous transmission ration, TR' will be smaller than the theoretical transmission ratio, TR.

In this study, it is assumed that the instantaneous transmission ratio is dominated by the incoming tooth pair at point A' in Figure 6 as it moves through one gear mesh stiffness cycle. The approximate variation/cycling of TR' is illustrated in Figure 9. The maximum variation in TR' is defined as ΔTR.

The described static analysis determines the variable-variable mesh stiffness (KGP), transmission ratios (TR), and the contact position vectors (RCP1, RCP2, RCCP1', etc.) for subsequent dynamic calculations.

DYNAMIC MODEL

A gear train shown in Figure 7 was used in dynamic simulations. This model is assumed to represent one of the practical cases in gearing. The model includes the input and load units; a pair of gears; interconnecting shafts; damping in shafting, gears and bearings; non-involute action caused by gear tooth deflections; and loss of contact.

The dynamic model is based on the same coordinates as the static model. The instantaneous parameters which were determined for various mesh arc positions in the static analysis will also be utilized in the dynamic simulation.

The equations of motion for this model along the instantaneous (non-involute) line of action can be given in the following form:

$$J_D \ddot{\Psi}_D + C_{BD} \dot{\Psi}_D + C_{B1} \dot{\Psi}_1 + C_{DS}(\dot{\Psi}_D - \dot{\Psi}_1) + K_{DS}(\Psi_D - \Psi_1) = T_D \qquad (19)$$

$$\begin{aligned} &J_{G1} \ddot{\Psi}_1 + C_{DS}(\dot{\Psi}_1 - \dot{\Psi}_D) + K_{DS}(\Psi_1 - \Psi_D) + \\ &[CGP_i(RBC1\dot{\Psi}_1 - RBC2'\dot{\Psi}_2) + KGP_i(RBC1\Psi_1 - RBC2'\Psi_2)]\, RBC1 = 0 \end{aligned} \qquad (20)$$

$$\begin{aligned} &J_{G2} \ddot{\Psi}_2 + C_{LS}(\dot{\Psi}_2 - \dot{\Psi}_L) + K_{LS}(\Psi_2 - \Psi_L) + \\ &[CGP_i(RBC2'\Psi_2 - RBC1\dot{\Psi}_1) + KGP_i\, (RBC2'\Psi - RBC1\Psi_1)]\, RBC2' = 0 \end{aligned} \qquad (21)$$

$$\begin{aligned} J_L \ddot{\Psi}_L + C_{BL}\dot{\Psi}_L + C_{B2} \dot{\Psi}_2 + C_{LS}(\dot{\Psi}_L - \dot{\Psi}_2) + K_{LS}(\Psi_L - \Psi_2) &= T_D \times TR' \\ &= T_L(TR') \end{aligned} \qquad (22)$$

The bearing damping on the drive and load shafts was lumped as effective damping at their respective drive and load masses.

The bracketed terms in equations (20) and (21) represent the dynamic gear mesh force which is dependent on the dynamic displacements of engaged gears, gear mesh stiffness and damping in the mesh.

In equations (20) and (21), KGP_i represents the variable-variable mesh stiffness. KGP_i is a function of gear tooth profile errors and modifications, deflections of gear teeth, load sharing, height of engagement, and an angular position i of engagement as the gear pairs move through the mesh zone. The mesh stiffness cycle is illustrated in Figures 9 and 10. The basic sources of excitation for a rotating pair of gears are the variable-variable mesh stiffness and the changes in the transmission ratio caused by non-involute action. The input torque T_D is assumed to be constant while the output or load torque T_L is a function of the instantaneous transmission ratio shown as T_L (TR'), and bearing losses. Also see Appendix 5. If contact occurs above the theoretical line of action, the effective base circle radius of the driven gear will be decreased by an amount equivalent to the percentage decrease in the transmission ratio.

Operational situations, which may involve momentary disengagement of gears in mesh can impost several conditions on the dynamic gear mesh forces in equations 20 and 21. By defining the relative dynamic displacement CRM as

$$CRM = RBC1 \times \Psi_1 - RBC2' \, \Psi_2 \, , \tag{23}$$

if CRM >0

$$(QDT)_i = CGP_i \times (RBC1\dot{\Psi}_1 - RBC2'\dot{\Psi}_2) + KGP_i \times CRM \tag{24}$$

if (CRM $\leq$ 0) and DDELT > |CRM| (25)

$$(QDT)_i = 0$$

if (CRM $\leq$ 0) and DDELT <|CRM|

$$(QDT)_i = CGP_i \times (RBC1\,\dot{\Psi}_1 - RBC2'\dot{\Psi}_2) + KGP_i \times (CRM-DDELT) \tag{26}$$

Also, when $KGP_i = 0$, $(QDT)_i = 0$

The equivalent damping in gear mesh CGP_i was related to KG_i by means of a critical damping coefficient (ζ).

$$CGP_i = 2\zeta \sqrt{KGP_i \frac{1}{\frac{(RBC1)^2}{J_{G1}} + \frac{(RBC2)^2}{J_{G2}}}} \qquad (27)$$

The indicated equations of motion (equations 19 - 22) were numerically integrated in the FAST routine by means of a 4th order Runge-Kutta integration scheme described in Appendix 5.

The initial displacements $\Psi_D(0)$, $\Psi_1(0)$, $\Psi_2(0)$ and $\Psi_L(0)$ were determined by statically twisting the entire system with the prescribed T_D and T_L torques. For the initial velocities $\dot{\Psi}_D(0)$, $\dot{\Psi}_1(0)$, $\dot{\Psi}_2(0)$ and $\dot{\Psi}_L(0)$ the anticipated steady state involute action velocities were selected.

The numerical integration of the equations of motion is carried out for a length of time equivalent for the time required for the start-up transient to decay. This time is assumed to be equal to five times the longest system natural period. The integration time step is taken either as one tenth of the shortest system natural period or one percent of the mesh stiffness period with CR < 2 (two percent for CR > 2), whichever is smaller. Also see Appendix 4.

As the first step, the FAST routine calculates the dynamic force in the mesh defined by equations 23-25. Next, the FAST routine interacts with the SLOWM subroutine to determine the adjunct dynamic information:

a. how the dynamic load is shared by contacting tooth pairs during periods when multiple tooth pairs are in contact.

b. the variation of the load magnitude along the tooth profiles of a contacting tooth pair as the pair moves through the contact zone.

c. the sliding velocity, the maximum hertz pressure and the sliding velocity-hertz pressure product along the tooth profiles.

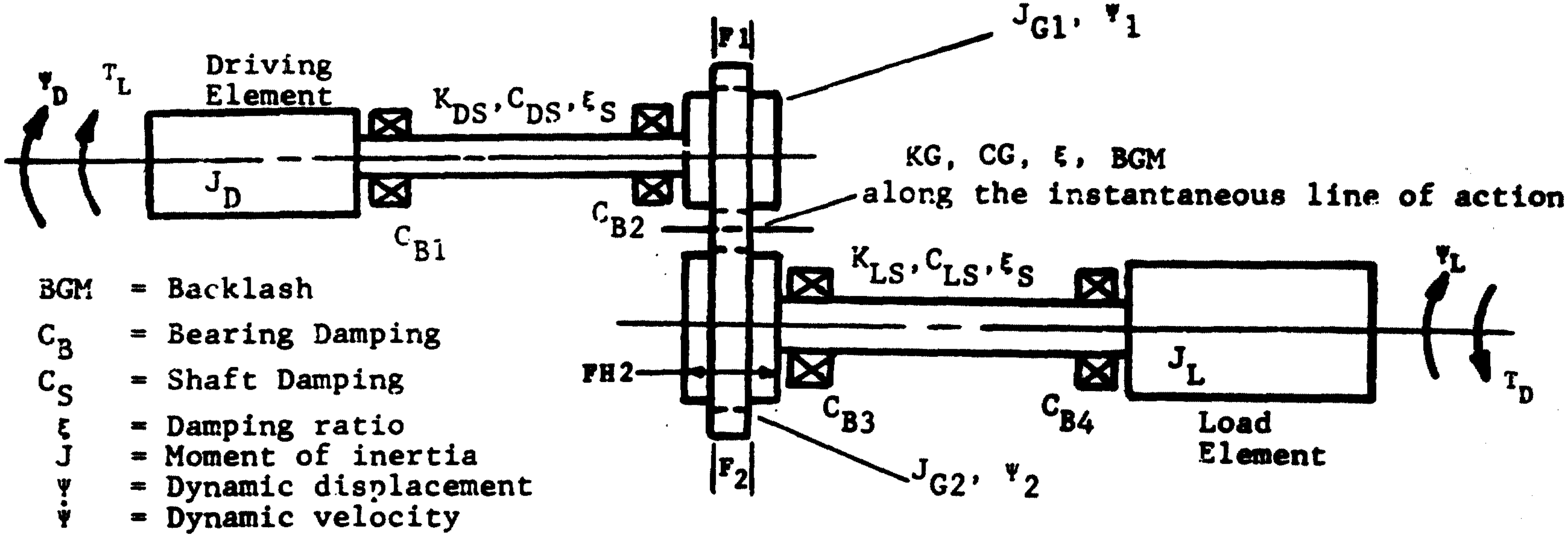

FIGURE 7 - GEAR TRAIN USED IN THE DYNAMIC ANALYSIS

In order to save computational time, it was assumed that the loaded meshing arcs (Points A'and B' in Figure 6) in the static and dynamic modes will be of the same length. It is believed that this is also a reasonable assumption because the rapidly fluctuating loads should not produce a lasting change of the meshing arc lengths. With this assumption the determined dynamic absolute angular displacements can be compared/interpolated with the equivalent mesh arc positions in the static mode PSI1TP(k), PSI2TP(k) for selecting the associated RCP1(k), RCP2(k), RCCP1(k), RCCP2(k) and other vectors for further calculations. Some of this information is illustrated in Figures 5 and 6. Consequently, the above-listed adjunct parameters a, b and c were determined by utilizing the calculated dynamic mesh force (can be zero for certain conditions) and interpolations between the dynamic and static mode positions.

For example, by establishing the correspondence between the Ψ_1, Ψ_2 and interpolated PSI1TP(k), PSI2TP(k) positions and associated RCP1(k), RCP2(k) vectors it is possible to calculate the sliding velocity for the dynamic mode.

The necessary vector relationships for determining the instantaneous sliding velocities can be seen in Figure 6. In the kinematics of gearing the tangential velocities V_1 and V_2 at the point of contact are perpendicular to their respective contact radii with the sliding velocity perpendicular to the line of action, Reference [21].

velocities $\dot{\psi}_1$ and $\dot{\psi}_2$, the instantaneous sliding velocity SV is determined by solving the vector equation 28 (vector polygon in Figure 5).

$$SV(k)_i = \overline{V}_1 - \overline{V}_2 = \overline{RCP1}'(k)\,\dot{\Psi}_1 - \overline{RCP2}'(k)\,\dot{\Psi}_2 \qquad (28)$$

(Equation 27 can also be written in a scalar form as Equation 28).

$$SV(k)_i = \sqrt{(V_1)^2 + (V_2)^2 - 2V_1\,V_2\,\cos\,(\alpha_{A1} + \alpha_{A2})} \qquad (29)$$

The dynamic load (QD(k) for a contacting gear tooth pair in the dynamic mesh position i was established as

$$QD(k)_i = \frac{KP(k)i}{KG_i}(QDT)_i \tag{30}$$

For the same position the Hertz stress P_H was calculated by using an equivalent cylinder approach, equation 30.

$$P_H\ (k)_i = \sqrt{\frac{QD(k)_i}{\pi\ FA}\left(\frac{1}{RCCP1'(k)} + \frac{1}{RCCP2'(k)}\right)} \tag{31}$$

where

RCCP1'(k), RCCP2'(k) = equivalent instantaneous radii of curvature

F = minimum gear tooth face width

$$A = \left(\frac{1-\mu_1^2}{E1}\right) + \left(\frac{1-\mu_2^2}{E2}\right)$$

In this study the dynamic load factors were defined as

$$(DF1)_i = \frac{(QDT)_i}{P} \tag{32}$$

and

$$(DF2)_i = \frac{QD(k)_i}{Q(k)i} \tag{33}$$

DF1 can be interpreted as the dynamic load factor for the mesh or as the dynamic load factor for the gear pair, adjacent shafts and bearings.

DF2 is the dynamic load factor for an individual gear tooth pair traversing the mesh arc. DF2 is of main importance when the strength of the gear teeth is of primary importance. The larger of the two dynamic load factors will be defined as the dynamic load factor for design, DF.

RESULTS AND DISCUSSION

In the extended modeling which includes the variable-variable mesh stiffness (VVMS) method, the gear train was modeled as a rotating system excited by the variable-variable mesh stiffness and the profile error-induced interruptions of the stiffness function. The non-involute action was described by the use of the instantaneous line of action and consequent variations in the transmission ratio.

The VVMS method defines the gear mesh stiffness as a function of load, errors and position of contact. This is in contrast with the fixed-variable stiffness (FVMS) method where the gear-mesh stiffness was treated independently of the transmitted loads and gear tooth errors. In the FVMS method it is generally assumed that the mesh stiffness function is the same for identical gears with or without errors with the contact in both cases occuring only on the theroretical line of action. The non-involute action of the gears in the FVMS method was simulated by means of the error/displacement strips acting along the line of action.

Static Analysis

The described digitized VVMS method removed many of the previous assumptions and simplifications thus improving the determination of the gear mesh stiffness. The extended modeling which includes the VVMS method will be illustrated in the static and dynamic modes by a few selected cases in the high contact ratio (HCR with CR≥2) and normal contact ratio (NCR with CR<2) gearing, respectively.

Tables 1A, 1B, and 2 and accompanying Figure 8 show the mesh stiffness characteristics for error-less gears. Presented results indicate the obscure but important influence of equivalent hub stiffness on the overall gear mesh stiffness. By increasing hub torsional stiffness (higher HSF, Appendix 2) the loaded contact ratio decreases, mesh stiffness increases, changes in transmission ratio decrease, and sensitivity to gear tooth errors increases. The opposite occurs by decreasing the hub stiffness.

The tabulated results indicate substantial changes in the contact ratio with increasing loads and/or gear hub flexibilities. For example, starting with a theoretical contact ratio of 2.14 for a 32 & 96 tooth gear pair the loaded contact ratio can be 2.47 or higher within practical load and gear hub flexibility ranges. In addition, some of the NCR gear pairs could be theoretically made to operate in the HCR regime by selecting an appropriate combination of the transmitted load and gear hub flexibilities.

Profile errors and pitting can affect the mesh stiffness characteristics to varying degrees. A case where only one of the meshing gears has surface imperfections will be considered first. With torsionally flexible hubs where the circumferential fixity is approximately equal to the minimum shaft size required to transmit the applied torques (HSF$\simeq$.5), the sinusoidal errors of .013mm (.0005 in.) and narrow surface pits .5mm wide (.02 in.) were absorbed by the mesh flexibility without affecting the errorless mesh stiffness characteristics. On the other hand, when the hubs were torsionally rigid (HSF = 1) the mesh flexibility was not able to absorb the errors of above magnitudes. Unabsorbed errors cause non-contact zones resulting in significant changes in the mesh stiffness characteristics (Figures 8 and 9). With increasing hub flexibility there was a gradual return to normal mesh stiffness characteristics, i.e. the flexibilities in the mesh were able to narrow or bridge the non-contact zones. For example, a 32 & 96 tooth gear pair mesh with HSF = .6 was able to absorb a portion of the sinusoidal error by eliminating about fifty percent of the mesh stiffness interruptions shown in Figure 9.

TABLE 1A

EFFECTS OF GEAR HUB FLEXIBILITY ON MESH STIFFNESS, TRANSMISSION RATIO AND CONTACT RATIO

Gears: 32 & 96T, 8DP, 14.5°PA, F = 25.4mm (1 in.), CR_T = 2.14
Normal Load: 4450N(1000 lb) or 175 N/mm (1000 lb/in)

$RH1_f$ mm	$RH2_f$ mm	KG_{max} N/m	KG_F N/mm^2	HSF	ΔTR * %	CR
10.0	14.5	3.07×10^8	1.21×10^4	.476	2.4	2.47
12.7	18.3	3.80×10^8	1.50×10^4	.591	1.9	2.42
12.7	38.1	5.08×10^8	2.00×10^4	.794	1.6	2.36
38.1	114.3	6.36×10^8	2.50×10^4	.992	1.0	2.32
47.2	148.8	6.45×10^8	2.54×10^4	1.0	1.0	2.32

TABLE 1B

LOAD EFFECTS ON MESH STIFFNESS, TRANSMISSION RATIO AND CONTACT RATIO

Gears: 32 & 96T, 8DP, 14.5°PA, F = 25.4mm (1 in.), CR_T = 2.14, HSF = .992

Load N/m	KG_{max} N/m	KG_F N/mm^2	ΔTR* %	CR
88	6.36×10^8	2.50×10^4	0.8	2.29
175	6.36×10^8	2.50×10^4	1.0	2.32
350	6.36×10^8	2.50×10^4	1.0	2.38
525	6.36×10^8	2.50×10^4	1.8	2.43
700	6.36×10^8	2.50×10^4	2.2	2.45

KG_{max} = maximum attainable stiffness in the meshing arc

All gears without errors or modifications

F1= F2= FH1= FH2 = 25.4mm (1.0 in.) $\qquad KG_F = \frac{KG_{max}}{F}$

RRC1 = 47.25mm RRC2 = 148.84mm

*Illustrated in Figure 9

TABLE 2

Gear Mesh Stiffness Characteristics

Normal Load: 4450N(1000 lb.) or 175 N/mm (1000 lb/in)

Gear Combination	$RH1_f$ mm	$RH2_f$ mm	KG_{max} N/m	KG_F N/mm^2	HSF	ΔTR %	CR
A	10.0	14.5	3.07×10^8	1.21×10^4	.476	2.4	2.47
	47.2	148.8	6.45×10^8	2.54×10^4	1.0	1.0	2.32
B	10.0	14.5	2.89×10^8	1.14×10^4	.714	2.6	1.67
	55.1	55.1	4.05×10^8	1.59×10^4	1.0	1.3	1.63
C	10.0	14.5	3.52×10^8	1.39×10^4	.852	3.1	2.03
	37.5	37.5	4.13×10^8	1.62×10^4	1.0	2.6	1.99
D	10.0	14.5	1.63×10^8	$.64 \times 10^4$	.517	.6	1.99
	37.5	37.5	4.89×10^8	1.92×10^4	1.0	0.5	1.87

A - 32 & 96T, 8DP, 14.5°PA, CR_T = 2.14

B - 20 & 20T, 4DP, 20°PA, CR_T = 1.56

C - 26 & 26T, 8DP, 14.5°PA, CR_T = 1.89

D - 40 & 40T, 4DP, 20°PA, CR_T = 1.71

All gears without errors or modifications

F1 = F2 = FH1 = FH2 = 25.4mm (1.0 in.)

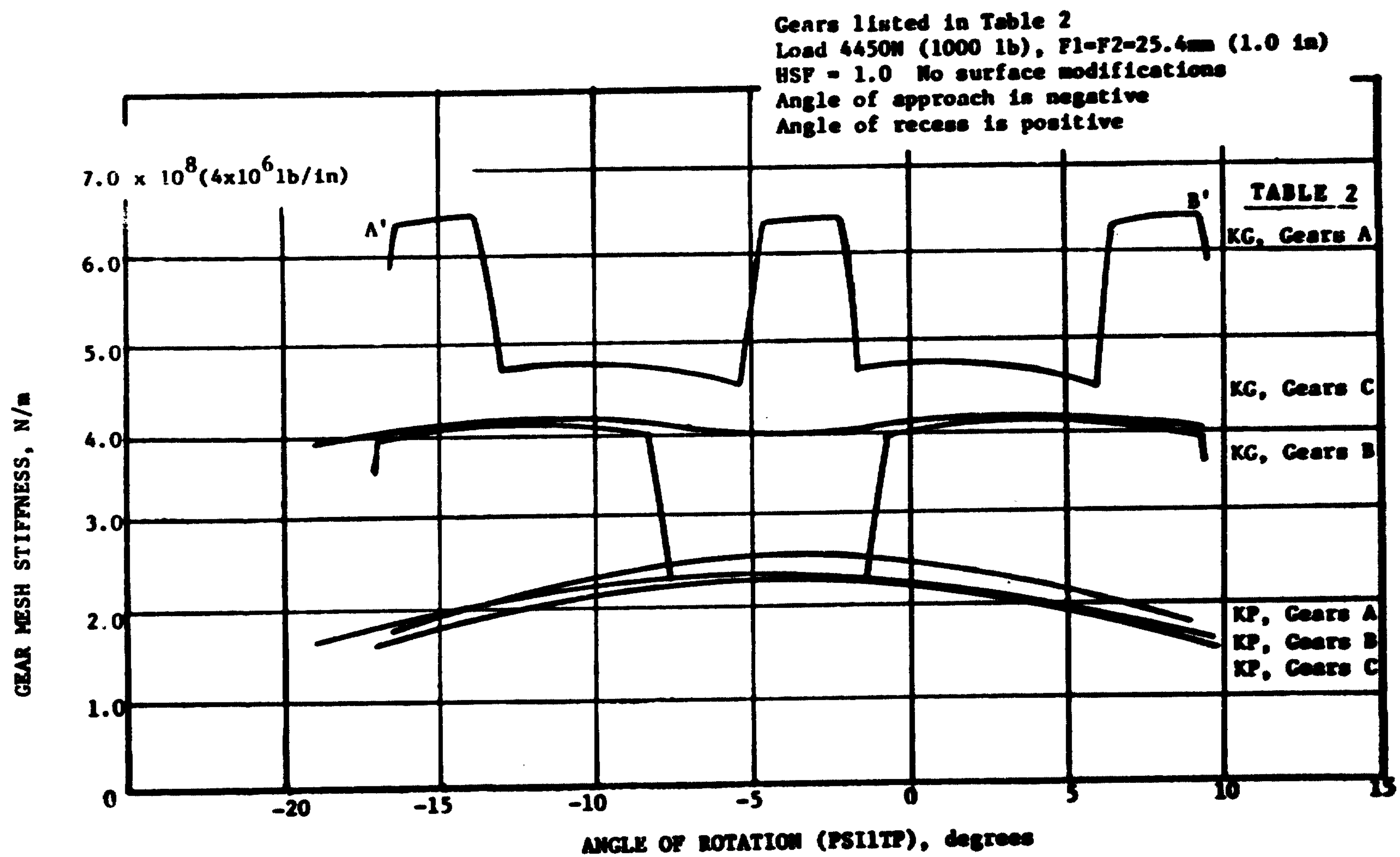

FIGURE 8 - GEAR MESH STIFFNESS FOR TYPICAL GEARS

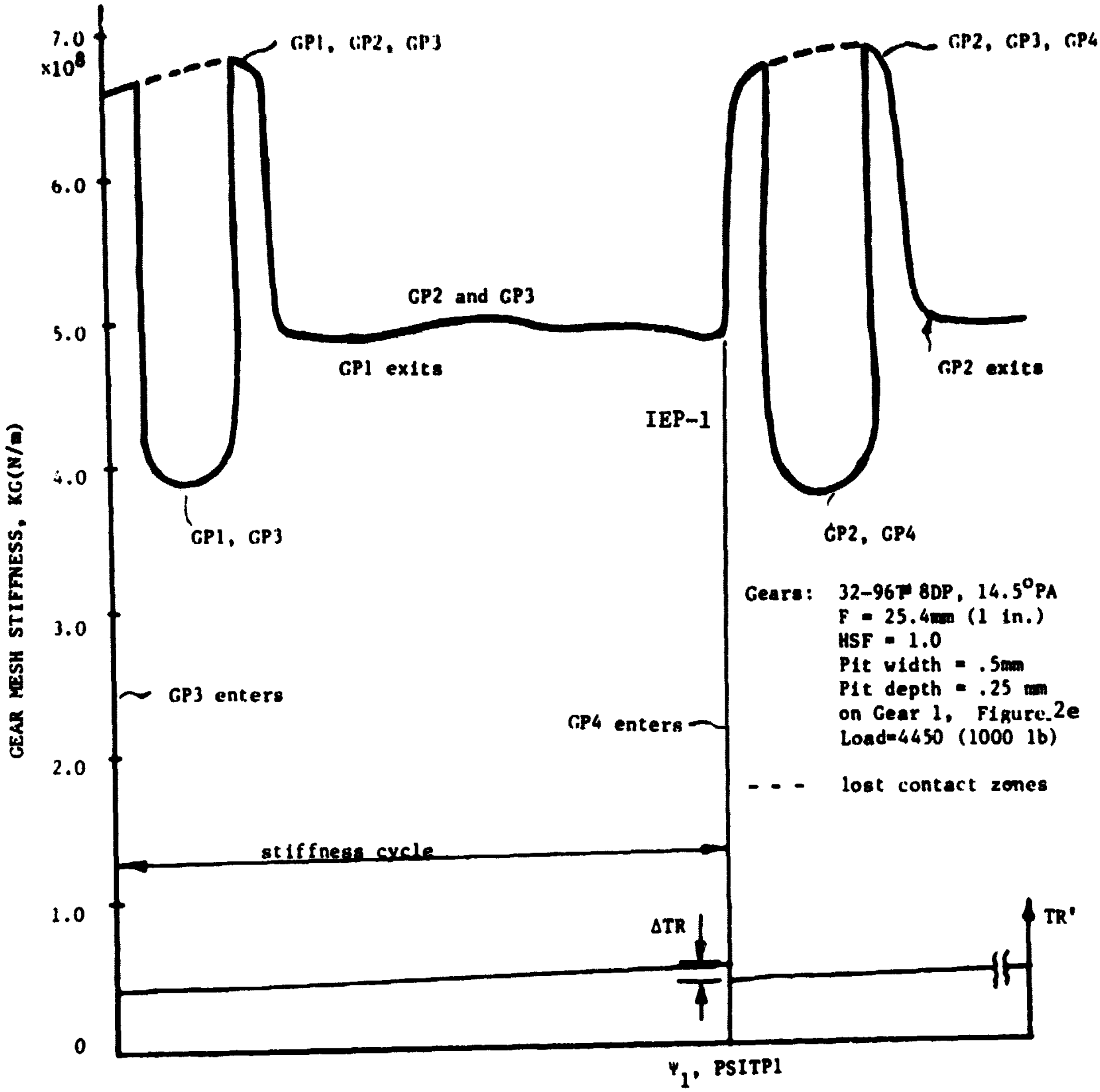

FIGURE 9 - EFFECT OF SURFACE PITS ON GEAR MESH STIFFNESS, (HCR GEARING)

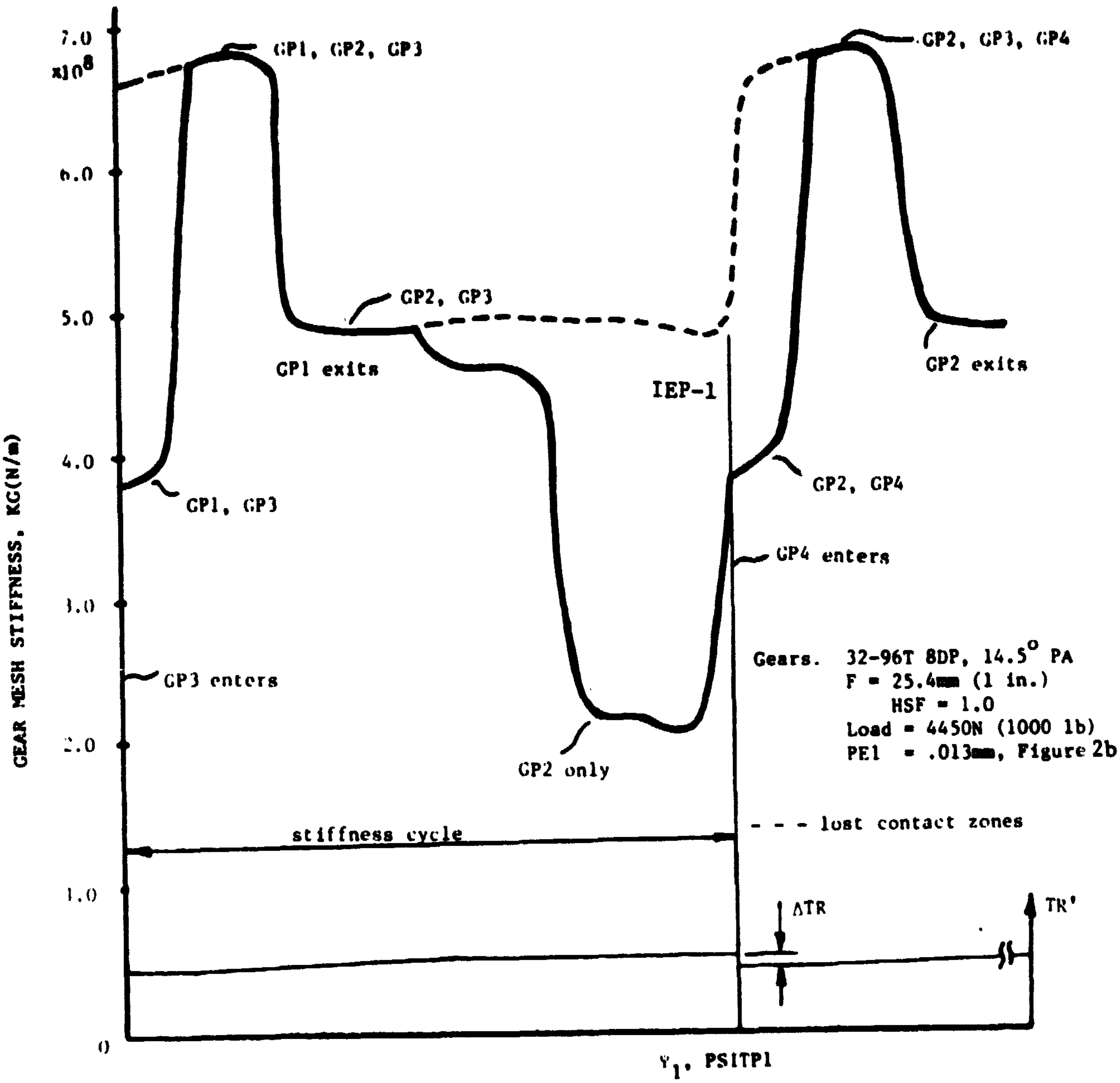

FIGURE 10 - EFFECT OF SINUSOIDAL ERROR ON GEAR MESH STIFFNESS, (HCR GEARING)

The VVMS method can also be used to investigate other error combinations acting on both gears. For example, errors shown in Figure 2b with PE1 and PE2 of .013mm are nearly self-compensating in terms of very small changes from the normal meshing stiffness function. Other profile error combinations, especially of large error magnitudes, could lead to non-operational contact ratios below 1.0 or to very frequent interruptions of the mesh stiffness function. The sinusoidal profile errors of approximately one cycle (Figures 1a, 1b) and .013mm in magnitude are probably the maximum tolerable profile errors in accurate spur gearing applications.

The gear tooth contacts due to deflections do not occur on the theoretical line of action. This results in non-involute action producing variations in the transmission ratio, ΔTR. The ΔTR can be viewed as a variation in the output torque. These variations are cyclic as illustrated in Figures 9 and 10 could reach 5% for high load and hub flexibility ranges. Some additional discussion of ΔTR is given in section on Dynamic Analysis.

The calculated results also indicated that the load distribution in a gear pair without errors remained practically the same for the considered hub flexibility ranges. Another observation could be made that for the gears with rigid hubs the attainable maximum gear mesh stiffness value remained approximately constant over a wide range of load.

It is important to indicate that the FVMS and similar methods can not directly consider the absorbtion of errors.

Dynamic Analysis

The dynamic loads are influenced by a large number of variables such as the mass moments of inertia of all elements, shaft stiffnesses, transmitted loads, gear mesh stiffness characteristics, damping in the system, amount of backlash and speed.

The presented information on dynamic loads in Figures 11, 12, and 13 is intended to show the limiting ranges and effects of some of the parameters.

Figure 11 shows the dynamic characteristics of a gear drive (Figure 7) with an errorless 32 and 96 tooth gear pair, "soft" and "stiff" shafting and gear hubs, and varying amounts of damping. The trends indicate that various gear drive systems could be designed for best performance in terms of acceptable dynamic load factors DF (equations 31 and 32) by proper selection of masses, gear mesh and shafting flexibilities, and damping.

The shaft stiffnesses and the masses of the drive and load elements in most cases will determine the lower natural frequencies of the system. The gear masses and mesh stiffness will dominate the highest natural frequency. The harmonic content of the mesh stiffness characteristics will excite at various speeds a number of natural modes. The mesh stiffness functions shown in Figures 8, 9, and 10 suggest a considerable variation of the harmonic contents for various situations. Changes in the transmission ratio TR' also refer to the same mesh stiffness cycle. The analyses tend to suggest that the main sources of excitation are the variable-variable mesh stiffness and its interruptions. The ΔTR quantity which represents variations of load torque due to non-involute action appear to be of secondary importance as a source of excitation as shown in Figure 14.

Two severe types of interruptions of the HCR mesh stiffness function resulting in a partial loss of mesh stiffness are shown in Figures 9 and 10. The effects of unabsorbed profile surface imperfections (sinusoidal and pitting) are illustrated in Figures 12 and 13 for the HCR and NCR gearing, respectively. In the presented cases, momentary gear separation can occur when DF>2. The resonant peaks are the average dynamic load factors based on the backlash between zero and .25mm.

The unabsorbed errors in the NCR situations considered caused a momentary loss of mesh stiffness resulting in high dynamic loads and gear separation over wide regions of considered speeds. In the slow speed range

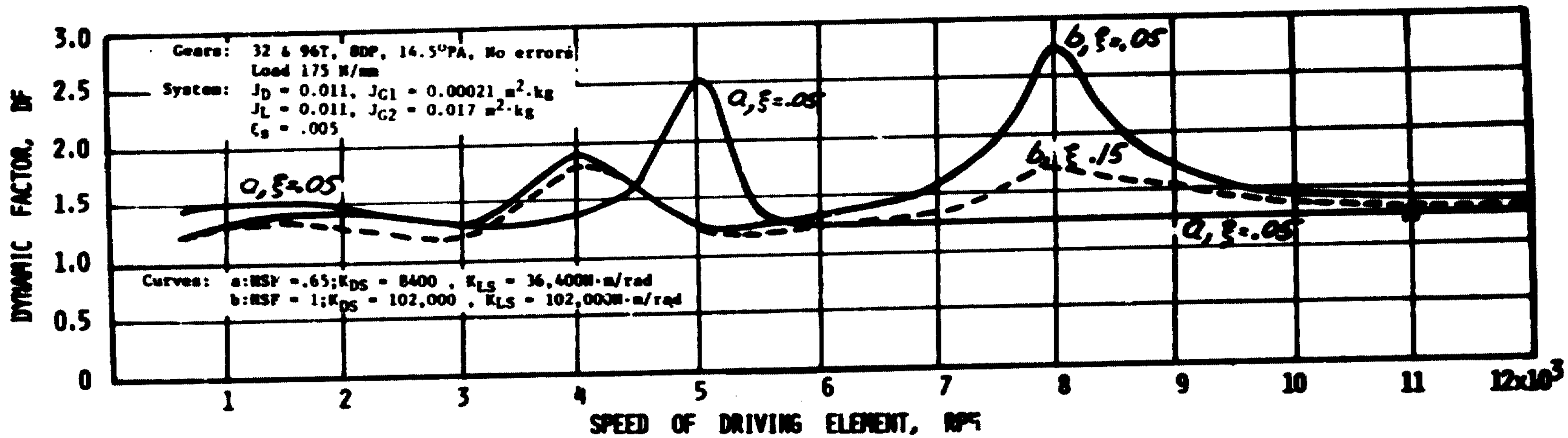

FIGURE 11 - DAMPING AND SYSTEM FLEXIBILITY EFFECTS ON DYNAMIC FACTORS FOR A CHARACTERISTIC HCR GEAR PAIR WITHOUT ERRORS

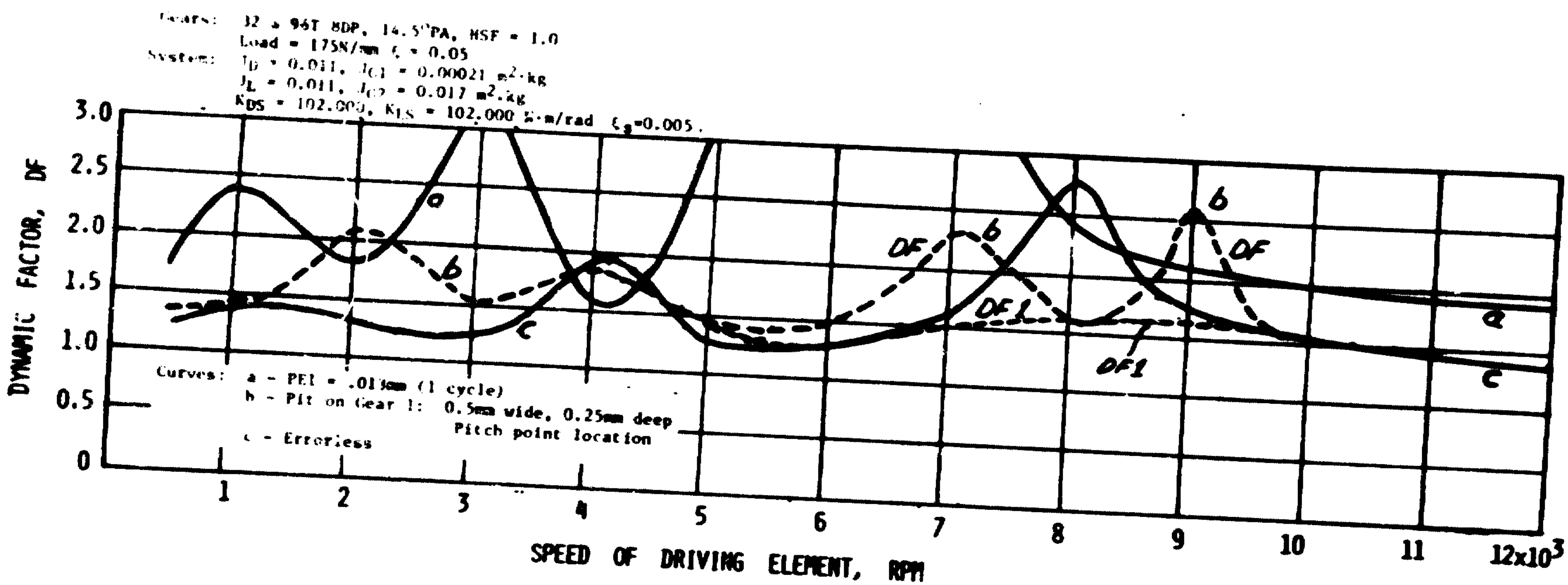

FIGURE 12 - INFLUENCE OF PROFILE FAULTS ON DYNAMIC FACTORS FOR A CHARACTERISTIC HCR GEAR PAIR

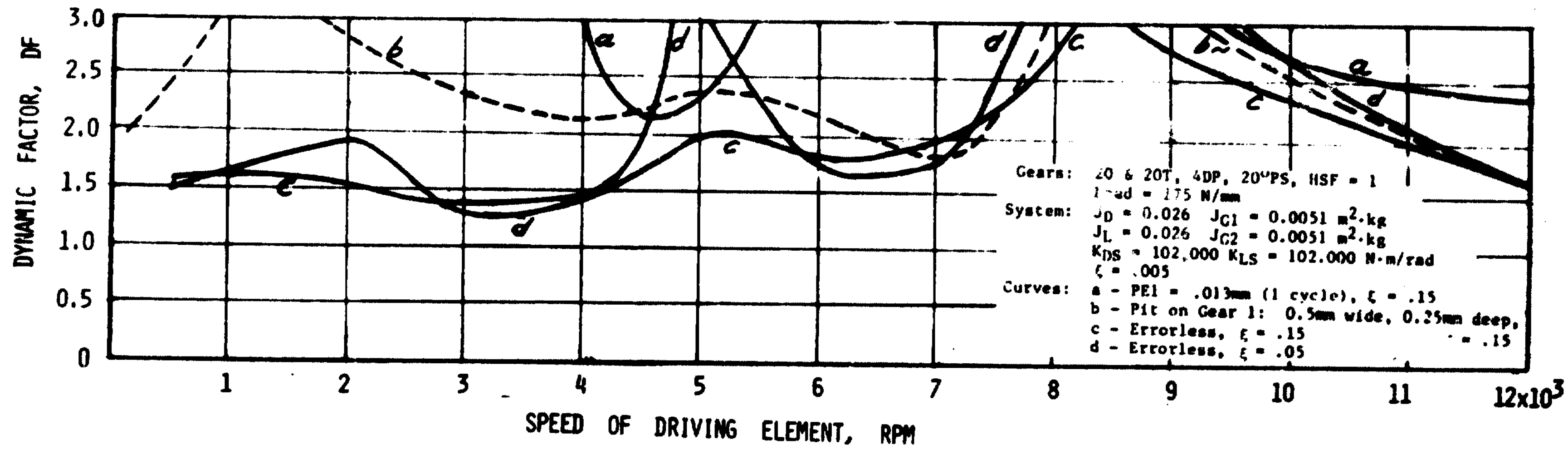

FIGURE 13 - INFLUENCE OF PROFILE FAULTS ON DYNAMIC FACTORS FOR A CHARACTERISTIC NCR GEAR PAIR

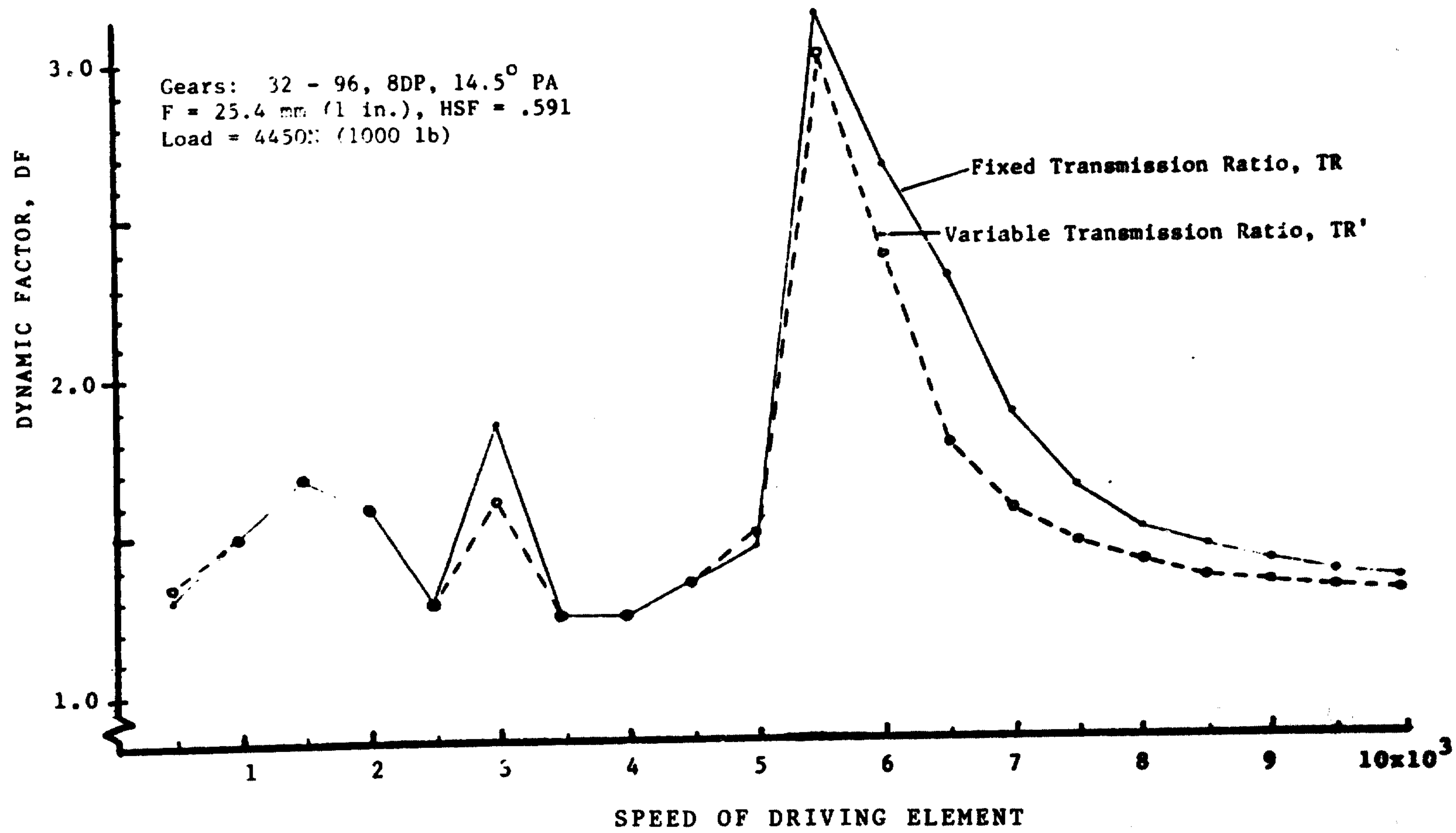

FIGURE 14 - EFFECT OF VARIABLE AND FIXED TRANSMISSION RATIOS ON DYNAMIC FORCES

there is a large zone of high dynamic load factors affected by a number of the mesh stiffness function harmonics and separation of gears. These high dynamic loads can be reduced by introducing higher damping, higher applied loads and lower HSF's. Reference [33] indicated a 300 percent increase in dynamic amplitudes caused by a zero stiffness zone due to a single tooth pit. In this study surface imperfections were assigned to all teeth for a given gear.

There is a requirement for a minimum amount of damping to prevent the Mathieu-Hill type instabilities [25, 32]. In the considered cases only for a 32 & 96 errorless gear pair, "soft" shaft, "soft" hub and zero backlash case there was a narrow instability band at approximately 11,000 rpm with $\xi = .05$ and $\xi_s = .005$. This instability was eliminated by increasing ξ to about .07. The above instability could also possibly be prevented without changing ξ by including the bearing damping. However, for limiting the number of variables the bearing damping in this study was taken to be zero. There are also additional remedies for removing or minimizing these instabilities [25, 32].

The extended modeling has the capability for analyzing the distribution of the dynamic loads, dynamic factors, load sharing, contact Hertz stress (P_H) and the contact stress-sliding velocity product (PV) for the entire meshing zone. The maximum dynamic loads, dynamic factors, maximum P_H, and maximum PV do not necessarily occur at the same or any fixed position. These quantities and their locations are dependent on the transmitted loads, speed, amount of damping, mesh stiffness function interruptions due to errors, and location of the contact points (contact point vectors and radii of curvature). Figures 14 and 15 show the range of the maximum P_H and maximum PV values corresponding to the dynamic conditions illustrated in Figures 11, 12, and 13. In general, these values were lower with higher damping and higher contact ratios.

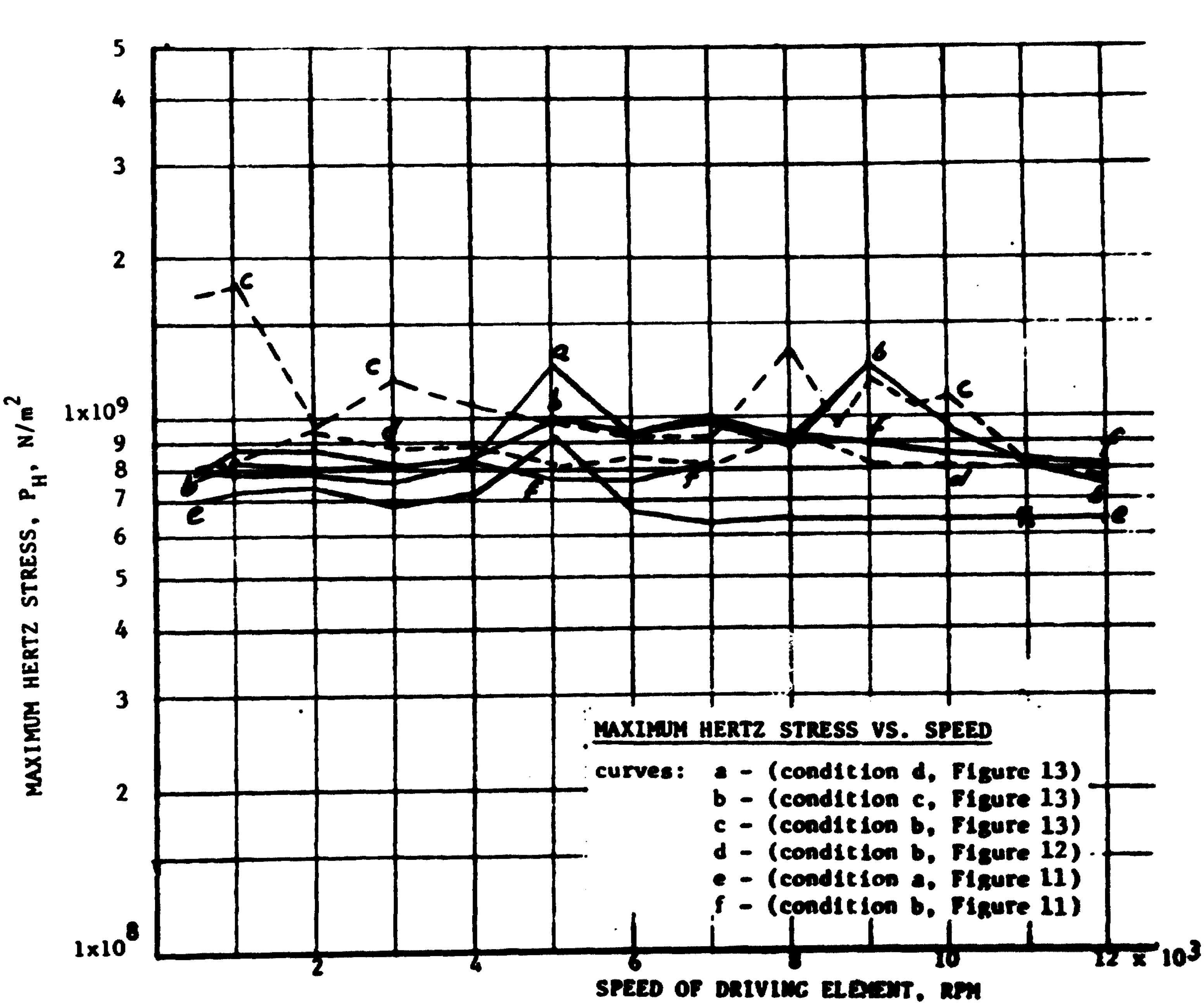

FIGURE 15 - MAXIMUM HERTZ STRESS IN CONTACT ZONE
FOR VARIOUS SPUR GEAR SITUATIONS

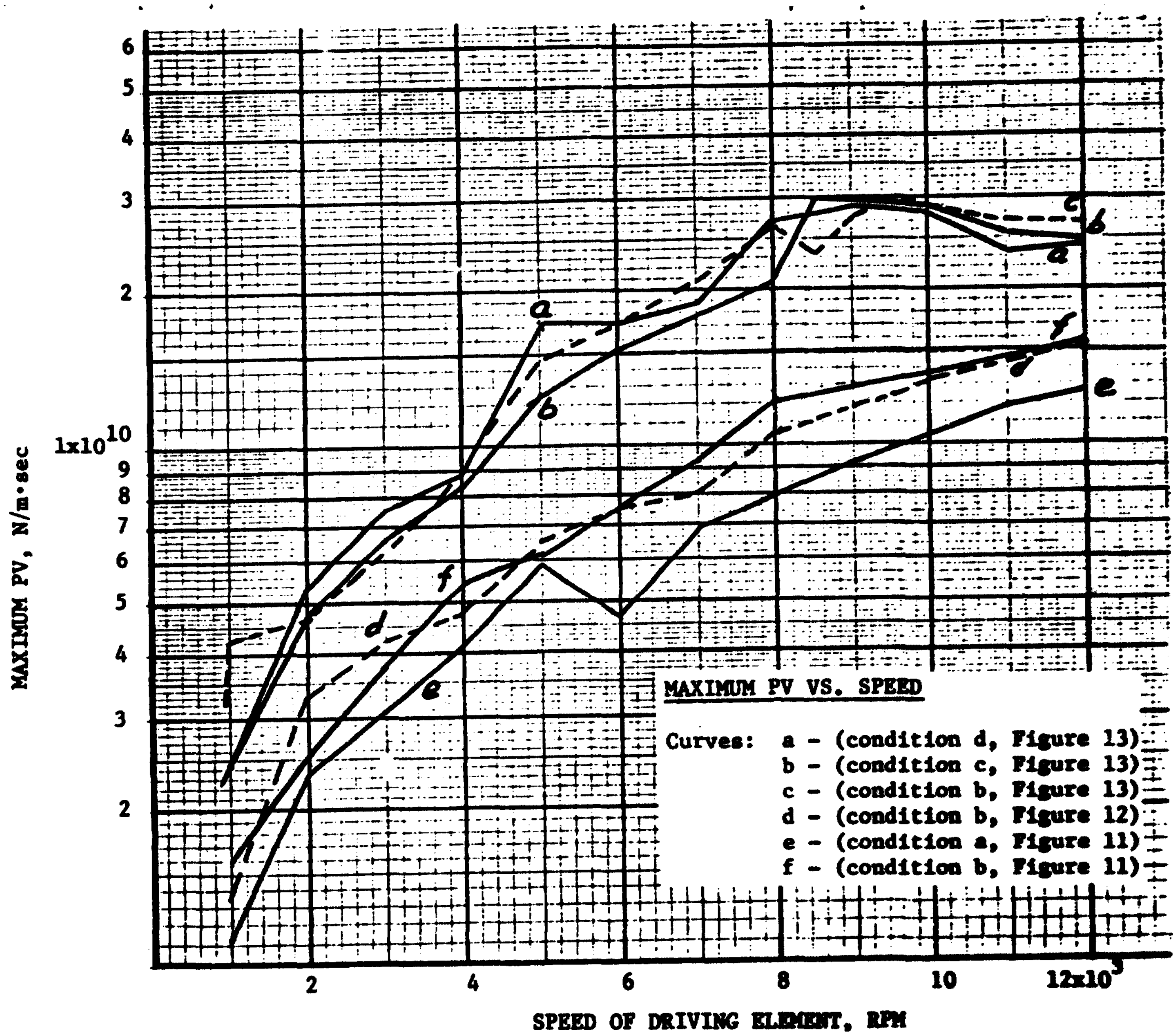

FIGURE 16 — MAXIMUM PRODUCT OF HERTZ STRESS AND SLIDING VELOCITY

The contact pressures in the approach arc using the method of instantaneous radius of curvature (eqs. 18 , 19 and 31) were, in many cases, somewhat lower in comparison with the true involute solutions. The incorporated gear tooth deflections increased the length of the contacting and curvature vectors thus causing a decrease in the contact pressures. These findings are supported by [27 and 36]. The instantaneous sliding velocities (eq. 28) on the other hand are higher than those in the true involute case.

SUMMARY

A large scale digitized extended gear modeling including the variable-variable mesh stiffness (VVMS) method was developed to analyze spur gearing in one uninterrupted sequence for both static and dynamic conditions. This approach can be used to eliminate many deficiencies of the currently used fixed-variable mesh stiffness (FVMS) modeling.

In the extended modeling an iterative procedure was used to calculate the VVMS by solving the statically indeterminate problem of multi-pair contacts, changes in contact ratio, and mesh deflections. The developed method can be used to analyze both the normal and high contact ratio gearing with a minimum number of simplifications.

The associated computer program package calculates the VVMS, the static and dynamic loads, and variations in transmission ratios, sliding velocities and the maximum contact pressures acting on the gear teeth as they move through the contact zone. The following findings were obtained for some typical single stage spur gear systems:

1. The gears and the adjacent drive and load systems can be matched for optimum performance in terms of minimum allowable dynamic loads for a wide range of operating speeds.
2. Torsionally flexible design of gear bodies/hubs/rims offers an excellent means for absorbing or minimizing the geometrical errors in mesh.
3. The gear mesh stiffness and its distribution are significantly affected by the transmitted loads and tooth profile imperfections.
4. The dynamic factors can be decreased by increasing the damping and/or contact ratio. Local damping appears to be the most efficient means for decreasing the dynamic load factors.
5. The high contact ratio (HCR) gearing has lower dynamic loads and peak Hertz stresses than the normal contact ratio (NCR) gearing.

REFERENCES

1. Buckingham, E., "Dynamic Loads on Gear Teeth," Report of Special Research Committee on the Strength of Gear Teeth, ASME, New York, 1931.

2. Walker, H., "Gear Tooth Deflections and Profile Modifications," The Engineer, Vol. 166, 1938, pp. 434-436 and Vol. 170, 1940, pp. 102-104.

3. Weber, C., "The Deformation of Loaded Gears and the Effect on Their Load-Carrying Capacity," Part I, Department of Scientific and Industrial Research, Sponsored Research (Germany) No. 3, London, 1949.

4. Tuplin, W.A., "Gear-Tooth Stresses at High Speed," Proceedings of the Institute of Mechanical Engineers, Vol. 163, 1950, p. 162.

5. Van Zandt, R.P., "Beam Strength of Spur Gears," Quarterly Transactions of the SAE, 1952, pp. 252-211.

6. Tuplin, W.A., "Dynamic Loads on Gear Teeth," Machine Design, Vol. 25, Oct. 1953, pp. 203-211.

7. Reswick, J.B., "Dynamic Loads on Spur and Helical Gear Teeth," Transactions of the ASME, Vol. 77, No. 5, July 1955, pp. 635-644.

8. Nakada, T., and Utagawa, M., "Dynamic Loads Caused by the Varying Elasticity of Mating Gear Teeth," Proceedings of the 6th Japan National Congress on Applied Mechanics, 1956, pp. 493-497.

9. Zeman, J., "Dynamische Zusatzkraefte in Zahnradetrieben," Zeitschrift des Vereines Deutscher Ingenieure, Vol. 99, 1957, pp. 244-254.

10. Harris, S.L., "Dynamic Loads on the Teeth of Spur Gears," Proceedings of the Institute of Mechanical Engineers, Vol. 172, 1958, pp. 87-112.

11. Richardson, H.H., "Static and Dynamic Load, Stress and Deflection Cycles in Spur Gearing," Sc.D. Thesis, Department of Mechanical Engineering. M.I.T., Cambridge, Mass., 1958.

12. Utagawa, M., "Dynamic Loads on Spur Gear Teeth," Bulletin of Japanese Society of Mechanical Engineers, Vol. 1, No. 4, 1958, pp. 397-403.

13. Bohm, F., "Drehschwingungen von Zahnradgetricben," Oesterreichisches Ingenieurarchiv, Col. 13, No. 2, 1959, pp. 82-103.

14. Cloutier, L.J., "Dynamic Loads on Precision Spur Gear Teeth According to the Theory of Variable Elasticity," Laval University,

15. Utagawa, M. and Harada, T., "Dynamic Loads on Spur Gear Teeth Having Pitch Errors at High Speed," Bulletin of JSME, Vol. 5, No. 18, 1962, pp. 374-381.

16. Kasuba, R., "An Analytical and Experimental Study of Dynamic Loads on Spur Gear Teeth," Ph.D, Thesis, Mechanical Engineering Department, University of Illinois, June, 1962.

17. Attia, A.Y., "Deflection of Spur Gear Teeth Cut in Thin Rims," ASME paper 63-WA-14, 1963.

18. Bollinger, J.G., "Darstellung des Dynamicschen Verhaltens Eines Nichlinearen Zahradgetriebesystems Auf Dem Analogrechner," Industrie-Anzeiger, June 7, 1963, pp. 961-966.

19. Gregory, R.W., Harris, S.L., and Munro, R.G., "Dynamic Behavior of Spur Gears," Proceedings of the Institute of Mechanical Engineers, London, Vol. 178, Part 1, No. 8, 1963, pp. 207-218.

20. Bollinger, J.G., and Bosch, M., "Ursachen and Auswirkungen Dynamischer Zahnkraefte in Stirnradgetrieben," Industrie-Anzeiger, No. 19, March 6, 1964, pp. 319-326.

21. Cowie, A., "The Kinematics of Contacting Surfaces," Trans. ASME, Journal of Engineering for Industry, August, 1968, pp. 450-454.

22. Hahn, F.W., "Study of Instantaneous Load to Which Gear Teeth are Subjected," Ph.D. Thesis, Mechanical Engineering Department, University of Illinois, Urbana, Ill., 1969.

23. Seireg, A., and Houser, D.R., "Evaluation of Dynamic Factors for Spur and Helical Gears," ASME Paper 69-WA/DE-9, 1969.

24. Niemann, G., and Baethge, J., "Drehwegfehler, Zahnfederharte und Gerausch bei Stirnradern," Zeitschrift des Vereines Deutscher Ingenieure, Vol. 112, No. 4, 1970, pp. 205-214.

25. Kasuba, R., "Dynamic Loads on Spur Gear Teeth by Analog Computation," ASME Paper 71-DE-26, 1971.

26. Franks, R.G.E., "Modeling and Simulation in Chemical Engineering," John Wiley & Sons, Inc., 1972.

27. Ichimaru, K. and Hirano, F., "Dynamic Behavior of Heavy-Loaded Spur Gears,' ASME Paper 72-PTG-14, 1972.

28. Wang, S.M., "Analysis of Non-Linear Transient Motion of a Geared Torsional System," ASME Paper 72-PTG-8, Presented at the International Symposium on Gearing and Transmissions, San Francisco, Calif., Oct. 1972.

29. Chakraborty, J., and Hunashikati, H.G., "Determination of the Combined Mesh Stiffness of a Spur Gear Pair Under Load," ASME Paper, 74-DET-39, 1974.

30. Seager, D.L., "Separation of Gear Teeth in Approach and Recess, and the Likelihood of Corner Contact," ASLE Transactions, Vol. 19, No. 2, 1975, pp. 164-170.

31. Staph, H.E., "A Parametric Analysis of High-Contact-Ratio Spur Gears," ASLE Transactions, Vol. 19, 3, 1976, pp. 201-215.

32. Tordion, G.V. and Gauvin, R., "Dynamic Stability of a Two-Stage Gear Train Under the Influence of Variable Meshing Stiffnesses," Trans. ASME, Journal of Engineering for Industry, August 1977, pp. 785-791.

33. Drosjack, M.J. and Houser, D.R., "An Experimental and Theoretical Study of the Effects of Simulated Pitch Line Pitting on the Vibration of a Geared System," ASME Paper 77-DET-123.

34. Cornell, R.W. and Westervelt, W.W., "Dynamic Tooth Loads and Stressing for High Contact Ratio Spur Gears," ASME Paper 77-DET-101.

35. Remmers, E.P., "Gear Mesh Excitation Spectra for Arbitrary Tooth Spacing Errors, Load and Design Contact Ratio," Trans. ASME, Journal of Mechanical Design, October 1978, pp. 715-722.

36. Krishnamurthy, R., "Influence of Addendum Correction on the Surface-Durability of Gears," ASME Paper 78-DET-65.

37. Wilson, E. L.; Taylor, R. L.; Doherty, W. P.; and Ghaboussi, J., Incompatible Displacement Models, Office of Naval Research Symposium, Numerical and Computer Methods in Structural Mechanics, September, 1971.

38. Lestingi, J.; Prachuktam, S., A Blocking Technique for Large-Scale Structural Analysis, Computers and Structure, 1973, 3, 669-714.

APPENDIX 1

CONTACT POINT SEARCH METHOD

Since the location of the contact point is not constant and directly affects the amount of tooth deflection and vice-versa, it was necessary to develop a search technique that was able to determine accurately where contact occurred. More importantly, because of gear errors, it was necessary to be able to predict where contact would not happen for a given angular position.

Figures A. 1-1 and A. 1-2 illustrate the search technique for the contacting points. In the search stage, the digitized points include the profile errors, modifications and appropriate deformations. Each gear tooth profile was described by one to tow hundred digitized points. In the majority of practical cases, this would translate into .13 to .25 mm (.005 to .01 in.) radial intervals between two adjacent digitized points.

Although basically the same, there are three distinct serach procedures in the SLOWM subroutine. These establish:

1. Location of first contact in the meshing arc and its angular position (Position 1);
2. Location of the contact point on the tooth profile as the tooth traverses through the contact zone (Positions 2 through 49);
3. Location of the final contact in the meshing arc and its angular position (Position 50).

Each procedure makes at least two checks in the distance between the gear teeth to establish whether or not contact occurs at that particular angular gear tooth position.

For example, for establishing the actual loaded initial point of the meshing arc, Point A', Figure 6, the gears were counter rotated to be outside the theoretical initial contact point equation A. 1-1. Then the loaded gears are rotated by subtracting small increments (DELTA x NLIM x DPELT) from P1SL in the direction of actual rotation and comparing the gaps between the approaching loaded teeth.

$$\text{P1SL} = \text{PSS1SL} + \text{DELTA} \times (\text{NLIM} \times \text{DELT}) \qquad \text{(A. 1-1)}$$

P1SL	-	starting search angle
PSS1SL	-	theoretical starting angle for meshing arc
DELTA	-	angular increment in the contact zone
NLIM	-	arbitrary number such that NLIM x DDELT = any integer greater than 5
DELT	-	1/N, where N is any interger greater than one

The product (NLIM x DELT) determines how many angular increments,
DELTA, the gear teeth are set back. The product (DELTA x DELT)
DELTA, the gear teeth are set back. The product (DELTA x DELT) will later determine how much the gear teeth are incremented in the search for the initial contact. Generally, for light loaded, fairly rigid, non-modified gear teeth, (NLIM x DELT) can be in the range of 5 to 8. NLIM should be larger for systems with modified teeth or relatively soft teeth or hubs. Smaller values of DELT will give more accurate results as to the location of the initial contact. Both large values of NLIM and small values of DDELT result in more interations, more accurate results, but require more computer time.

Each gear tooth is described in space by the U1 (J), V1 (J) and U2 (L), V2 (L) coordinates. In searching for the initial point of contact, the search is started with the tip of the driven gear, point L = 1 by examining the gaps between the tooth profiles of both gears.

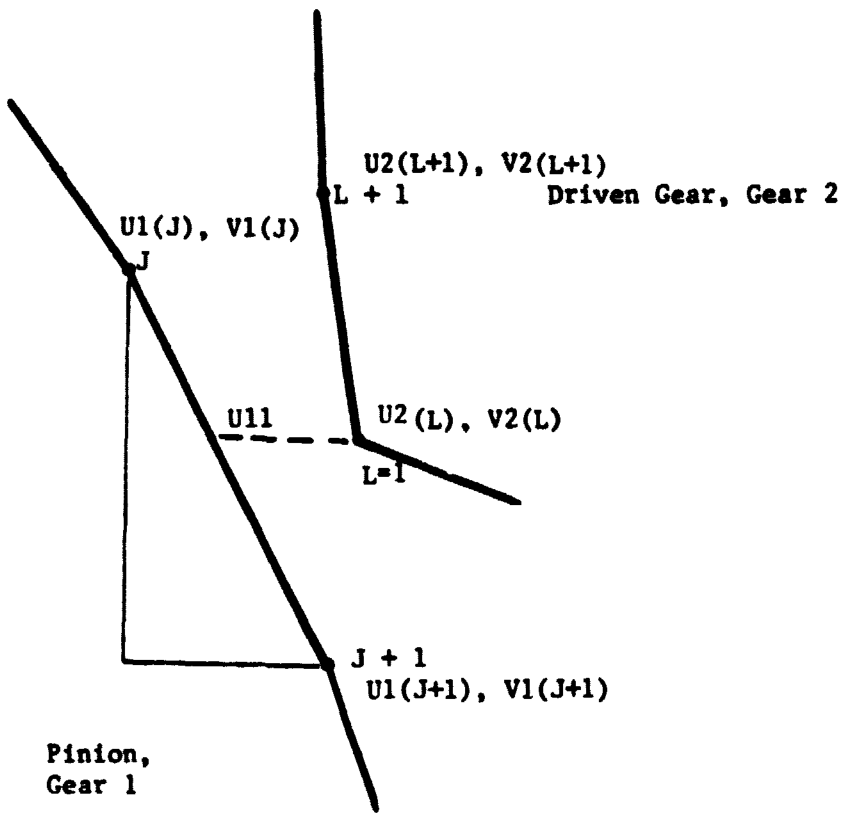

Figure A. 1-1 SEARCH FOR INITIAL MESH ARC CONTACT

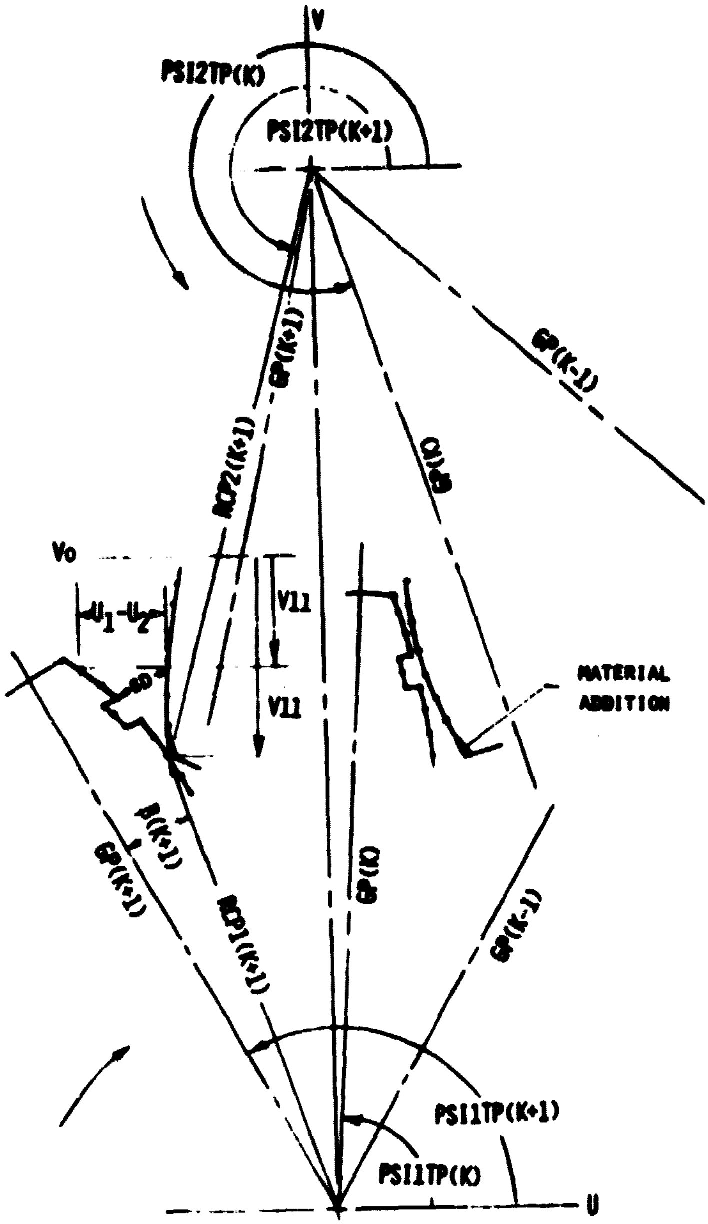

FIGURE A. 1-2 - CONTACT POINT SEARCH METHOD - I th MESH ARC POSITION

For any

$$V1\ (J) \geq V2\ (L) > V1(J+1)$$

U11 can be calculated by similar triangles from Figure A. 1-1 to be

$$U11 = \frac{V2(L) - V1(J)}{V1(J+1) - V1(J)} \times \left[U1(J+1) - U1(J)\right] + U1(J) \qquad \text{(A. 1-2)}$$

If, $U11 > U2\ (L)$

and

$$(U11 - U2\ (L)) \leq 0.00010 \text{ in. or } .0025 \text{ mm.}, \qquad \text{(A. 1-3)}$$

a permissible amount of jamming or overlap has occurred; contact is established and the rotational angles for this position defined (Point A', Figure 6).

If the condition (A. 1-3) was not satisfied by any of the digitized profile points, then the same points were reanalyzed for the "minimum contact/gap" condition (A. 1-4)

$$\text{abs}\left|U11 - U2\ (L)\right| < (.00001 \text{ in. or } .00025 \text{ mm.}) \qquad \text{(A. 1-4)}$$

Using this second test, a contact was declared if the condition (A. 1-4) was satisfied.

There is no contact, if neither of the above two conditions are met. In this case, L is incremented by one, and the process repeated. If all the values of L in the search region have been exhausted and no contact found, then the angular position of the gears is advanced by an amount (DELTA x DELT), and the search process repeated with L = 1, etc.

The technique for finding the final contact point is similar to the one just described. This time, the search is initiated with the tip of the pinion point J, J = 1.

After the initial and final contact positions are found, the contact positions for the remaining 48 meshing arc positions are determined.

For any i^{th} mesh arc angular position, the contact points or absence of them are established by analyzing from 20 to 40 digitized points for each gear pair profiles in the approach or estimated contact zones. This is accomplished by incrementing the vertical search distance V11 (common for each pair profiles) and comparing the corresponding horizontal "U" distances between the profiles by means of the previously discussed conditions A. 1-3 and A. 1-4.

The allowance (A. 1-4) was introduced to account for small deviations in the profile digitizing and other numerical processes. It should be noted that the longer horizontal rather than the shorter perpendicular distances were analyzed thus increasing the probability of contact. The (A. 1-3) and (A. 1-4) conditions were established by investigating a large number of gears for the known theoretical "contact" and "no contact" points. For the situations failing both tests, there was an unacceptable gap or no contact. In the search method the initial or the highest point for the pair in the i^{th} angular mesh arc position.

This process was repeated for all tooth pairs expected to be in contact in the i^{th} mesh arc position. Referring to Figure A. 1-1, contact was established at point P for the gear pair GP (k+1). There is no contact for GP (k). Next, the gears are advanced to a new angular position, and the process is repeated for the entire loaded mesh arc.

APPENDIX 2

DEFLECTION AT POINT OF CONTACT

Numerical integration of digitized gear tooth slices (Figure A. 2-1) was used to obtain the bending (δ_M), shear (δ_S) and normal force (δ_N) deflections used in equations 3 and 4. These calculation were performed in the DEFL subroutine. The circumferential deformation of the gear hub and deformation of the adjacent part of the gear body were reflected to the contacting point as (δ_R) and (δ_B) deflections, respectively.

The methods for calculating the δ_B and the localized hertzian deflection δ_H are amply described in [3, 17, and 29]. The δ_{R1}, δ_B and δ_H deflections were calculated in the SLOWM subroutine.

The δ_R deflections cannot be easily defined. Following [17], these deflections can be approximated for Gears 1 and 2 as shown below.

$$\delta_{R1}(k)_i = \frac{Q(k)i\ (RCP1(k)i)^2 \cos\alpha\ B1}{4\ \pi\ G1(FH1)} \left[\left(\frac{1}{RH1_f}\right)^2 - \left(\frac{1}{RH1_o}\right)^2 \right] \quad \text{(A. 2-1)}$$

where

$Q(k)_i$ = load along the instantaneous line of action at the contact point, k^{th} pair.

RCP1(k)= radius to the contacting point, Gear 1, k^{th} pair

FH1 = hub face, Gear 1

$RH1_0$ = outside hub/rim radius, Gear 1

$RH1_f$ = effective radius of circumferential hub fixity, Gear 1

G1 = torsional modulus of elasticity, Gear 1

Similarly, for Gear 2

$$\delta_{R2}(k)_i = \frac{Q(k)i\ (RCP2(k)i)^2 \cos\alpha\ B2}{4\ \pi\ G2(FH2)} \left[\left(\frac{1}{RH2_f}\right)^2 - \left(\frac{1}{RH2_o}\right)^2 \right] \quad \text{(A.2-2)}$$

In many cases, it could be assumed that $RH1_0$ and $RH2_0$ will be approximately equal to RRC1 and RRC2, respectively. The radius of circumferential fixity RH_f for individual hubs cannot be as readily assumed. RH_f will depend on the hub disk face width (HF), hub web thickness (HW), type of gear mounting, shaft size, cutouts, etc.

The torsionally rigid hubs can be theoretically obtained when the radius of circumferential or torsional fixity will coincide with the root circle resulting in $\delta_R = 0$. The opposite case can be visualized with the thin hubs being fixed to small shafts. In general, an increase in the hub/rim flexibility will increase the total deflection of the tooth and thus will decrease the gear mesh stiffness. The hub stiffness factor (HSF, eq. A2-3) will be used to indicate a degree of influence of the hub flexibility on the overall gear mesh stiffness.

$$HSF = \frac{KGmax}{KG^{*}max} \qquad \text{(A. 2-3)}$$

where

KG^{*}_{max} = maximum mesh stiffness with torsionally rigid hubs

KG_{max} = maximum mesh stiffness with designated hubs

A combination of rigid hubs will be identified by HSF = 1.

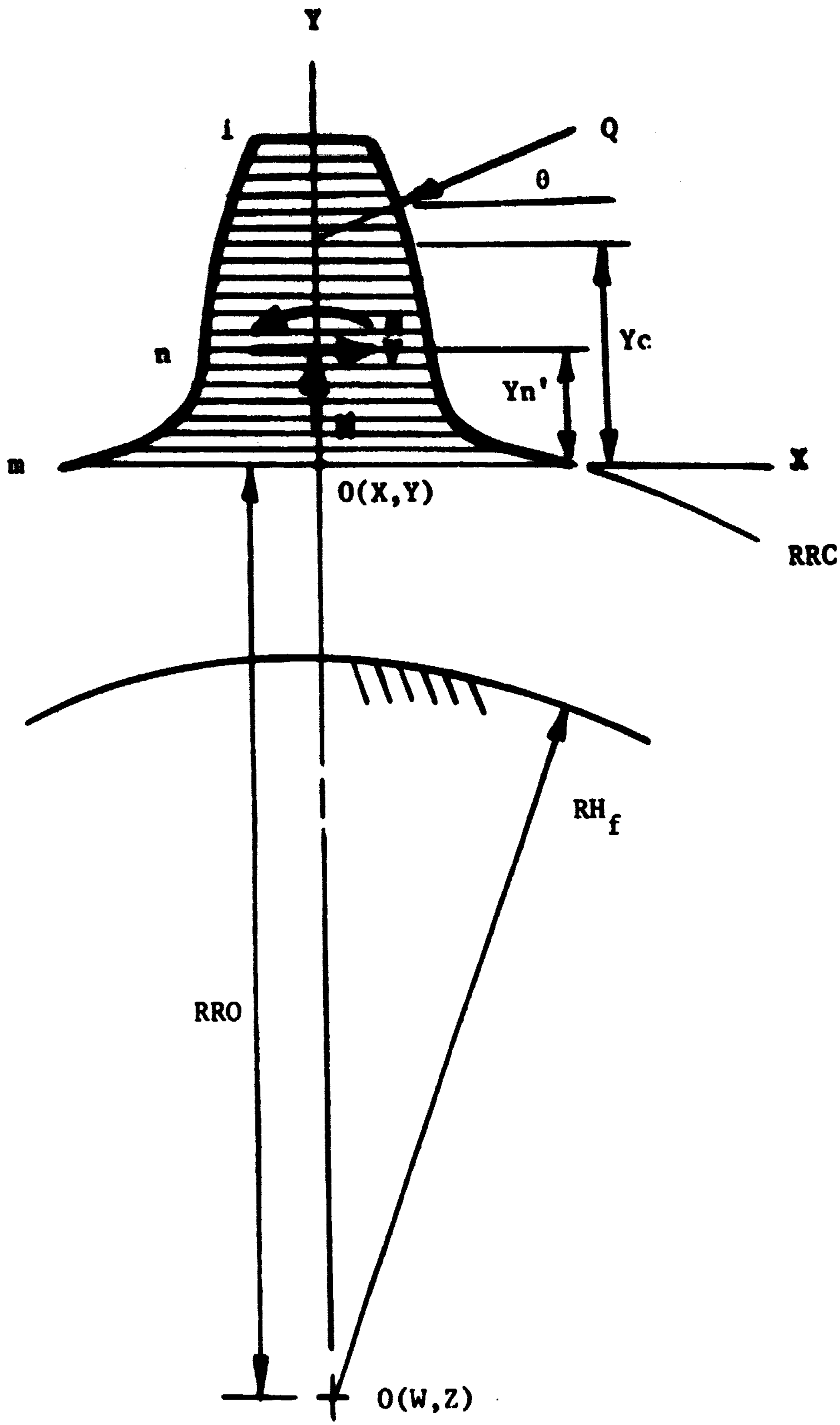

FIGURE A. 2-1 - GEAR TOOTH BENDING, SHEAR AND NORMAL DEFLECTION MODEL

APPENDIX 3

PROFILE DIGITIZING SUBROUTINE-MOD

The MOD subroutine is used for digitizing the spur gear tooth profiles. Both standard and non-standard gear forms can be digitized. This subroutine can accomodate the parabolic and straight line modifications of the tip and root zones, sinusoidal profile errors and surface pits as shown in Figures 2 and 3 and discussed in the static analysis section.

The main parameters needed for describing standard and/or non-standard profiles for each gear are:

DP	-	diametral pitch (English input only)
M	-	gear module (metric module only)
PHID	-	pressure angle, degrees
TG	-	number of gear teeth
AD	-	addendum
WD	-	working depth
GRRF	-	generating fillet radius of basic rack
PATM	-	parabolic tip modification
STTM	-	straight line tip modification
RATM	-	roll angle of tip modification, degrees
PABM	-	parabolic bottom modification
STBM	-	straight line bottom modification
RABM	-	roll angle of bottom modification, degrees
PER	-	amplitude of sinusoidal error
PAP	-	phase angle of sinusoidal error
CYC	-	number of cycles of sinusoidal errors
IPIT	-	profile coordinate points over which pit occurs
DEEP	-	depth of pit

Other symbols used in the computerized profile equation in the MOD subroutine are defined in the Program Listing, Appendix 8.

A number of figures are included in this Appendix to show the graphical relationship of the principal profile-defining symbols.

Figure A.3-1 shows a basic standard involute tooth profile. Figures A.3-2 through A.3-4 depict several modifications of a standard involute tooth profile. The fillet radius RF1 for gear 1 is described as

```
RF1 = .7*(GRRF1+WD1-AD1-GRRF1**2)/
         (.5*PD1*WD1-AD1*GRRF1)
```
(A.3-1)

and, similarly, for Gear 2. In equation A.3-1, PD1 is the pitch diameter. Other symbols are defined at the beginning of this Appendix.

The sinusoidal profile error PE1 for Gear 1 was defined as

```
PE1(J) = PER1*SIN((*RATI1-RA1(J))
         *CYC1/RATIP1)+PAP1)                    (A.3-2)
```

and, similary, for Gear 2.

In equation A.3-2 the phase angle PAP1 refers to the peak of the error from the pitch point. The sinusoidal error covers the region between the tip and root profile modifications as shown in Figure A.3-3.

A straight line tip and root profile modification model in terms is shown in Figure A.3-3. A similar model was used for Gear 2 as well as for the parabolic tip and bottom modifications.

By introducing negative profile modification in the root zone as shown in Figure A.3-4 several types of undercuts can be developed.

The program has several protective features. For example, in the case of very severe profile modifications the contact ratio could fall below 1 or there could be an interference, then a special notice will be printed and the program execution stopped.

Case: RBC ≥ RTF
RBC ≥ RRC
RLM ≥ RTF

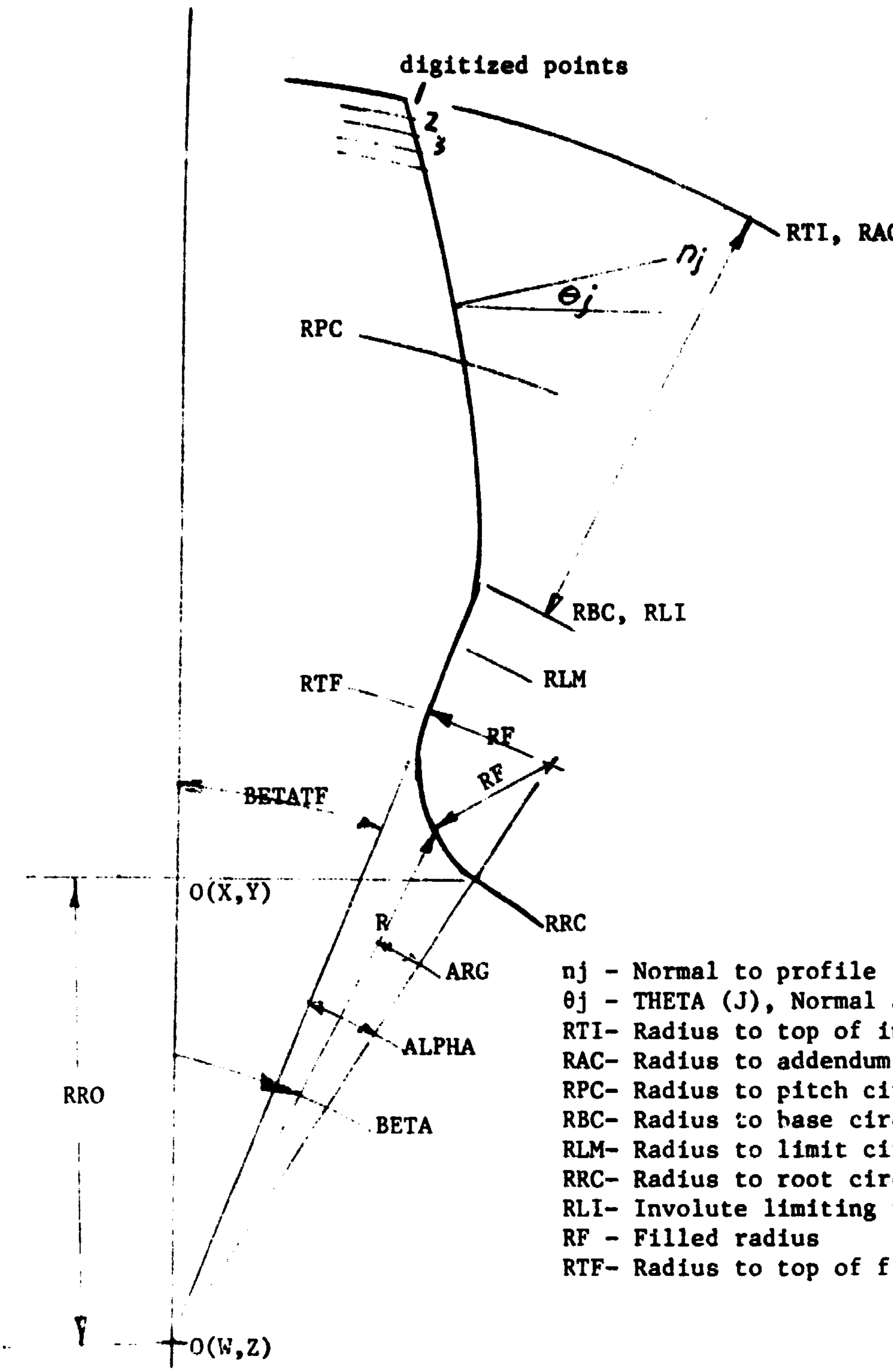

nj - Normal to profile
θj - THETA (J), Normal angle
RTI- Radius to top of involute
RAC- Radius to addendum circle
RPC- Radius to pitch circle
RBC- Radius to base circle
RLM- Radius to limit circle
RRC- Radius to root circle
RLI- Involute limiting radius
RF - Filled radius
RTF- Radius to top of fillet

Figure A. 3-1 PRINCIPAL SYMBOLS - STANDARD INVOLUTE TOOTH PROFILE

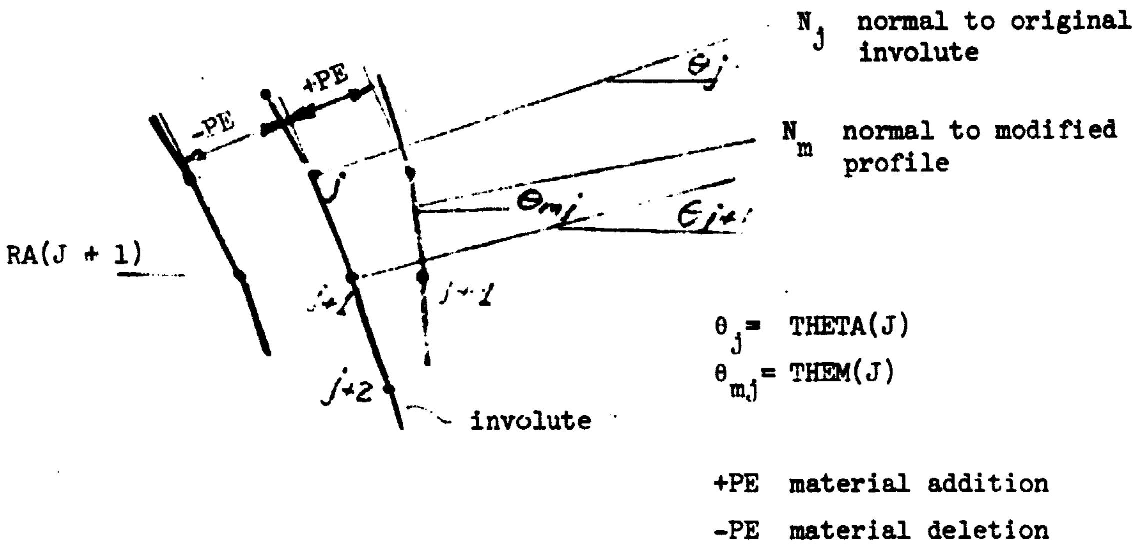

Figure A.3-2 MATERIAL ADDITION OR SUBTRACTION FOR A TYPICAL PROFILE LOCATION

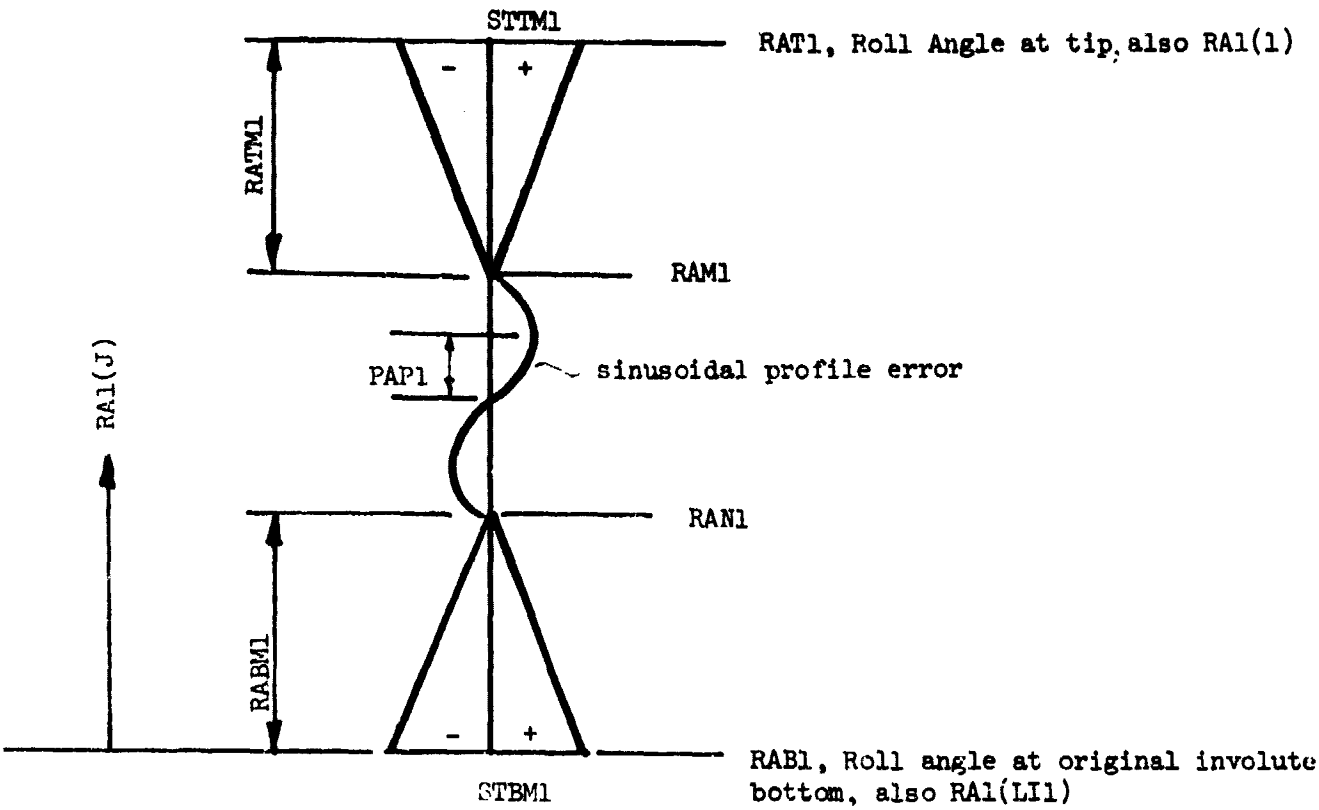

Figure A.3-3 STRAIGHT LINE MODIFICATION OF PROFILE AT TIP AND ROOT

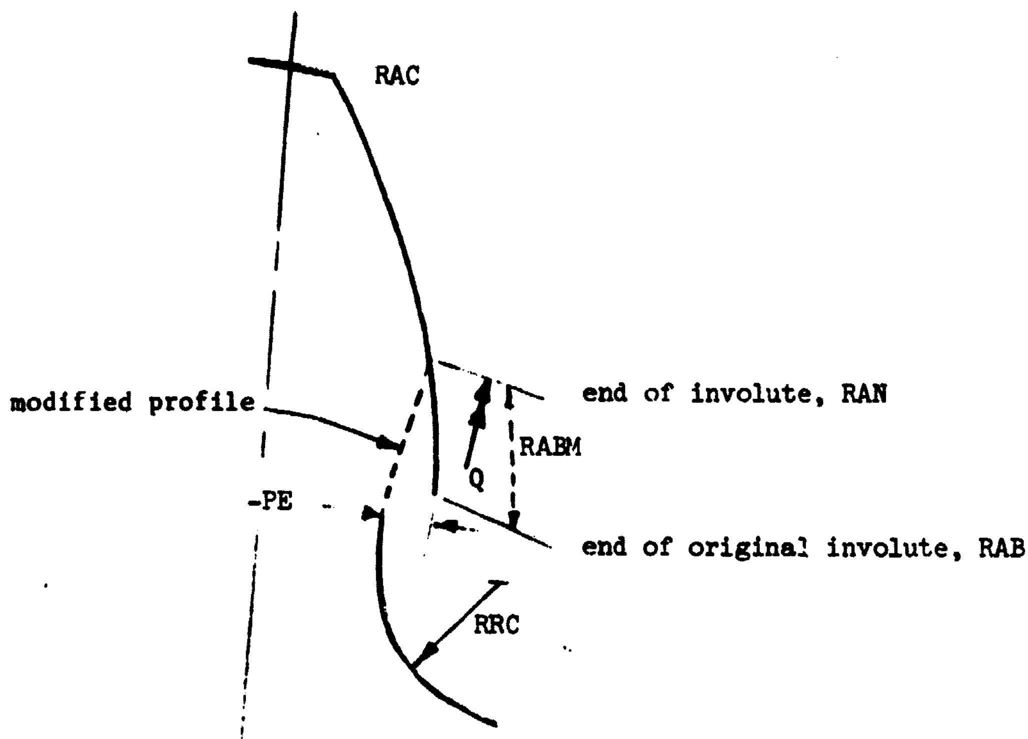

Figure A.3-4 TOOTH ROOT MODIFICATION-MATERIAL REMOVAL

APPENDIX 4

VIBS SUBROUTINE

The VIBS subroutine based on a Jacobi interation technique is used to determine the eigen-values of the gear train from which the length of the numerical integration as well as the integration time step were determined. Using the undamped version of the model shown in Figure 7, the equations of motion expressed in matrix form become

$$[J]\{\ddot{\Psi}\} + [K]\{\Psi\} = \{0\} \qquad \text{(A. 4-1)}$$

The inertia matrix (J) is

$$\begin{bmatrix} {}^{*}DJD & 0 & 0 & 0 \\ 0 & DJG1 & 0 & 0 \\ 0 & 0 & DJG2 & 0 \\ 0 & 0 & 0 & DJL \end{bmatrix} \qquad \text{(A. 4-2)}$$

The stiffness matrix (K) is

$$\begin{bmatrix} DKDS & -DKDS & 0 & 0 \\ -DKDS & DKDS + DKAVG \times (DRBC1)^2 & -(DKAVG \times DRBC1 \times DRBC2) & 0 \\ 0 & -(DKAVG \times DRBC1 \times DRBC2) & DKDS + DKAVG \times (DRBC2)^2 & -DKLS \\ 0 & 0 & -DKLS & DKLS \end{bmatrix} \qquad \text{(A. 4-3)}$$

DKAVG is the average gear mesh stiffness. It is determined by summing up the stiffness function over one cycle and dividing by the number of positions in the cycle,

$$DKAVG = \frac{1}{n}\sum_{i=0}^{n} KGP_i \quad ; \qquad n = IEP - 1 \qquad \text{(A. 4-4)}$$

* Shown in double precision format

In equation A. 4-4:

KGP_i - gear mesh stiffness at the i^{th} position of the mesh arc.

n = number of the mesh arc positions in one stiffness cycle

IEP = start position index for new stiffness cycle (Figure 9)

Having defined the constituent parts of the above matrix equation, the VIZS routine is called to determine the natural frequencies and the modal shapes. The natural frequencies were used to determine the time period over which the system is to be evaluated and the length of the integration time steps. It was assumed that the startup transients would decay within a time period equivalent to five times the longest natural period. This time period plus the time required for 2 or 3 additional cycles, depending on the contact ratio, constitutes the total time span TTOTAL in the integration portion of the FAST routine. The integration time step DT is taken either as one tenth of the shortest system natural period or one percent of the stiffness period with CR <2 (two percent for CR > 2), whichever is smaller.

APPENDIX 5

PROGRAM INTEGRATION

The Fast routine has been developed to analyze a four mass, mathematical model of a geared torsional system shown in Figure 7. This model also includes the gear mesh stiffness variations; damping in the shafts, gears and bearings; non-involute action effects and loss of gear tooth contact due to dynamic conditions.

The Fast routine (Figure 1), which constitutes the dynamic portion of the entire program, consists of the natural frequency subroutine VIBS, the integrating subroutines RKUTTA and MORERK, and the storing and plotting subroutines STORE and XTPLOT, respectively.

The differential equations of motion were programmed in the double precision on IBM 370/158 computer. The equations of motion (equations 19 - 22) are shown in the computerized symbols as equations A.5-1 through A.5-4. All variables used in these equations were declared double precision. This also includes the symbols preceded with letter D.

```
PSDPDD  = (-DCDS*((PSDPD+DOMGAD)-(PSIPD+DOMGA1))
           -DCBD*(PSDPD+DOMGAD)-DCB1*(PS1PD*DOMGA1)          (A.5-1)
           -DKDS*((PSDP+DT*DOMGAD)-(PS1P+DT*DOMGA1))+ TD)/DJD

PS1PDD = (-DCDS*((PS1PD+DOMGA1)-(PSDPD+DOMGAD))
          -DKDS*((PS1P+DT*DOMGA1)-(PSDP+DT*DOMGAD))          (A.5-2)
          -CGP*(DRBC1*(PS1PD+DOMGA1)-(DRBCN*PS2PD + DRBC2*DOMGA2))
             *DRBC1
          -KGP*(DRBC1*(PS1P+DT*DOMGA1)-(DRBCN*PS2P + DRBC2*DT
             *DOMGA2))*DRBC1)/DJG1

PS2PDD = (-DCLS*((PS2PD+DOMGA2)-(PSLPD+DOMGAL))
          -DKLS*((PS2P+DT*DOMGA2)-(PSLS+DT*DOMGAL))           (A.5-3)
          -CGP*((DRBCN*PS2PD+DRBC2*DOMGA2)-DRBC1*(PS1PD+DOMGA1))
              *DRBCN
          -KGP*((DRBCN*PS2P*DT*DOMGA2)-DRBC1*(PS1P+DT*DOMGA1))
              *DRBCN/DJG2

PSLPDD = (-DCLS*((PSLPD+DOMGAL)-(PS2PD+DOMGA2))
          -DCBL*(PSLPD+DOMGAL)- DCB2*(PS2PD+DOMGA2)          (A.5-4)
          -DKLS*((PSLP+DT*DOMGAL)-(PS2P+DT*DOMGA2))- TL)/DJL
```

The effective load torque is equation (A.5-4) is decreased to account for the bearing losses by redefining the load torque as

```
TL = (TD-DCBD*(PSDPD+DOMGAD) - DCB1*(PSIPD+DOMGA1))*TRN
     - DCB2*(PS2PD+DOMGA2) - DCBL*(PALPD+DOMGAL)
```

For maintaining greater numerical accuracy by working with larger numbers the absolute angular displacements and velocities were introduced into equations A.5-1 through A.5-4. For example, in equation A.5-2, DPS1P is the angular oscillatory displacement and DT*DOMGA1 is the swept out constant angular displacement of Gear 1. The absolute angular velocity at any instance consists of DPS1PD+DOMGA1 terms where DPS1PD is the oscillatory component of the constant angular velocity of gear 1, DOMGA1. Similar expression were introduced for gear 2 by using the effective base circle radius DRBCN, DT and DOMGA2 values. The initial displacements were determined by statically twisting the entire system with the drive and load torques, TD and TL, respectively. Thus, at time equal zero, the initial displacements are:

Text		Computer Program			
$\Psi_D(0)$	-	DPSID	=	TD/DKKS	(radians)
$\Psi_1(0)$	-	DPSI1	=	0.0	
$\Psi_2(0)$	-	DPSI2	=	- TD/KGP x DRBC1 x DRBC2)	
$\Psi_L(0)$	-	DPSIL	=	DPSI2 - TL/DKLS.	

The initial velocities are set to nominal steady-state velocities

Text	Computer Program					
$\dot{\Psi}_D(0) = \dot{\Psi}_1(0)$	DPSIDD	=	DPSI1D	=	2 x RPMIN/60	(rad/sec)
$\dot{\Psi}_2(0) = \dot{\Psi}_L(0)$	DPSI2D	=	DPSILD	=	(DRBC1/DRBC2) x DPSIDD.	

The general integration schemetic for program integration in the FAST routine is shown in Figure A.5-1. The actual numerical integration is performed in the RKUTTA and MORERK subroutines based on the fourth order Runge-Kutta method [26]. The RKUTTA subroutine (Figure A.5-2) keeps track of the iterations across the integration interval. The MORERK subroutine (Figure A.5-3) evaluates the derivatives and performs the summations.

The RKUTTA call statement argument contains the integration step size. The MORERK call statement argument contains the variable to be integrated, its derivative value, and the integration time step. At first glance, it would seem that the variables are being integrated in reverse order. But, it must be remembered that the integrated values are those that will be used in the next integration step. Therefore, the positional values are integrated first, and then the angular velocities. The MORERK subroutine is called eight consecutive times after RKUTTA to evaluate each element's change in position and velocity; PSDP, PADPD, PSIP, PS1PD, PS2P, PS2PD, PSLP, and PSLPD. The variable NE is a counter used to index the integrated variable and its derivative in two- eight element vectors, XI and DXI. It is reset to zero at the start of every interation. NP is the variable controlling the iteration time step and denoting the iteration step for MORERK. NRK is a variable used in the calling subroutine to check for the conclusion of integration for a given time interval.

The integrated values of angular displacements and velocities (equations A.5-1a through A.5-4a) for each element represent the deviations from the nominal constant velocities and swept out displacements. These values are when added to the constant velocities and swept out displacements to give the espective absolute angular velocities and displacements. In addition to being used to initialize the next integration step, the absolute angular position is used to interpolate a new value for KGP_i and TRN_i.

Calculations in FAST are based on a stiffness cycling shown in Figures 8 and 9. The cycle starts with the initiation of contact on a tooth entering the contact zone and ends with the initiation of contact with the tooth immediately following it. In the program, this is done in the SLOWM subroutine by examining the developed stiffness function. The position of tooth #3 when #4 comes into contact is defined as IEP. Consequently, (IEP-1) is the endpoint of the stiffness cycle started when tooth # 3 came into contact as illustrated in Figure 9. This process is repeated until the total number of stiffness cycles (NCT) equivalent to TTOTAL is reached.

At this point, it is assumed that the system is at a steady state and the values of gear pair stiffness, dynamic force, angular position, angular velocity, stiffness, hertz stresses and dynamic load factors are printed out. The RCP1, RCP2, RCCP1, RCCP2 vectors needed in some of these calculations were similarly interpolated as KGP.

The total integration time TTOTAL and the integration time step DT are based on the lowest natural frequency of the system. More details on TTOTAL and DT are given in Appendix 4.

The description of parameters and relationship between the text and computer program symbols is given in Table A.5-1.

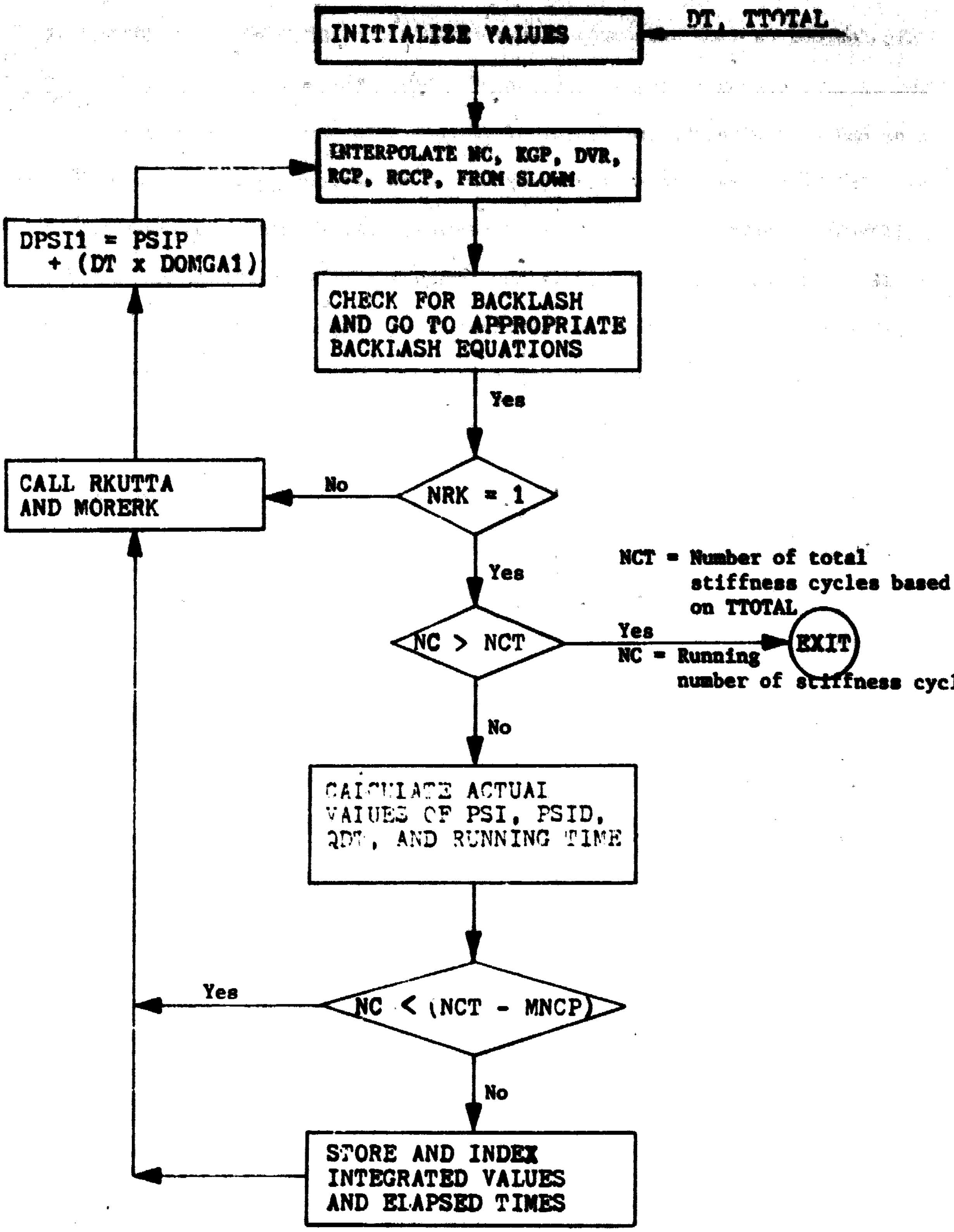

Figure A. 5-1 PROGRAM INTEGRATION

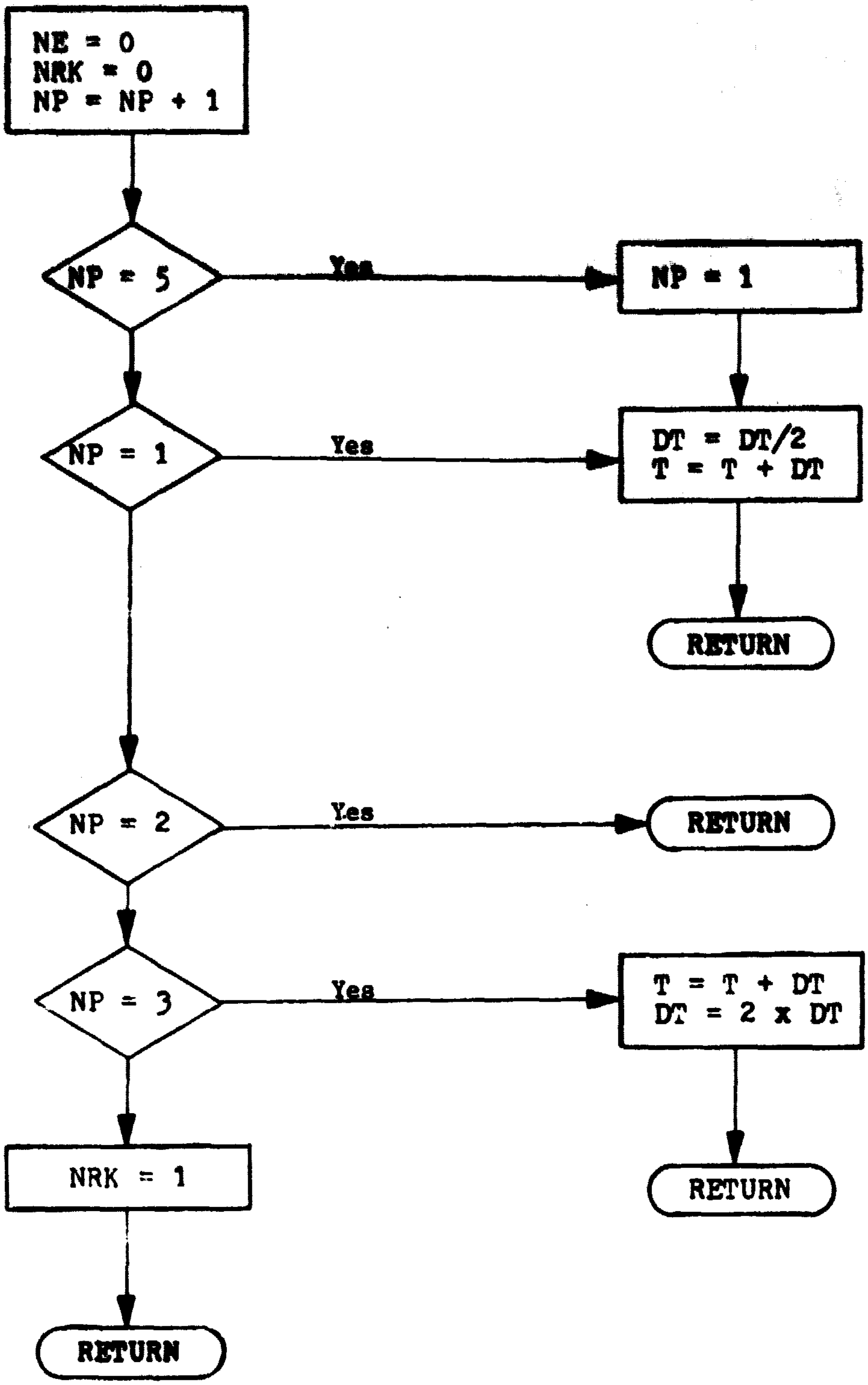

Figure A. 5-2 SUBROUTINE RKUTTA

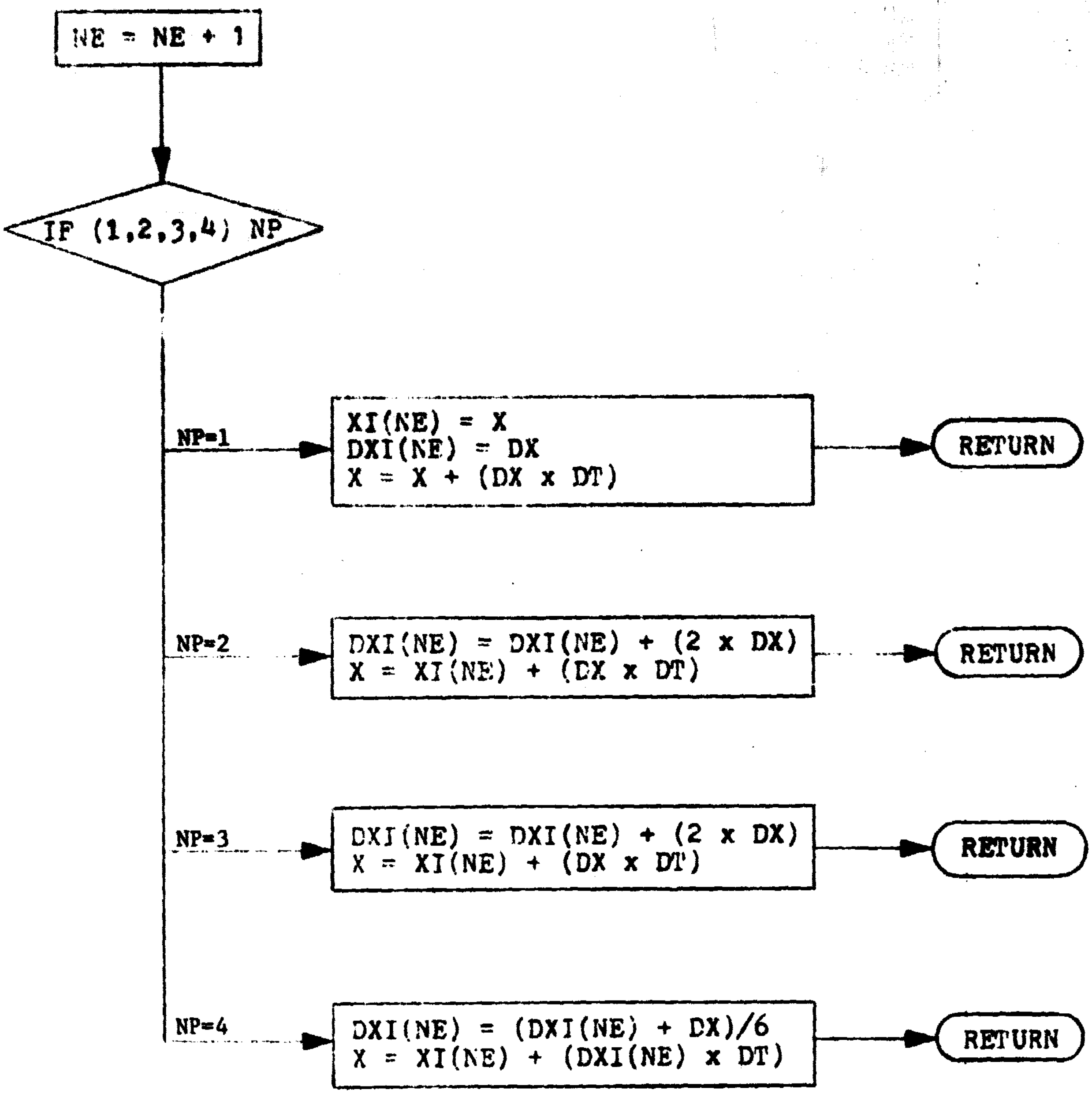

Figure A.5-3 SUBROUTINE MORERK

TABLE A.5-1

RELATIONSHIP BETWEEN THE
TEXT AND PROGRAM SYMBOLS

TEXT	PROGRAM	DESCRIPTION
μ	PR	Poisson's ratio
δ_1, δ_2	TDEFL1, TDEFL2	Tooth deflection, Gear 1 and 2
ζ	ZETAG	Gear mesh, critical damping ratio
ζ_s	ZETAS	Shaft critical damping ratio
TR'	TRN	Instantaneous transmission ratio
RBC2'	DRBCN	Instantaneous base circle, Gear 2
RCCP1' RCCP2'	RCC1 RCC2	Instantaneous radius of curvature
[J]	[MM]	Inertia matrix
[K]	[SM]	Stiffness matrix
$\Psi_D, \dot{\Psi}_D, \ddot{\Psi}_D$	PSDP, PSDPD, PSDPDD	Dynamic Displacement, Velocity, and Acceleration, Driving Unit
$\Psi_1, \dot{\Psi}_1, \ddot{\Psi}_1$	PS1P, PS1PD, PS1PDD	Dynamic Displacement, Velocity, and Acceleration, Gear 1
$\Psi_2\ \dot{\Psi}_2\ \ddot{\Psi}_2$	PS2P, PS2PD, PSPDD	Dynamic Displacement, Velocity, and Acceleration, Gear 2
$\Psi_L, \dot{\Psi}_L, \ddot{\Psi}_L$	PSLP, PSLPD, PSLPDD	Dynamic Displacement, Velocity, abd Acceleration, Load Unit
T_D T_L	TD, TDIN TL, TOUT	Input torque Output torque
	OMGAD	Constant angular velocity, driver, rad/sec
	OMGA1	Constant angular velocity, gear 1, rad/sec
	OMGA2	Constant angular velocity, gear 2, rad/sec
	OMGAL	Constant angular velocity, load, rad/sec

NOTE: Letter D preceding the computerized symbols identify double precision.

APPENDIX 6

PROPOSED FINITE ELEMENT PROGRAM - STRESS

INTRODUCTION

The external spur gear program which was developed by the Mechanical Engineering Department, Cleveland State University under NASA grant NAS3-18547 currently has the capability to solve for the instantaneous static and dynamic loads of an external spur gear mesh. The program also calculates the instantaneous transmission ratio, sliding velocities, maximum contact pressure, and maximum PV values. For determining the gear tooth bending stresses the finite element approach is proposed.

Several types of elements and mesh generators were considered. In order to conserve computing time without compromising the accuracy, it was decided to use an isoparametric incompatible displacement finite element. The entire external spur gear program was developed in a modular form, thus facilitating introduction (if needed) of other types of finite elements or even the major finite element programs such as NASTRAN, SAP IV etc.

The quadrilateral elements used are a four node quadrilateral having two incompatible displacement modes that were developed by Wilson, et. al., [37]. This element was selected because it gives excellent results for bending applications, while maintaining a narrow band width. For large computer systems where the band width is no problem, the more common eight or nine node isoparametric elements could be used. The incompatible displacement model is discussed in more detail in the subsequent sections of the appendix. A special purpose finite element mesh generation routine was developed that takes into account the digitized spur gear tooth shapes from the MOD routine thus minimizing the input on the part of the analyst. The static and dynamic portions of the external spur gear program contain the required definitions of the gear tooth geometry, definitions of the material properties as well as the instantaneous gear load, its location and orientation.

The finite element and mesh generation routines were combined as a single STRESS routine as shown in Figure A. 6-1. Linking, the proposed STRESS routine with the above described external spur gear program is a function of computer size and type. This finite element program, due to its large scale, at this time is not an integral portion of the gear load analysis program. Currently the proposed STRESS program uses the pre-processed data from the above external spur gear program - there is no direct link between the load and finite stress analyses. Work is to be continued to develop a direct link between these two programs for usage on various computers.

In the STRESS program the stresses can be calculated on a gear or pinion tooth at any profile position along the line of action. For efficiency, the stiffness matrix is assembled and decomposed only once for each structure as shown in Figure A. 6-1.

The decomposed matrix is then stored on a disk file for subsequent use for each selected load case. Since most of the computer time involved in the stress calculation is in the assembly and decomposition procedure, this approach represents a considerable savings in execution time for gear sets having the stress routine called more than once. The following load cases can be called:

a. Maximum dynamic load (at any position).
   The calling index FELGR = 1, Control Name List, CONTRL.

b. Dynamic load at pitch
   The calling index FELGR = 2, Control Name List, CONTRL

c. Maximum dynamic bending moment
   The calling index FELGR = 3, Control Name List, CONTRL

d. Maximum static load (at any position)
   The calling index FELGR = 4, Control Name List, CONTRL

MESH GENERATION

This program takes advantage of generic shape of the spur gear tooth. The finite element mesh is divided into two separate areas, the tooth (Figure A.6-2) and the gear blank (Figure A.6-3) modeled as a triangular zone.

The gear tooth portion is composed of quadrilateral elements as illustrated in Figure A.6-2. An algorithm was devised that causes nodal points near the gear surface to be more closely spaced than those near the centerline of the gear tooth. In the horizontal direction using symmetry six nodal points were selected. The relative coarseness in the horizontal direction - X direction is shown in Figure A.6-2. In the vertical direction, the total number of nodal points must be even. It is felt that about six to eight nodal points will be sufficient to describe the working portion of the profile. The fillet zone can be described also by 6 to 8 nodal points. The vertical distance between two adjacent nodal points encompass several digitized profile points. The relative coarseness between the nodal points on the gear tooth profiles is suggested in Figure A. 6-2.

The only input that is required for the stress analysis is the desired total number of the surface nodes on the gear tooth profile (NNODE) and their respective index numbers (NODES). The name list heading is FINLEM for NNODE and NODES. The coordinates of the desired nodal points are contained in the MOD and STRESS routines. The grid generator automatically generates the required data from the designated surface nodal points for the analysis of the tooth based on a symmetrical side input. Coordinates of the involute profile points are transferred by a common block statement. The mesh is generated by defining the number of nodal points (NNODE) and their respective index number (NODES).

The lower portion of the structure is a triangular shape as illustrated in Figure A. 6-3. Point O is the center of the gear. This area is composed of triangular and quadrilateral elements. The locations of the nodal points are dictated by the nodal points at the base of the tooth and the geometry of the of the triangle AOB as illustrated. No nodal point inputs are required in this case.

INCOMPATIBLE DISPLACEMENT FINITE ELEMENT

This analysis uses an isoparametric finite element having two incompatible displacement modes. This type of element allows for a linear strain field having comparable accuracy for bending problems of eight or nine node isoparametric elements, but result in a band width identical to a constant strain element.

The basic problem with constant strain elements is that they behave poorly under pure bending. When using this type of element for the analysis of a structure in a location when bending stresses predominate (for example in the area of a gross structural discontinuity on a pressure vessel) the stress analyst must take special care to define a finite element mesh that is sufficiently refined to assure reasonable convergence. As a result, this type of analysis often requires large amounts of the stress analyst's time to be devoted to setting up analytical models and to interpret a large amount of output data. Also, by refining the finite element mesh, an increased number of equations must be solved. This may appreciably increase the computer time.

The usual approach to circumvent these problems is to use a higher order element. This type of element uses a higher degree polynomial to approximate the displacement field and usually has one or more mid-side nodes. One type of higher order element which has no mid-side nodes and is used in this study was reported by Wilson, Taylor, Doherty and Ghaboussi [37].

The approach used by Wilson, et. al., in their higher order element development is to add higher order terms to the displacement modes of lower order elements to compensate for the errors in the lower order element. A brief discussion of their technique follows.

Consider the two-dimensional element which is illustrated in Figure A. 6-4. The exact displacements are of the form

$$u = c_1 xy \quad \text{(A.6-1)}$$

$$v = 1/2\ c_1 (a^2 - x^2) + c_2 (b^2 - y^2) \quad \text{(A.6-2)}$$

These displacements are illustrated in Figure A. 6-4b. For a constant strain element, the assumed displacements are of the form

$$u = c_1 xy \quad \text{(A.6-3)}$$

$$v = 0 \quad \text{(A.6-4)}$$

and illustrated in Figure A. 6-4C.

From equations A.6-1 through A. 6-4, it can be seen that the error in the constant strain solution is of the form:

$$v = d_1 (a^2 - x^2) + d_2 (b^2 - y^2) \quad \text{(A. 6-3)}$$

Wilson et al. proposed that the error described by equation A.6-3 could be eliminated by adding displacements of the form of equation A.6-5 to equations A. 6-3 and A. 6-4. In this way pure bending, free of shear strain, may be represented exactly. The complete displacement fields for this element are given by:

$$u = \sum_{i=1}^{4} N_i u_i + (1 - s^2)\ u_5 + (1 - t^2)\ u_6 \quad \text{(A.6-6)}$$

$$v = \sum_{i=1}^{4} N_i v_i + (1 - s^2)\ v_5 + (1 - t^2)\ v_6 \quad \text{(A.6-7)}$$

The displacement modes which are represented by $i = 5$ and 6 in Equations A. 6-6, and A. 6-7 are associated with internal degrees of freedom and are illustrated in Figure A. 6-5. These displacements are quadratic and are defined by only two nodal points along the edge of the elements. Since a quadratic can not be uniquely defined by two points, the displacement field along a common edge of two elements generally not equal; hence, the displacements are referred to as incompatible.

Since one condition for monotonic convergence is that compatibility must exist between the elements. Since displacements in general are not compatible, monotonic convergence is not assured. However, since the incompatible modes satisfy the requirements for pure bending, an inproved solution is obtained.

BOUNDARY CONDITIONS

The boundary condition at the support are illustrated in figure A. 6-3. Point O is assumed to be fixed, while other nodal points along lines OA and OB are assumed to be on roller supports. This was accomplished by rotating the degrees of freedom associated with each of these supports into a local coordinate system that is parallel and normal to the roller supports. The force and displacement vectors in this coordinate system are:

$$\{F'\} = [R]\ \{F\}$$

$$\{\delta'\} = [R]\ \{\delta\}$$

where $\{F\}$ and $\{\delta\}$ represent the force and displacement vector respectively. The prime indicates the local coordinate system, and $[R]$ is a rotation matrix as follows:

$$[R] = \begin{bmatrix} \cos\theta & \sin\theta \\ -\sin\theta & \cos\theta \end{bmatrix}$$

where θ is the angle between the global x axis and the local x axis.

The above matrix equation is performed on the element stiffness matrices only. All elements in the triangular portion of the structures are checked to determine if one or more of its nodal points are one of the rotated supports. The only terms in the stiffness matrix that are modified are those that correspond to the rotated support.

SOLUTION ALGORITHM

The computer program developed used a blocking algorithm for an out of core equation solver that was presented by Lestingi and Prachuktam [38] This approach permits a very large number of equations to be solved on a computer having limited core capacity. This is because during the assembly and decomposition steps only a portion of the structure stiffness matrix has to be in core. The balance can be stored on a disk. Similarly, during the back substitution step, only a portion of the decomposed stiffness matrix must be in core.

It should be noted that this solution algorithm takes advantage of the symmetry and banded nature of the stiffness matrix. The only terms stored are the main diagonal and the upper triangular portion within the upper band width. Therefore, all of the zero terms outside the band width are not processed.

Since $[R]$ is an orthonormal matrix

$$[R]^{-1} = [R]^T$$

be stiffness equation in the global coordinate system

$$\{F\} > [K] \{\delta\}$$

becomes $$\{F'\} = [R]\ [K]\ [R]^T\ \{\delta'\}$$

in the local coordinate system. The stiffness matrix in the local system becomes

$$[K'] = [R]\,[K]\,[R]^T$$

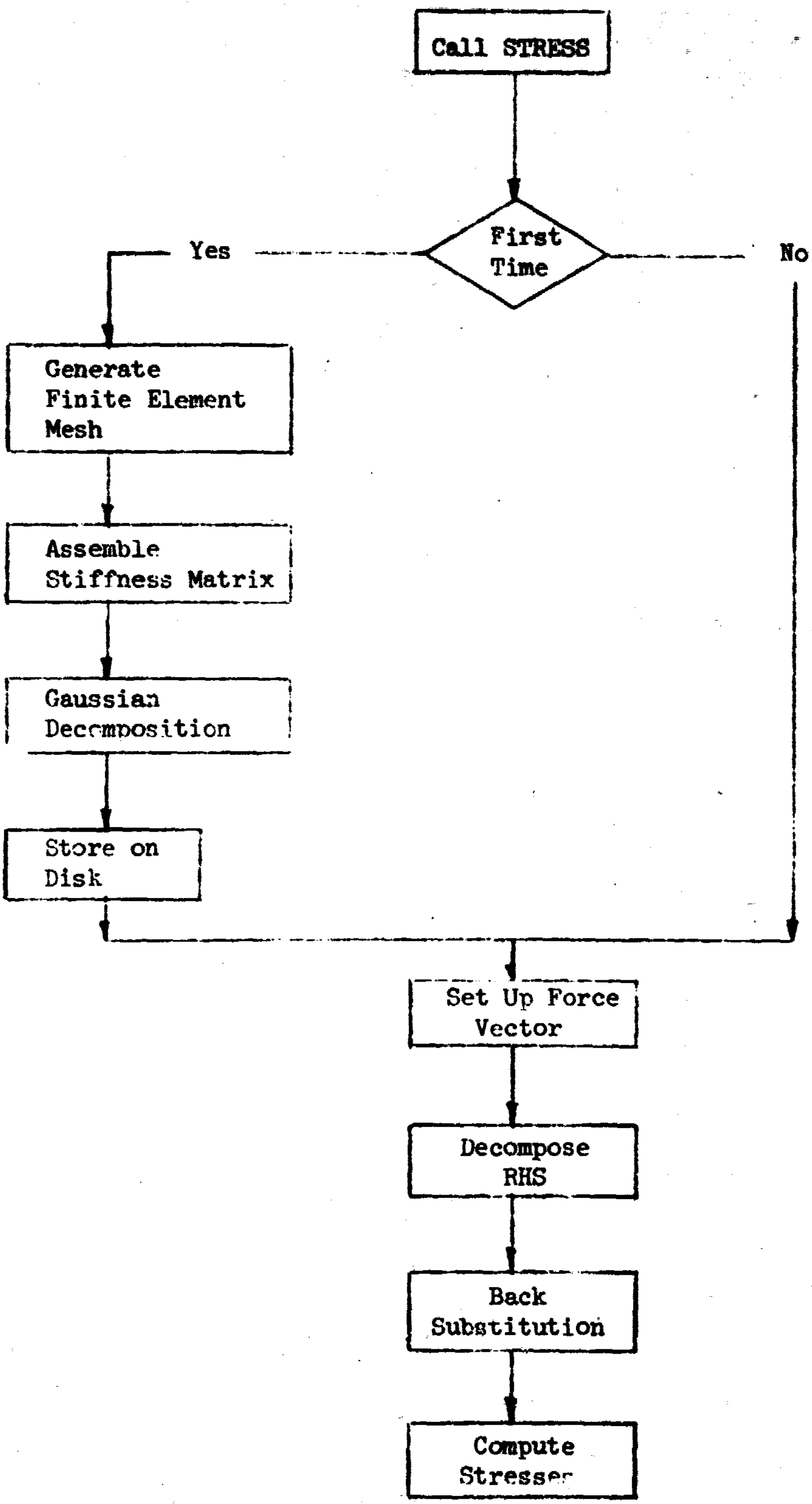

Figure A.6-1 SCHEMATIC OF FINITE ELEMENT PROGRAM

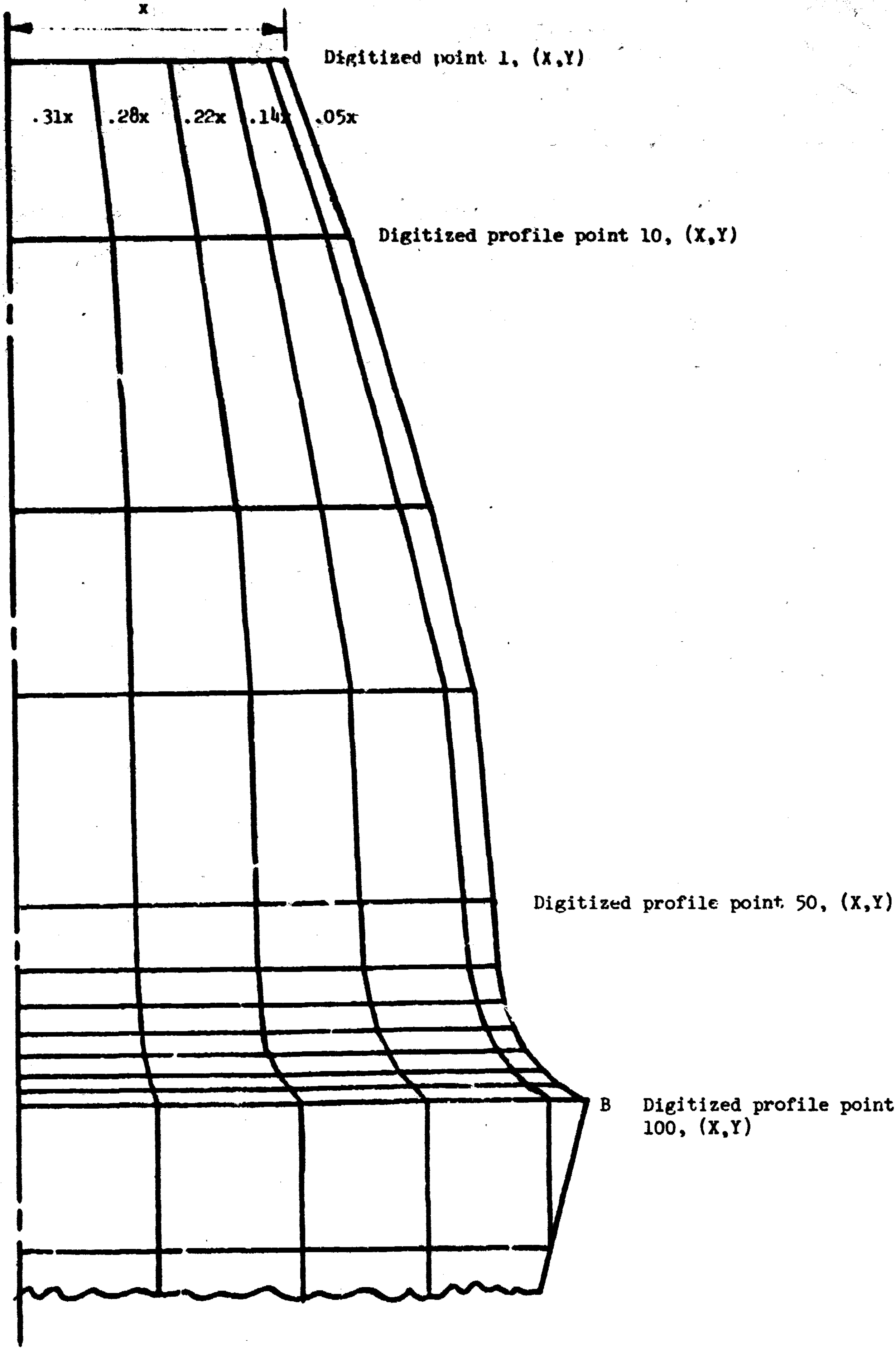

Figure A.6-2 GEAR TOOTH PORTION

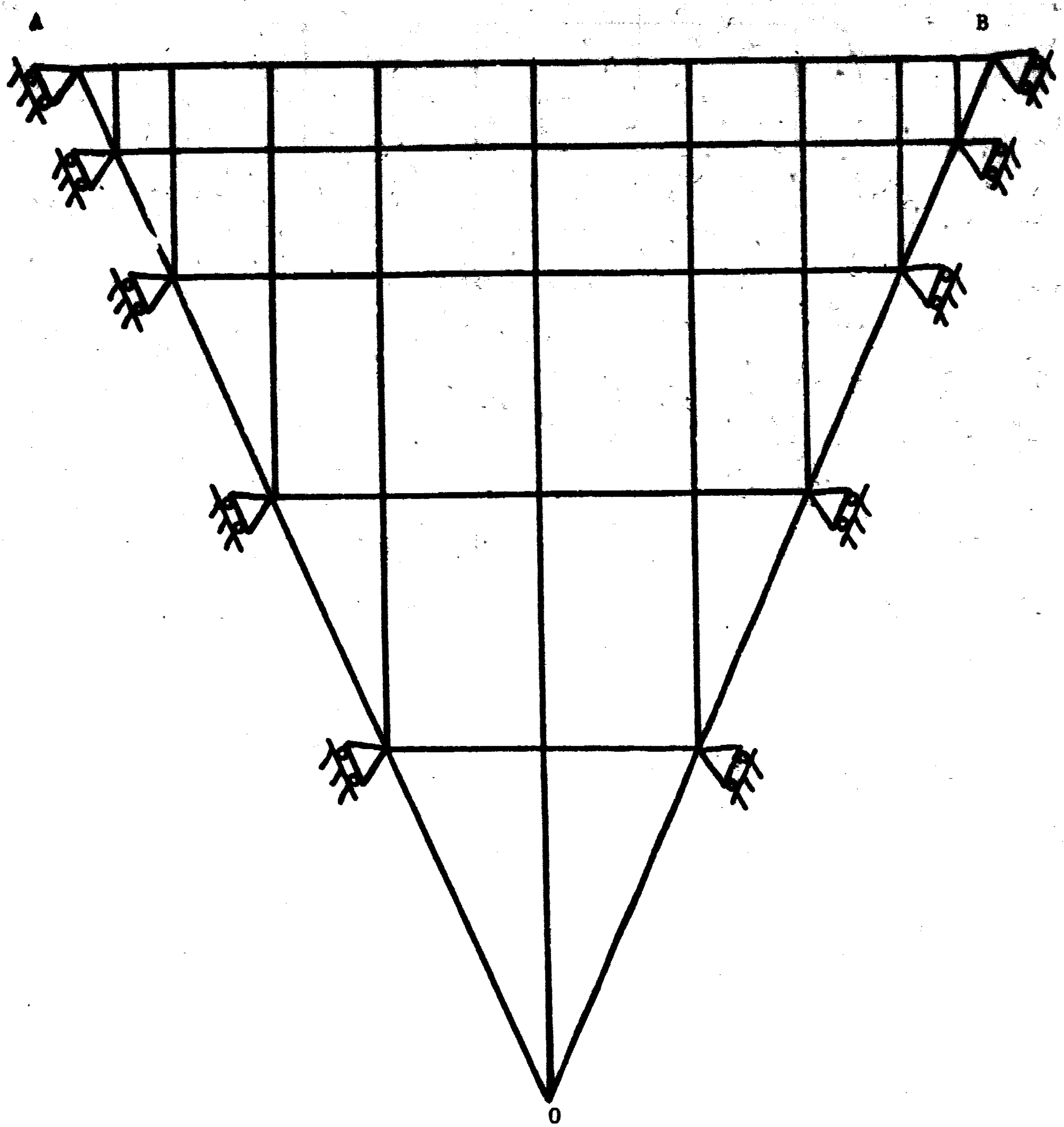

Figure A.6-3 GEAR TOOTH LOWER PORTION - BLANK

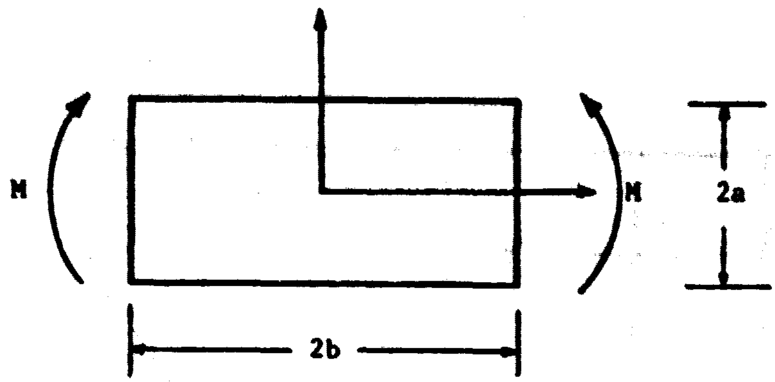

a. Element Under Simple Bending

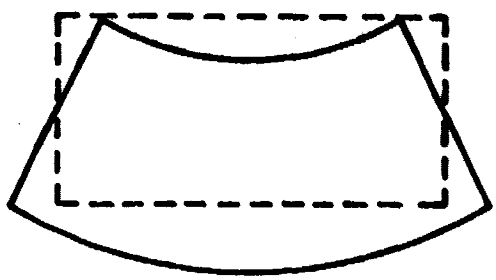

b. Exact Displacements

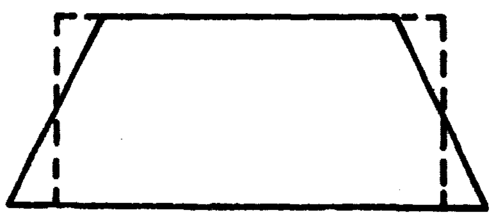

c. Finite Element Displacements

Figure A.6-4 ERROR DUE TO PURE BENDING STRESSES.

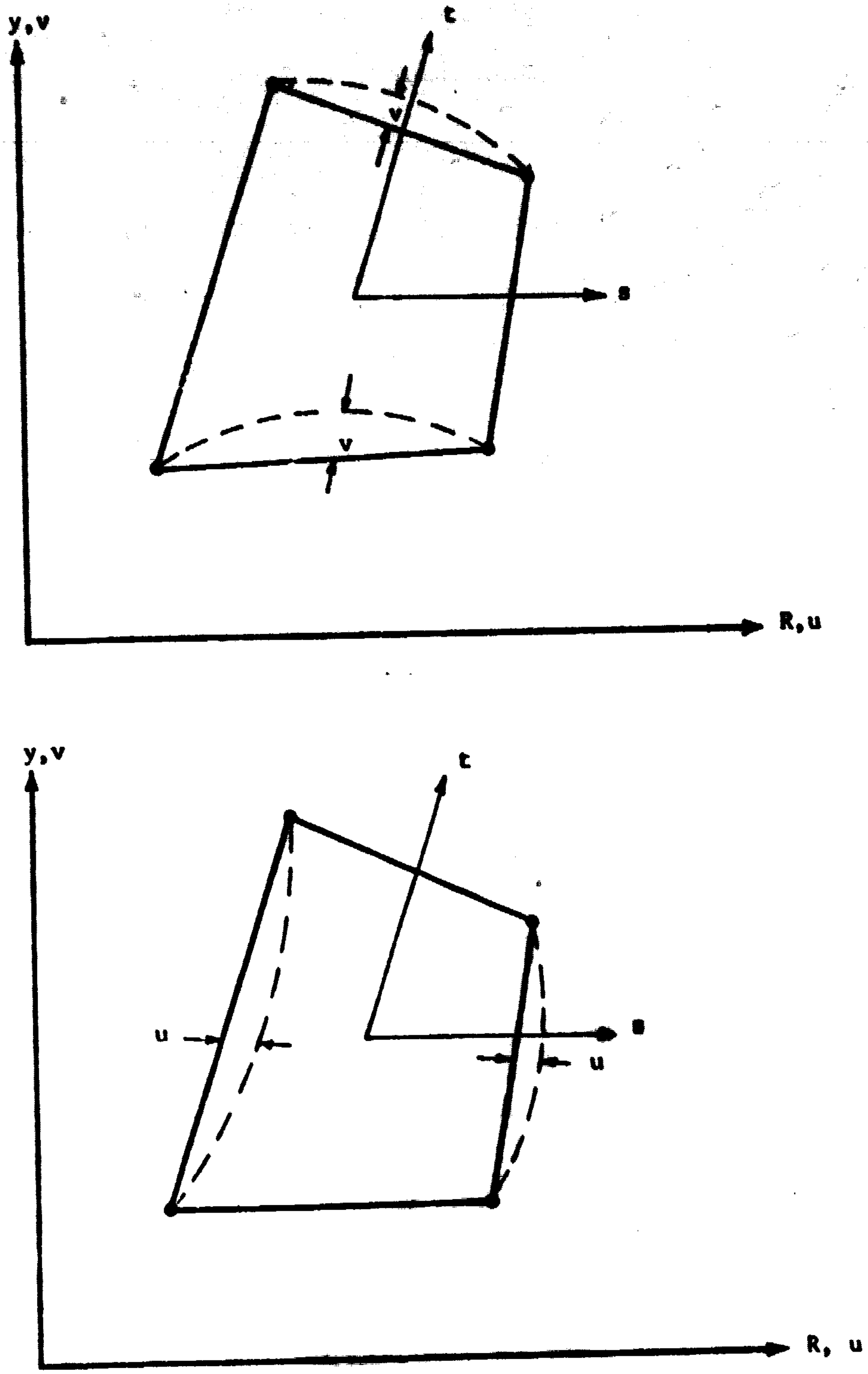

Figure A.6-5 INCOMPATIBLE MODES.

APPENDIX 7

DATA INPUT

The gear data set is input via the NAMELIST arrays defined in the main program. Numerical data maybe input without format statements, and fields are generated as required. The input variables required, along with their respective NAMELIST headings are:

/CONTRL/

INPUT - alphanumeric code used to designate type of input data
'ENGL' - English (lbf,in.,sec.)
'SI' - metric (newtons,mm,sec.)

OUTPUT - alphanumeric code used to designate output; codes used are same as for input

IPLOT - 0; tabulate all dynamic results
1; plot frequency response starting at time = 0
2; plot steady - state frequency response

MODF - alphanumeric code used to designate whether or not profile modifications are input

'NO' - no modifications
'YES' - modifications listed under /PRFDEF/

NTYPE - 1; static analysis only
2; static and dynamic analysis only
3; finite element analysis based on static loads
4; finite element analysis based on dynamic loads

FELGR - 1; finite element analysis based on maximum dynamic load experienced
2; finite element analysis based on maximum dynamic load applied at pitch point
3; finite element analysis based on maximum dynamic bending moment
4; finite element analysis based on maximum static bending moment

/PHYPAR/ (two data points (one for each gear) required per variable)

E - Young's modulus
PR - Poisson's ratio
GAMA - specific weight
* JG - polar moment of inertia

/GENPAR/

`	DP	- diametral pitch (English input only)
	M	- gear module (metric moduel only)
	DELTP	- backlash
	TIN	- input torque
	RPMIN	- input RPM
	ZETAS	- damping coefficient of shaft
	ZETAG	- damping coefficient between gear teeth
	PHID	- pressure angle (degrees)
	CBD	- driver bearing damping coefficient
	CB1	- pinion bearing damping coefficient
	CB2	- driven gear bearing damping coefficient
	CBL	- load bearing damping coefficient
*	JD	- mass moment of inertia of driver
*	JL	- mass moment of inertia of load
*	KDS	- torsional spring stiffness of driving shaft
*	KLS	- torsional spring stiffness of load shaft
*	LDS	- length of drive shaft
*	LLS	- length of load shaft

/GEOPAR/ (two data points required per variable)

	TG	- number of gear teeth
	AD	- addendum
	WD	- working depth
	GRRF	- fillet radius of basic rack
*	RI	- hub radius
	FW	- face width

/FINELM/

NNODE	- even number of profile points used in mesh generation
NODES	- index number of those profile points used in mesh generation
NGEAR	- 1; stress analysis done on pinion 2; stress analysis done on driven gear 3; stress analysis done on gear set

* optional, if no value entered. Program will generate values as shown at the end of this section.

The gear thooth profile can also be modified to simulate tip relief or undercutting. Sinusoidal errors can be introduced, as well as pits, to simulate involute errors due to manufacturing and surface damage, respectively. These modifications are introduced in /PRFDEF/ namelist. If MODF= NO, /PRFDEF/ need not be included in the data card set.

/PRFDEF/ (two data points required per variable)

PATM	- parabolic tip modification
STTM	- straight line tip modification
RATM	- roll angle of tip modification

PABM	- parabolic bottom modificaton
STBM	- straight line bottom modification
RABM	- roll angle of bottom modification
PER	- amplitude of sinusoidal error
PAP	- phase angle of sinusoidal error
CYC	- number of cycles of sinusoidal errors
IPIT	- profile coordinate points over which pit occurs
DEEP	- depth of pit
Q	- radius to top of undercut, Fig. A.3-4 automatically calculated, if not given.

Use of the NAMELIST arrays offers a simple, unformatted means of inputting data and is convenient for looping more than one data set. After the initial data set, subsequent data sets need just to input revisions. If a later NAMELIST array contains no revisions, only a card with the array heading and ending need be submitted. Unlisted variables default to the previous values. Examples of input data card sets illustrate the following NAMELIST data card format (Figure A. 7-1);

1. Column one is blank.
2. '&' is used to signify new NAMELIST array.
3. '&' is followed by the NAMELIST name.
4. A blank separates the NAMELIST name and the first variable name. Subsequent variables are separated by commas.
5. There are two methods for defining the two element variables. The elements are defined in the order they are to be entered in the variable and separated by commas, i.e., TG=32,96 defines TG(1)=32, and TG(2)=96. If both elements are equal, they may be entered by listing the number of identical values, the multiplication symbol, and then the value itself, i.e., AD=2*0.125, defines AD(1)=0.125 and AD(2)=0.125.
6. The last listed array value is followed by a blank and then the symbol from column 2 is repeated. The word END immediately follows the symbol and signifies the end of that array.

The program has the capability for accepting either SI or English gear input data and has options to print the results in either SI or English units. Input and output do not necessarily have to be of the same regime, i.e., SI output can be obtained from English input and vica-versa. Data submitted under the 'ENGL' code should be in poundsforce, inches, and seconds. The data submitted under the 'SI' code should be in newtons, millimeters, and seconds. The only exception to this is the density value under the 'SI' code should be in kg/m^3.

PROGRAM DEFAULT VALUES

```
RI(1) = (8.0 * TIN)/[(PI * TAUMAX) ** (1/3)] in.
RI(2) = (8.0 * TOUT)/[PI * TAUMAX) ** (1/3)] in.
                                    TAUMAX = 10,000 psi

JG(1) = 0.5 * GAMA(1) * PI * FW(1) * (RPC1 ** 4)/386.   in.-lbf -s^2/radian
JG(2) = 0.5 * GAME(2) * PI * FW(2) * (RPC2 ** 4)/386.   in.-lbf -s^2/radian

JD = 0.5 * JG(1)     in.-lbf-S^2/radian
JL = 0.5 * JG(2)     in.-lbf-S^2/radian

LDS = 6 in.
LLS = 6 in.

KDS = PI * (2.* RI(1) ** 4) * [E/(2.* (1 + PR))]/(32.* LDS)  in.-lbf /radian
KLS = PI * (2.* RI(2) ** 4) * [E/(2.* (1 + PR))]/(32.* LLS)  in.-lbf /radian
```

The listing of the program could be obtained by contacting the Project Manager at NASA Lewis Research Center.

Figure A. 7-1 SAMPLE DATA CARD SET (W/O PROFILE MODIFICATIONS OR ERRORS)

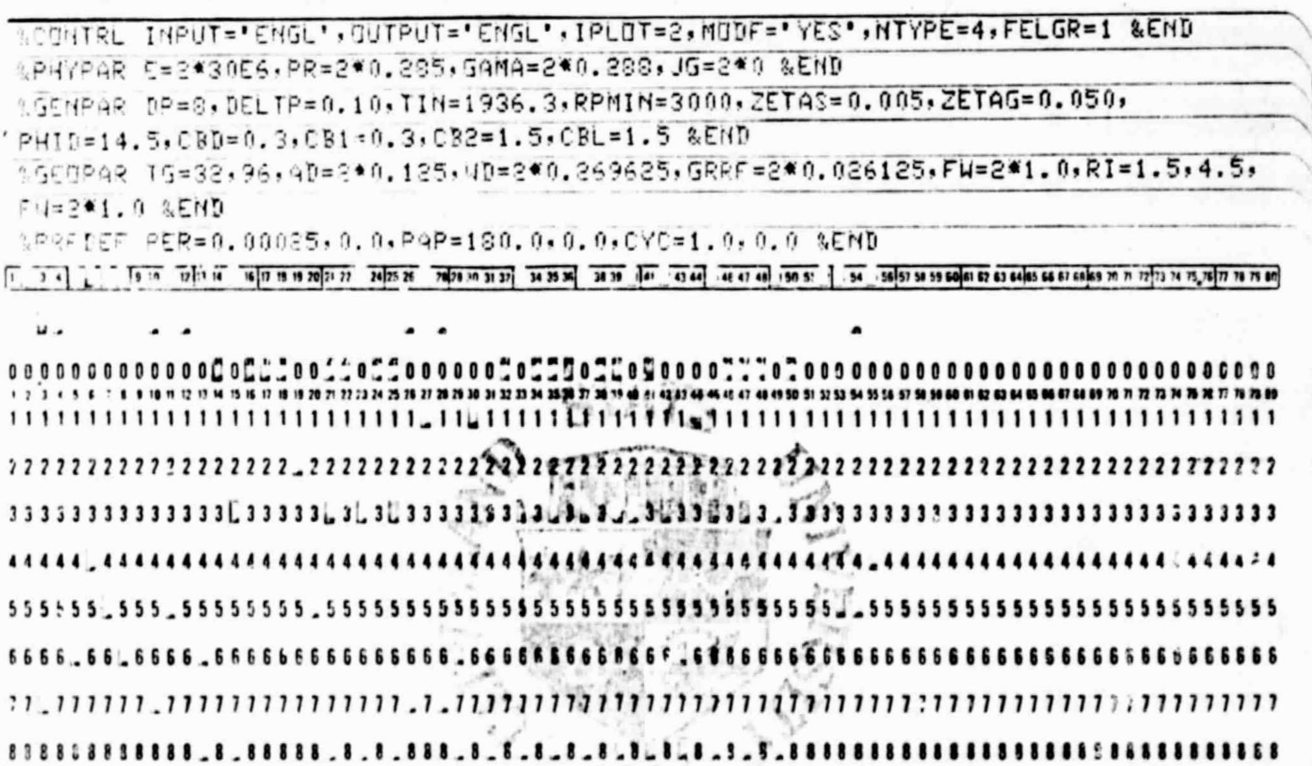

Figure A. 7-1 SAMPLE DATA CARD SET (WITH PROFILE ERRORS)

ORIGINAL PAGE IS
OF POOR QUALITY

APPENDIX 8

SAMPLE OUTPUTS

In the static and dynamic portions the following basic groups of parameters are calculated:

a. Gear tooth and mesh deflections and the accompanying gear mesh and gear tooth pair stiffness.

b. Load distribution among the contacting tooth pairs.

c. The sliding velocity, the maximum Hertz contact pressure, and the sliding velocity-hertz pressure product (PV) along the tooth profiles.

These parameters can be printed out in tabular form or plotted as individual graphs on a line printer for both static and dynamic conditions.

Some of theses plots are illustrated for 32-96 T, 20^{o} PA, 8 DP, standard full depth tooth form, gear pair, HSF $\approx$.5, transmitting a torque equivalent to a normal load of 175 N/mm (1000 lb/in) at 2000 rpm. CR_T = 1.758, CR = 2.123. Gears are without profile modifications and errors. ξ = .05, ξ_s = .005

Figure A. 8-1 Gear Tooth Deflections
Figure A. 8-2 Gear Mesh and Gear Tooth Pair Stiffness
Figure A. 8-3 Load Distribution
Figure A. 8-4 Hertz Contact Stress
Figure A. 8-5 Sliding Velocity
Figure A. 8-6 PV: Hertz Contact Stress - Sliding Velocity Product

Firues A.8-1 through A.8-6 are for the pinion (Gear 1) for equivalent static load condition at 2000 rpm. Similar plots can be generated for Gear 2, and as well as for the dynamic load conditions. The program accomodates the AGMA and metric gears,as well as the English and SI units.

The dynamic simulation results can be also given in both the tabular and graph forms. For example,

Figure A. 8-7 Gear Mesh Dynamic Load
Figure A. 8-8 Tabulation of Dynamic Load Factors
Figure A. 8-9 Dynamic Load Between Contacting Gear Tooth Pair
Figure A. 8-10 Dynamic Hertz Stress

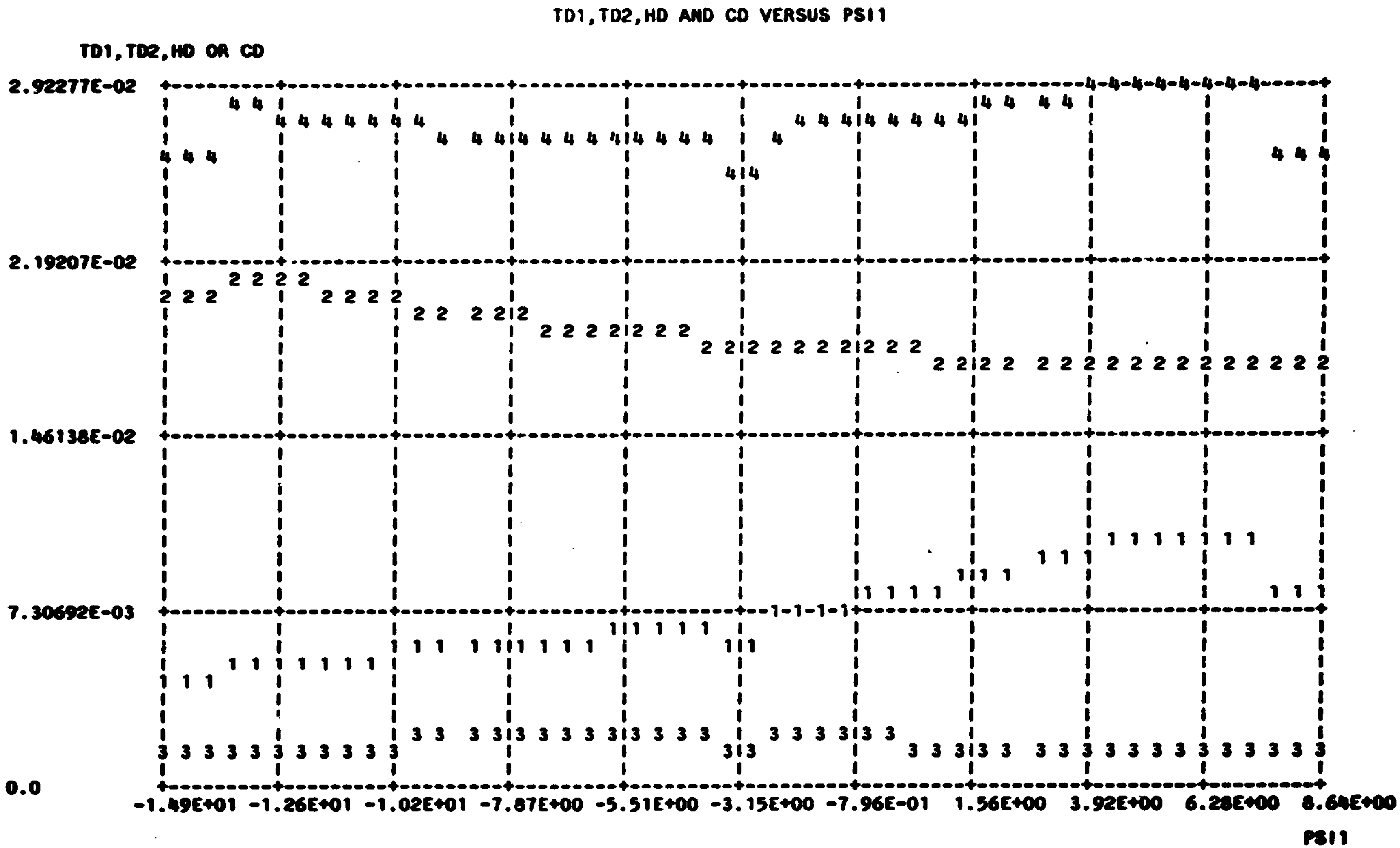

1 - TD1, THE TOOTH DEFLECTION ON GEAR 1; MM.
2 - TD2, THE TOOTH DEFLECTION ON GEAR 2; MM.
3 - HD, THE HERTZIAN DEFLECTION OF THE CONTACT POINT; MM.
4 - CD, THE COMBINED DEFLECTION OF THE CONTACT POINT; MM.
(ALL DEFLECTIONS ARE MEASURED ALONG THE LINE OF ACTION)
PSI1 IS THE ANGLE OF ROTATION OF THE DRIVING GEAR (IN DEGREES) MEASURED FROM THE LINE OF CENTERS.

Figure A. 8-1 GEAR TOOTH DEFLECTIONS

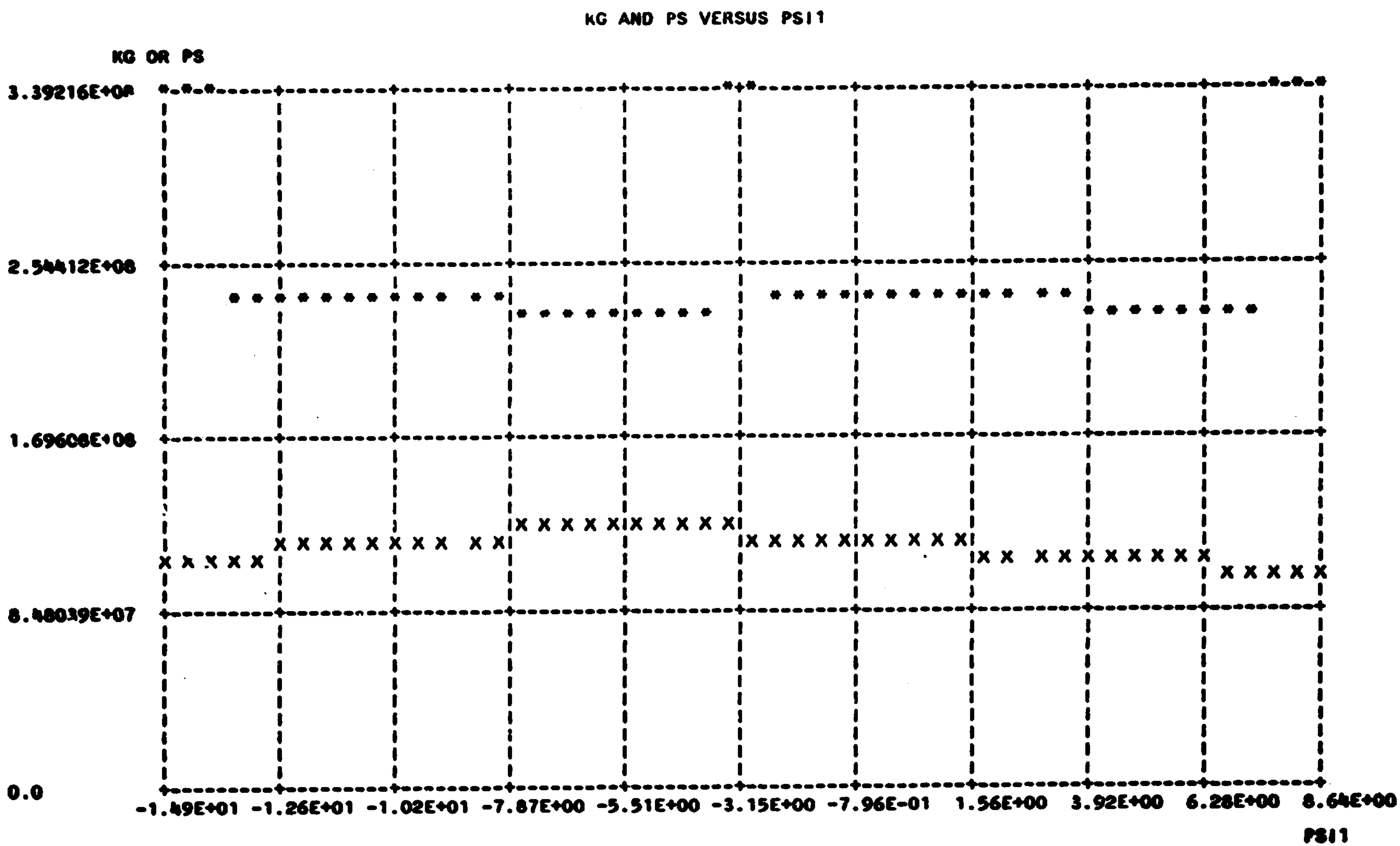

* - KG, THE GEAR STIFFNESS; N /M
X - THE TOOTH PAIR STIFFNESS; N /M
PSI1 IS THE ANGLE OF ROTATION OF THE DRIVING GEAR (IN DEGREES) MEASURED FROM THE LINE OF CENTERS.

Figure A. 8-2 GEAR MESH AND GEAR TOOTH PAIR STIFFNESS

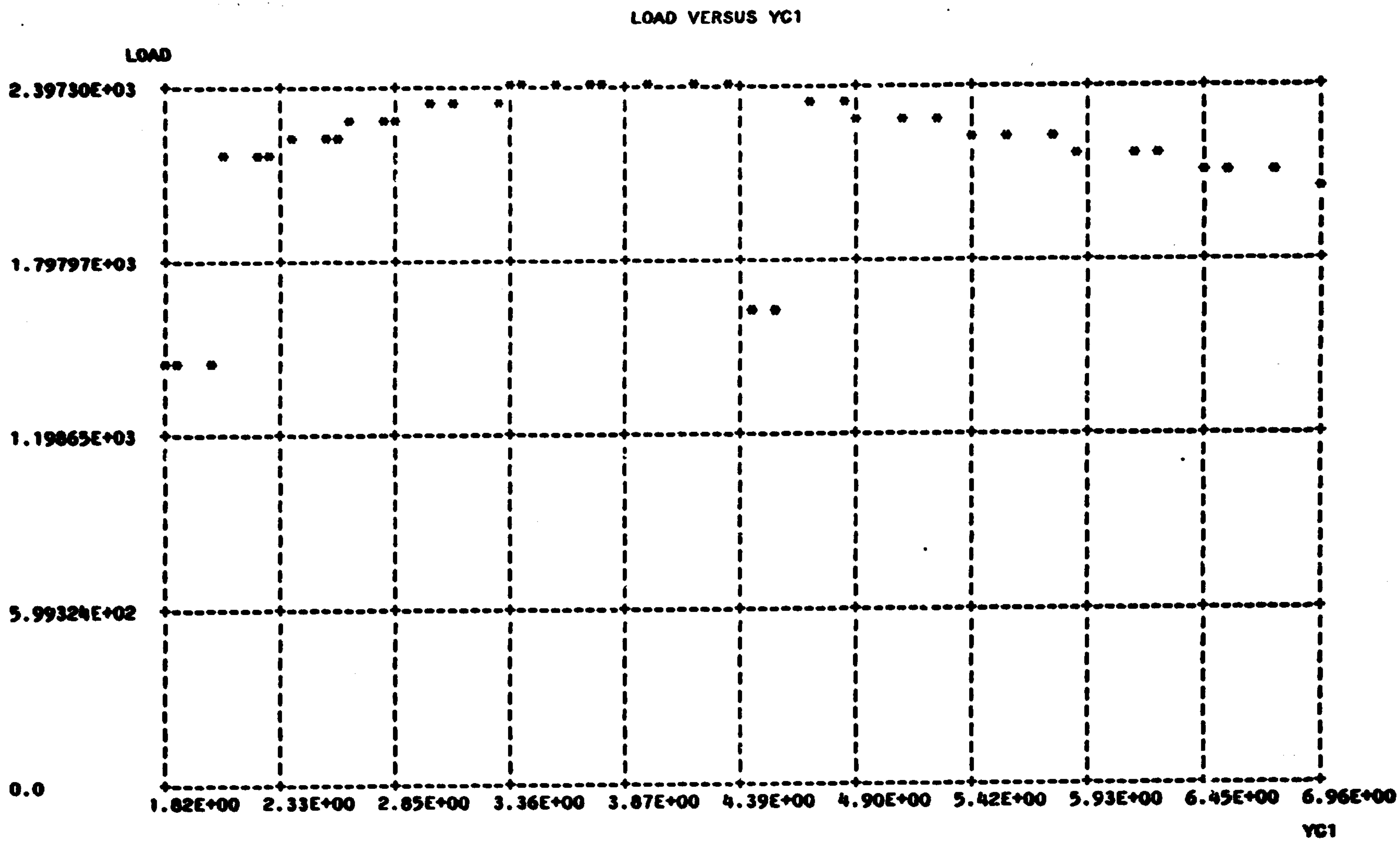

LOAD IS THE FORCE IN N ACTING BETWEEN THE CONTACTING TOOTH PAIR.
YC1 IS THE LOCATION OF THE CONTACT POINT ALONG THE TOOTH PROFILE OF GEAR 1; MM.

Figure A. 8-3 LOAD DISTRIBUTION

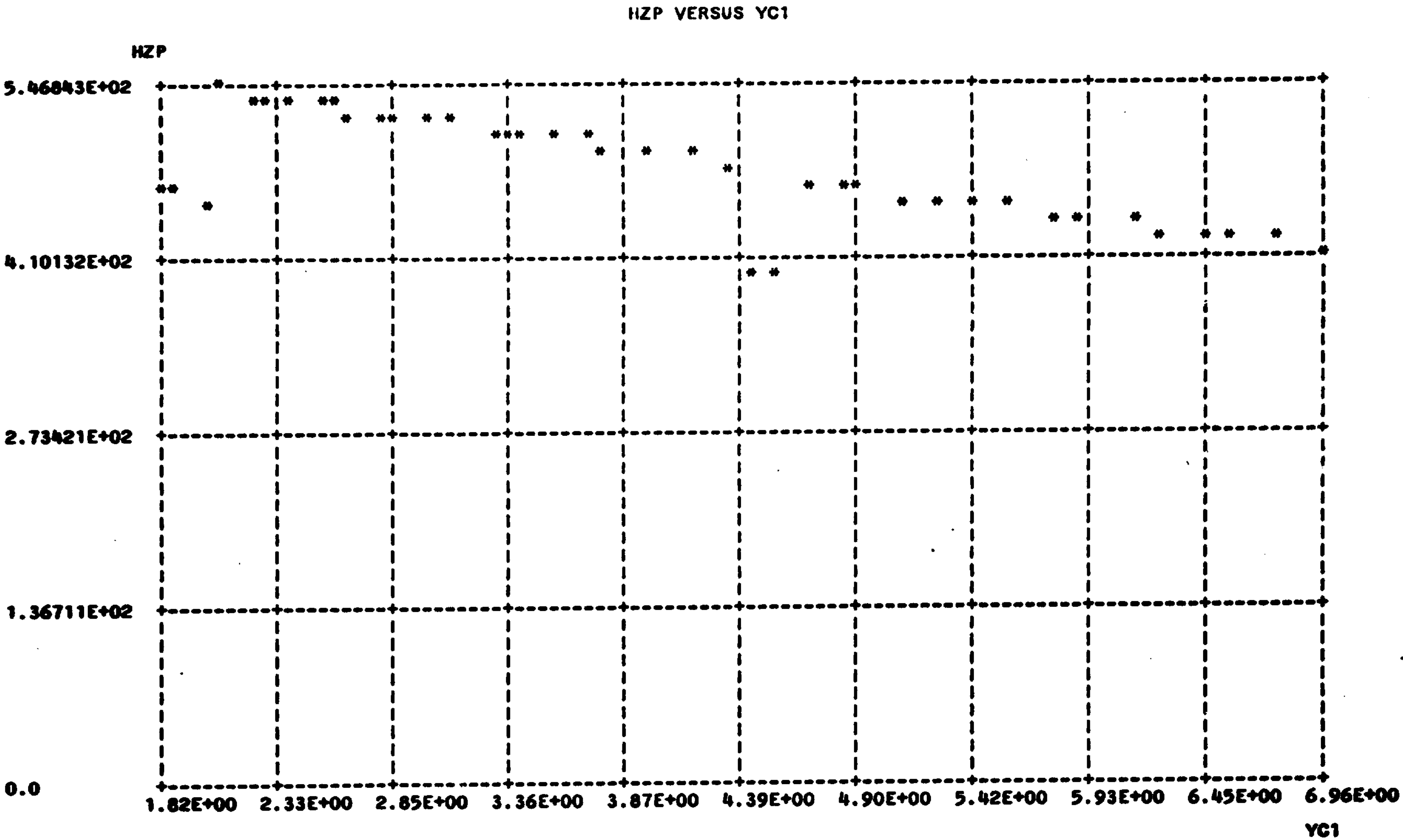

HZP IS THE MAXIMUN HERTZ CONTACT PRESSURE AT THE CONTACT POINT; MPA
YC1 IS THE LOCATION OF THE CONTACT POINT ALONG THE TOOTH PROFILE OF GEAR 1; MM.

C-2

Figure A. 8-4 HERTZ CONTACT STRESS

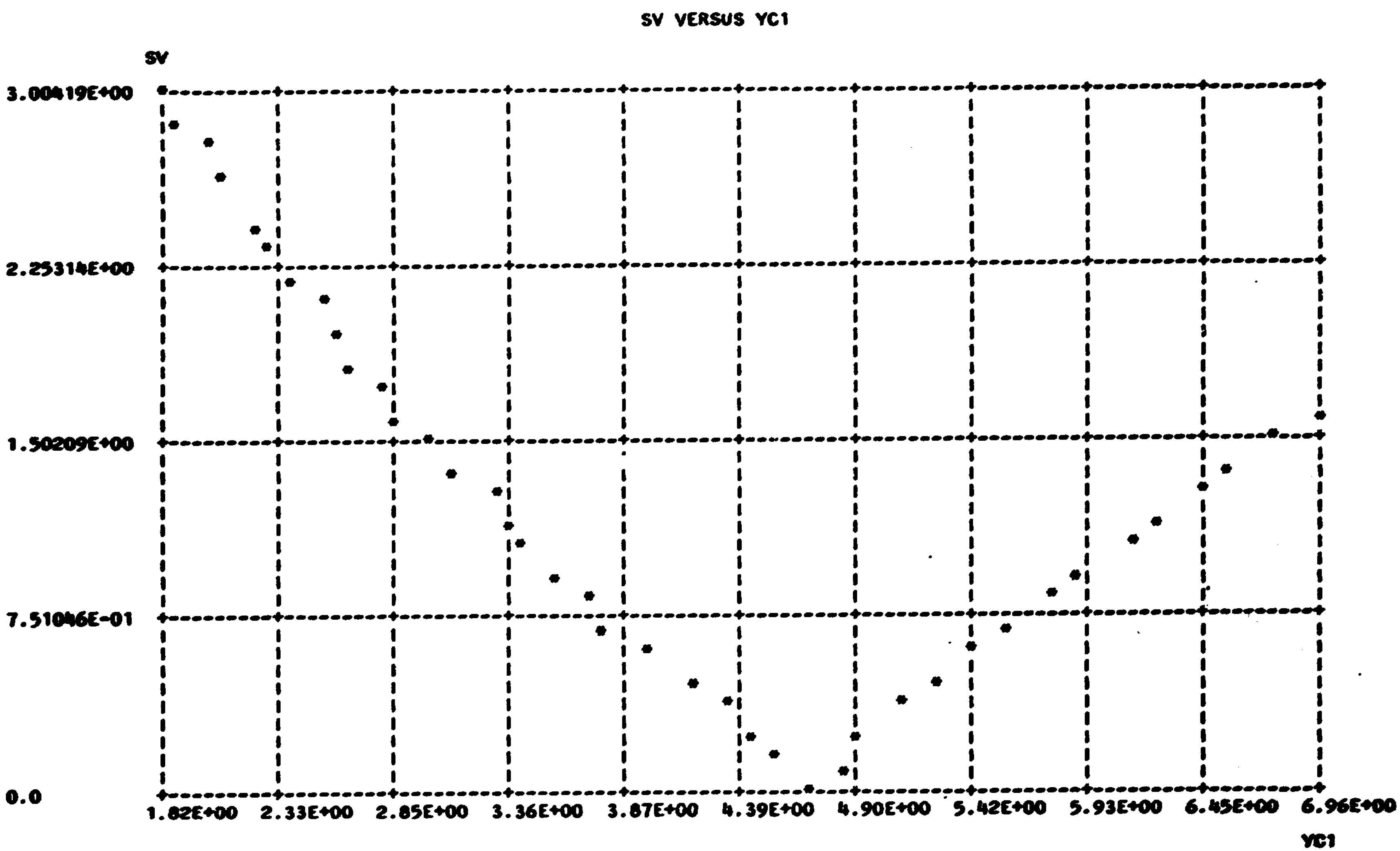

SV IS THE SLIDING VELOCITY AT THE CONTACT POINT; M/SEC
YC1 IS THE LOCATION OF THE CONTACT POINT ALONG THE TOOTH PROFILE OF GEAR 1; MM.

(NOTE: THE ABSOLUTE VALUE OF SV IS SHOWN - THERE IS A SIGN REVERSAL IN SV AT THE PITCH POINT)

Figure A. 8-5 SLIDING VELOCITY

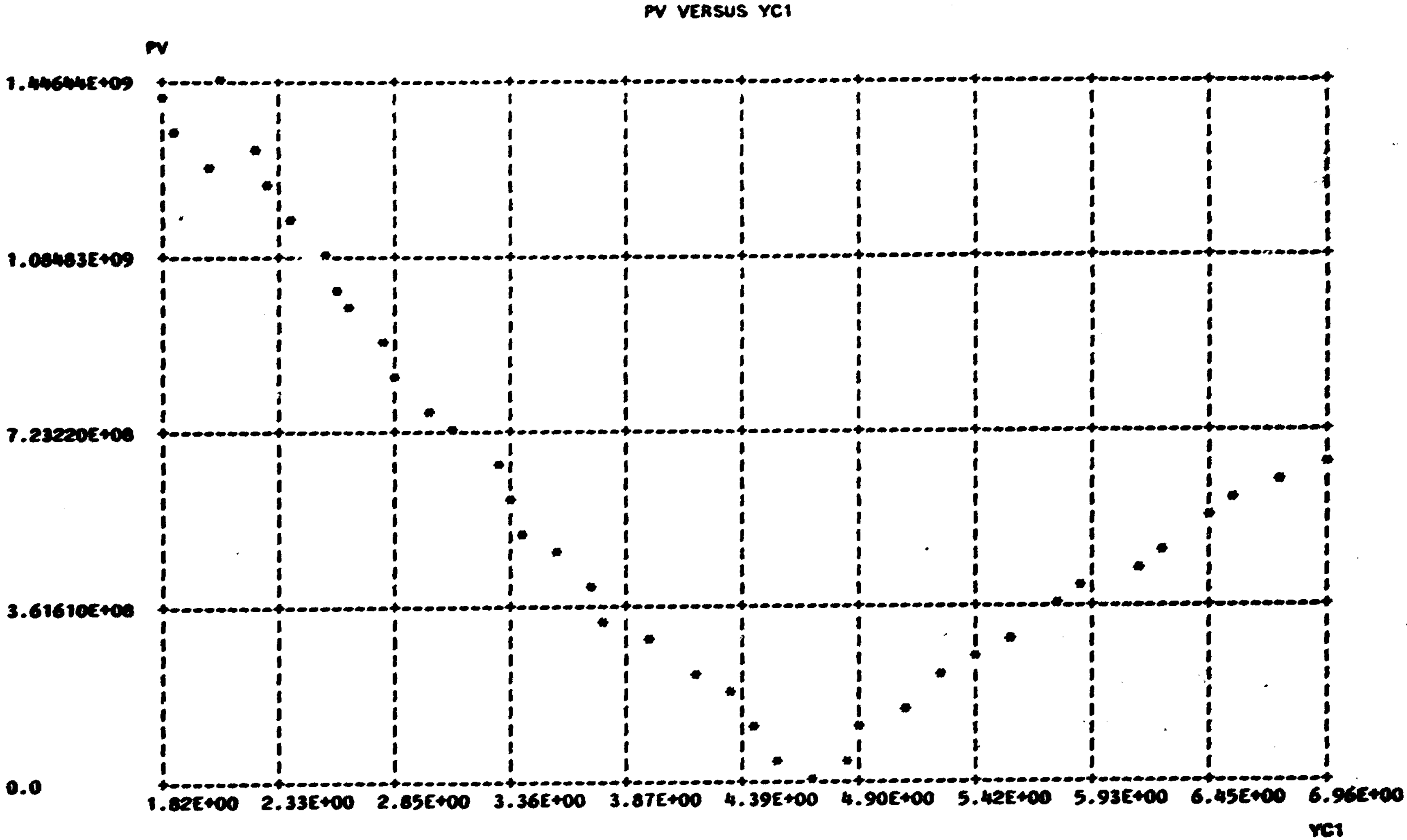

PV IS THE HERTZ PRESSURE-SLIDING VELOCITY PRODUCT; N /(M -SEC).
YC1 IS THE LOCATION OF THE CONTACT POINT ALONG THE TOOTH PROFILE OF GEAR 1; MM.

Figure A. 8-6 PV: HERTZ CONTACT STRESS

XT PLOT OF THE RESULTS OF
THE NUMERICAL INTEGRATION

THE DATA DEPICTED IN THE FOLLOWING X VERSUS T PLOTS ARE OBTAINED BY NUMERICALLY INTEGRATING THE DIFFERENTIAL EQUATIONS OF MOTION. IN THESE PLOTS:

TIME IS THE INTEGRATION TIME; SECONDS
KG IS THE GEAR STIFFNESS; N /M
DF IS THE DYNAMIC FORCE; N

THE DYNAMIC FORCE PLOT DISPLAYS A NORMALIZED DYNAMIC FORCE, I.E. THE DYNAMIC FORCE DIVIDED BY THE NOMINAL TRANSMITTED FORCE.

THIS PLOT REPRESENTS ONLY THAT TIME PERIOD IN THE NUMERICAL INTEGRATION SEQUENCE COVERING THE LAST PASSAGE OF A TOOTH PAIR THRU THE CONTACT ZONE. IT IS ASSUMED THAT THE SYSTEM IS OPERATING IN A STEADY STATE CONDITION DURING THIS PERIOD.

INPUT SPEED IS 2000.00 RPM BACKLASH IS 0.254000 MM.

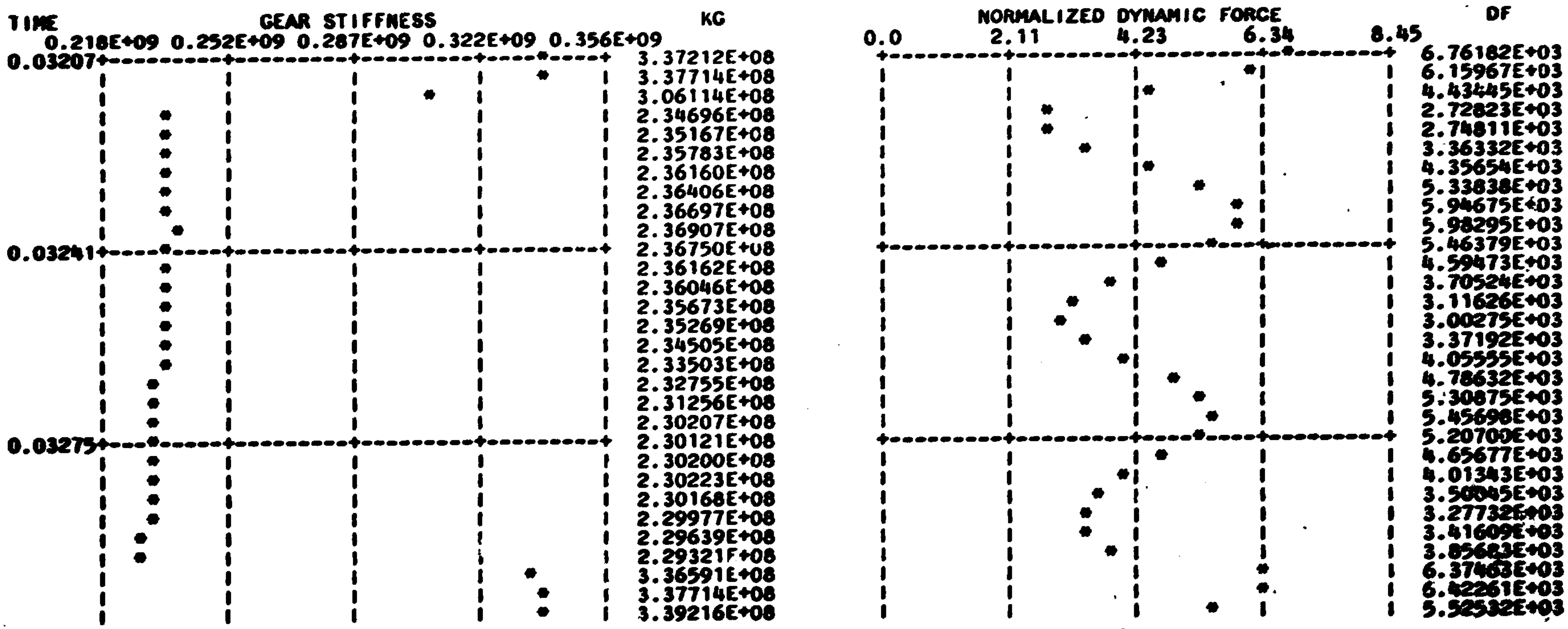

Figure A. 8-7 GEAR MESH DYNAMIC LOAD

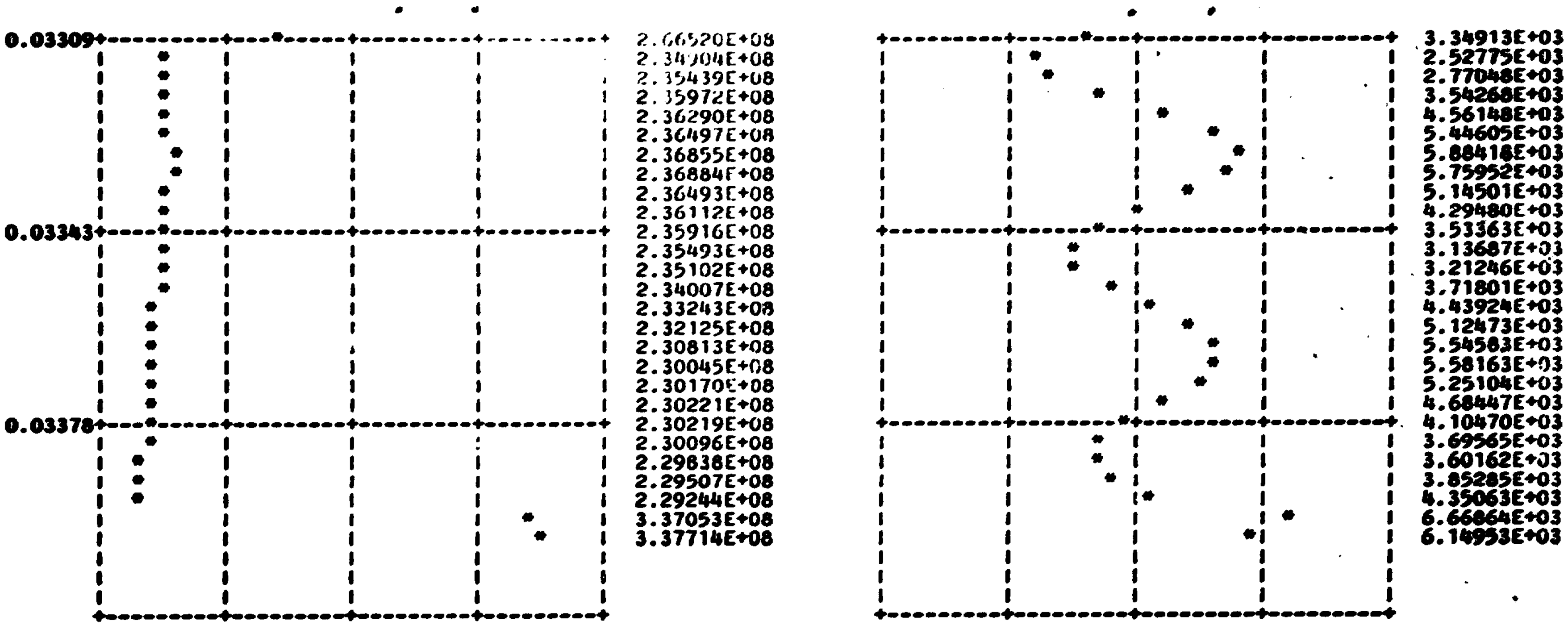

Figure A. 8-7 (Continued) GEAR MESH DYNAMIC LOAD

THE INFORMATION IN THIS TABLE COMES FROM AN ANALYSIS OF THE NUMERICAL INTEGRATION SEQUENCE COVERING THE LAST PASSAGE OF A TOOTH PAIR THROUGH THE CONTACT ZONE. POSITION 1 CORRESPONDS TO THE STARTING POINT OF CONTACT WHILE POSITION 100 CORRESPONDS TO THE END POINT OF CONTACT. THE FOLLOWING SYMBOLS ARE UTILIZED IN THIS TABLE:

SF IS THE NOMINAL TRANSMITTED FORCE ALONG THE LINE OF ACTION; N
DF IS THE TOTAL DYNAMIC FORCE BEING TRANSMITTED ALONG THE LINE OF ACTION; N
DF1 IS THE DYNAMIC LOAD FACTOR FOR THE GEAR PAIR, ADJACENT SHAFTS, AND BEARINGS
SL IS THE FORCE IN N ACTING BETWEEN THE CONTACTING TOOTH PAIR FROM THE STATIC ANALYSIS
DL IS THE FORCE IN N ACTING BETWEEN THE CONTACTING TOOTH PAIR FROM THE DYNAMIC ANALYSIS
DF2 IS THE DYNAMIC FACTOR FOR AN INDIVIDUAL GEAR TOOTH PAIR TRAVERSING THE MESH ARC

POSITION	SF	DF	DF1	SL	DL	DF2
1	4448.25	6761.82	1.52	1419.75	2158.17	1.52
2	4448.25	6411.30	1.44	1427.59	2046.30	1.43
3	4448.25	5874.64	1.32	1435.43	1895.72	1.32
4	4448.25	4864.62	1.09	1445.88	1569.79	1.09
5	4448.25	3861.62	0.87	1456.33	1264.27	0.87
6	4448.25	2863.77	0.64	1794.35	1360.93	0.76
7	4448.25	2738.21	0.62	2132.37	1312.62	0.62
8	4448.25	2798.45	0.63	2137.73	1341.50	0.63
9	4448.25	3153.09	0.71	2143.09	1519.10	0.7[illegible]
10	4448.25	3595.36	0.81	2155.29	1732.18	0.8[illegible]
11	4448.25	4165.19	0.94	2167.49	2029.56	0.94
12	4448.25	4730.51	1.06	2176.01	2305.02	1.06
13	4448.25	5293.55	1.19	2184.54	2599.66	1.19
14	4448.25	5660.63	1.27	2193.04	2779.93	[illegible].27
15	4448.25	5950.57	1.34	2201.55	2945.08	1.34
16	4448.25	5971.54	1.34	2211.35	2955.45	1.34
17	4448.25	5845.14	1.31	2221.15	2918.65	1.31
18	4448.25	5542.54	1.25	2229.13	2767.56	1.24
19	4448.25	5087.46	1.14	2237.12	2558.59	1.14
20	4448.25	4578.25	1.03	2247.53	2302.50	1.02
21	4448.25	4057.02	0.91	2257.95	2059.36	0.91
22	4448.25	35[illegible].31	0.81	2267.08	1823.97	0.80
23	4448.25	32[illegible]9.11	0.73	2276.22	1662.60	0.73
24	4448.25	3075.74	0.69	2284.22	1573.89	0.69
25	4448.25	3009.75	0.68	2292.22	1550.94	0.68
26	4448.25	3193.55	0.72	2301.18	1645.66	0.72
27	4448.25	3436.66	0.77	2310.14	1784.78	0.77
28	4448.25	3830.28	0.86	2321.11	1989.21	0.86
29	4448.25	4235.37	0.95	2332.08	2220.47	0.95
30	4448.25	4655.71	1.05	2341.30	2440.84	1.04
31	4448.25	4993.82	1.12	2350.52	2638.80	1.12
32	4448.25	5294.91	1.19	2362.31	2797.91	1.18
33	4448.25	5390.60	1.21	2374.10	2877.04	1.21
34	4448.25	5424.10	1.22	2382.67	2894.92	1.21
35	4448.25	5278.72	1.19	2391.24	2837.67	1.19
36	4448.25	5044.21	1.13	2392.57	2711.61	1.13
37	4448.25	4722.90	1.06	2393.90	2541.70	1.06
38	4448.25	4357.96	0.98	2394.87	2345.30	0.98
39	4448.25	3988.11	0.90	2395.83	2148.00	0.90
40	4448.25	3688.38	0.83	2396.56	1986.56	0.83
41	4448.25	3451.96	0.78	2397.30	1860.36	0.78
42	4448.25	3321.99	0.75	2397.25	1790.32	0.75
43	4448.25	3330.14	0.75	2397.20	1794.64	0.75
44	4448.25	3410.63	0.77	2396.45	1838.02	0.77
45	4448.25	3653.53	0.82	2395.70	1967.68	0.82
to 100						

Figure A. 8-8 TABULATION OF DYNAMIC LOAD FACTORS

LOAD VERSUS YC1

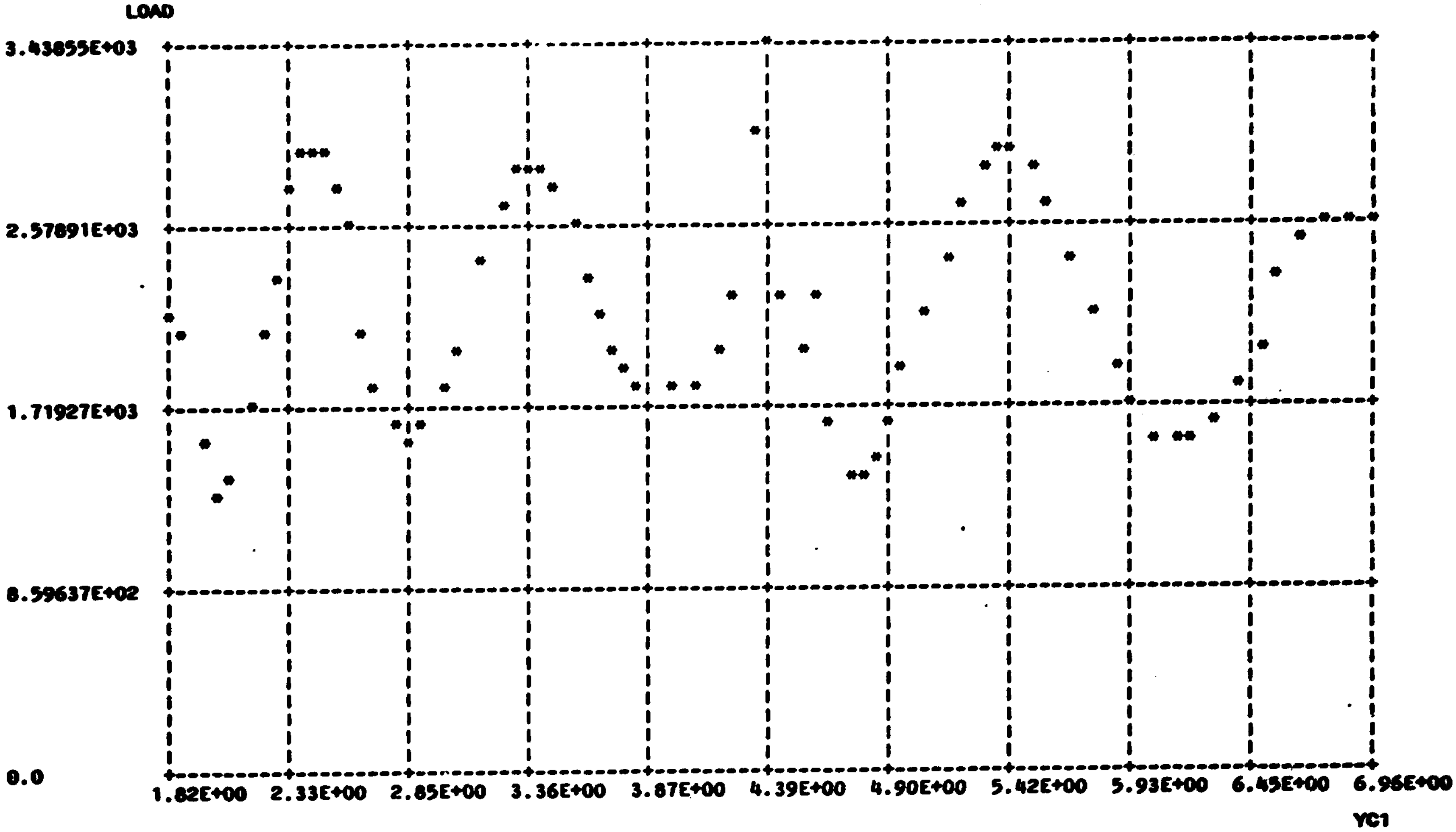

LOAD IS THE FORCE IN N ACTING BETWEEN THE CONTACTING TOOTH PAIR.
YC1 IS THE LOCATION OF THE CONTACT POINT ALONG THE TOOTH PROFILE OF GEAR 1; MM.

Figure A. 8-9 DYNAMIC LOAD BETWEEN CONTACTING GEAR TOOTH PAIR

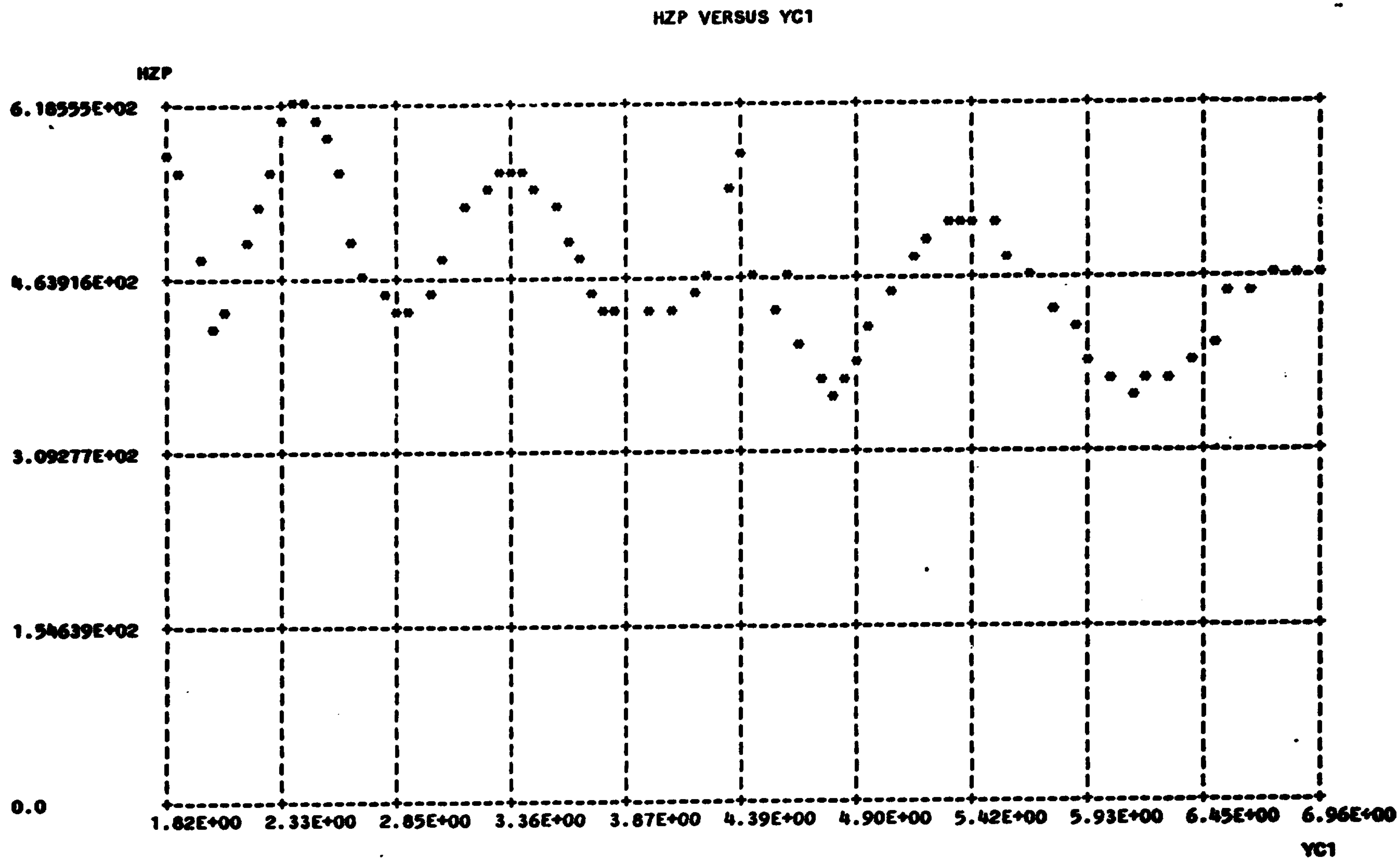

HZP IS THE MAXIMUM HERTZ CONTACT PRESSURE AT THE CONTACT POINT; MPA.
YC1 IS THE LOCATION OF THE CONTACT POINT ALONG THE TOOTH PROFILE OF GEAR 1; MM.

Figure A. 8-10 DYNAMIC HERTZ STRESS